The Thesis Committee for Woong Mo Koo
Certifies that this is the approved version of the following thesis:

Architecture and Evolution of Submarine-Fans, and Coupling with Shelf-Edge Processes in Supply-Dominated Margins: Example from Maastrichtian Washakie Basin

APPROVED BY
SUPERVISING COMMITTEE:

Supervisor:

Ronald J. Steel

Co-Supervisor:

Wonsuck Kim

Cornel Olariu

Architecture and Evolution of Submarine-Fans, and Coupling with Shelf-Edge Processes in Supply-Dominated Margins: Example from Maastrichtian Washakie Basin

by

Woong Mo Koo, B.S., M.S.

Thesis

Presented to the Faculty of the Graduate School of

The University of Texas at Austin

in Partial Fulfillment

of the Requirements

for the Degree of

Master of Science in Geological Sciences

The University of Texas at Austin

May 2015

Dedication

To my wife, children, and my mother who consistently love and support me unconditionally with patience

Acknowledgements

First of all, I would like to express my sincere thanks to my advisors Ronald Steel and Wonsuck Kim who have guided me to formulate and address the important geological problems in this project. I would like to extend my thanks to Cornel Olariu, a committee member, for his generous help during field trips and for his patience to listen my endless questions. I appreciate support for field and core work with funds from the RioMAR consortium (Shell, Statoil, Woodside, ENI, BHP, Devon, PDVSA, and Chevron) and the William Dow Hamm AAPG Grant-in-Aid. The field trip in Rawlins, Wyoming would not have been possible without Kathryn Sanger and Niels Hansen giving me permission to access their ranches to visit outcrops. Korea National Oil Corporation is appreciated for supporting tuition and living costs during my master's program. My officemates, David Conwell, Rattanaporn Fongngern, and Valentina Rossi, and all members of Dr. Steel and Dr. Kim's groups (Sarah Bateman, Emily Chatmas, Si Chen, Michael Cloos, Max Daniller-Varghese, Chenglin Gong, Eunsil Jung, Ye Jin Lim, Julio Leva López, Shunli Li, Kimberly Miller, Brandon Minton, Yang Pang, Anastasia Piliouras, Moonsoo Shin, Jeremy Slaugenwhite, Eugen P Tudor, Xiaojie Wei, Logan West, Yu Ye, and Jinyu Zhang) are thanked for their valuable suggestions on the project and their friendship which made me happy and full of energy. Cristian Carvajal and Mariana Olariu are deeply thanked for their constructive discussion on the variability of shelf margins and submarine-fan deposits. Austin Clayton is thanked for his assistance on digitization of multiple gamma-ray logs. I also thank USGS for permission to use their facilities to look at the cores.

Finally, my special thanks are dedicated to my father, Bon-Dong Koo, who watches me in heaven, for his encouragement and support in every aspect that built the foundation of Woong Mo Koo's study.

Abstract

Architecture and Evolution of Submarine-Fans, and Coupling with Shelf-Edge Processes in Supply-Dominated Margins: Example from Maastrichtian Washakie Basin

Woong Mo Koo, M.S. Geo.Sci.

The University of Texas at Austin, 2015

Supervisors: Ronald J. Steel and Wonsuck Kim

Along high-sediment supply margins, sediment delivered from shallow to deep-water by shelf-edge deltas is considered as the a main source for submarine-fans on the basin floor. As the consequence of direct feed, the architecture and spatio-temporal evolution of submarine-fans are closely related with processes on shelf margins. This thesis investigates 1) the linkage between shelf-edge architecture and evolution (stacking pattern) of basin-floor fans in two basin-scale clinothems (Clinothems 9 and 10) and 2) the lithofacies variability on the fringes of submarine-fans, using about 1,500 gamma well-logs and four cores in the Maastrichtian Washakie Basin, Wyoming.

Based on the correlation of gamma-ray logs, submarine fan-lobe complexes in Washakie Basin are shown to develop through stages of initiation, progradation and/or aggradation, and retreat. The aggradational stacking pattern of Clinothem 9 lobe complexes and progradational stacking pattern of Clinothem 10 lobe complexes are shown to be linked to the coeval shelf-edge trajectory behavior. This direct linkage between shelf-edge

trajectories and submarine fan-behavior was possible firstly because Washakie Basin was a sediment supply-dominated margin despite times of strong accommodation influence. Secondly, the sediment in shelf margins was transported quasi-continuously to deep-water via slope channels, which were continuously connected between shelf-edges and basin-floor during most of the sea-level cycle. In high sediment-supply systems, rivers commonly overcome the significant reworking power of waves and tides and are thus able to deliver sediments from the shelf edge to deep water.

Cores in Washakie Basin show that there was variable lithofacies patterns in mapped submarine fan-fringes. Multiple transitions of lithofacies occur within the same bed, without significant erosion between high-concentration turbidites (e.g., structureless sandstones) and debrites (e.g., mud-clasts rich muddy sandstones) are identified in distal fringes of submarine fans. In contrast, in the lateral fringes of fans, there is a significantly shorter transition from turbidites to debrites. One explanation of facies variability is correlated with the run-out distance of flow that enhances transitions of flow. The longer axial run-out distance of flows results in deposition of mud-clast rich debrites. The shorter, transverse to lobe run-out distance causes only partial or non-transformed flows, resulting in deposition of muddy and sandy turbidites respectively. In the longitudinally elongated submarine fans in Washakie Basin, developed by long run-out distance of flow, the distal fan-fringes are thus significantly muddier than the lateral fringes, something of importance to hydrocarbon productivity on fan lobes.

Table of Contents

List of Tables

List of Figures

Figure 2.10: Parts of Markov chain of lithofacies with cutoff 8% from A) Clinothem 4 at the location of Well API No. 4900722141, B) Clinothem 5 at the location of Well API No. 4900722141, C) Clinothem 12 at the location of Well API No. 4903721922, and D) Clinothem 11 at the location of Well API No. 4903721741. Inset chain diagrams are full Markov chain with cutoff 8%. The transitions related with mudstones (SM, DM1, DM2, LM) and deformed sandstones (DS1) are excluded from chains in order to compare transitions mainly among structureless sandstones (SS1, SS2), mud-clast sandstones (MS1, MS2), and laminated sandstones (LS1, LS2). For convenience, transitions over 30% are marked in pink color. Inset fan diagrams show the relative locations (green circles) of core interval in the fringes of fans. Note that transitions of deformed sandstones (DS1) - structureless sandstones (SS1), laminated sandstones (LS1, LS2) - laminated mudstones (LM)/structureless mudstones (SM), and structureless mudstones / laminated mudstones - structureless sandstones are well observed in any locations fan-fringes. In distal fringes (A, B, C) transitions among SS1, SS2, MS1, and MS2 occur frequently. In lateral fringe (D) the interaction between MS2 and other facies is less common but active between MS1 and other facies. 57

Chapter 1: Conditions for Coupling between Shelf-Edge Architecture and Submarine-Fan Growth Style in Supply-Dominated Margin

ABSTRACT

The linkage between relative sea-level change, shelf-edge architecture, and evolution of Maastrichtian basin-floor fans in Washakie Basin, Wyoming has been investigated at the scale of lobes, lobe complexes, and submarine fans using 630 wireline logs. The basin-floor fan deposits of two clinothems (9 and 10) form lobate shapes on the toe-of-slope and basin floor. At lobe scale, amalgamated channels, channel-levees, unconfined lobe sheets and muddy deposits are recognized in the axis, fringe, and distal fringe of lobes respectively. The lobe complexes of the two clinothems are initially only weakly developed, indicating minor sediment volumes delivered to deep-water. Later, the lobe complexes of Clinothem 9 aggraded with fixed slope channels and without strong basinward or lateral migration and did so in concert with a highly aggradational shelf-edge during a period of interpreted relative sea-level rise. In contrast, the deep-water lobe complexes of Clinothem 10 prograded continuously for 20 km on the basin floor coeval with a flattish shelf-edge progradation and an interpreted slight sea-level fall. The depocenters of lobe complexes in Clinothem 10 switched laterally by compensational stacking and slope-channel avulsions. During the late development of both clinothems, the deep-water lobe complexes became smaller or retreated concurrent with shelf flooding. Washakie Basin deep-water fan-lobe complexes thus evolved through stages of initiation, aggradation, progradation, and retreat. The lobe complex growth stages of these deep-water depocenters were surprisingly well linked to coeval shelf-edge trajectory changes between successive, ca. 100 Ky maximum flooding events on the shelf. We suggest that the

surprisingly close linkage of lobe-complex stacking pattern with shelf-edge behavior was because the Greenhouse Washakie Basin had a continuously, high, Laramide sediment discharge to the deep-water fans while the feeder deltas were at the shelf edge, despite significant sediment reworking of shelf-edge deltas by waves and tides.

INTRODUCTION

The lowstand of sea-level has been conventionally considered as the conducive condition of submarine fan deposition (Van Wagoner et al., 1987; Posamentier and Vail, 1988). However, researchers argued conceptually (Burgess and Hovius, 1998) and demonstrated with ancient datasets that rising and high sea-level stand can also produce deep-water fans in high sediment-supply basins (Carvajal and Steel, 2006; Covault et al., 2007; Kim et al., 2013) though the volume of lowstand submarine fans would be larger than that produced at highstand. The behavior and process regime of shelf-edge deltas (sediment feeder to deep water) in high sediment-supply basins is also now known to impact the presence and volume of deep-water fan-lobe complexes (Dixon et al., 2012). The stacking pattern of submarine fans has been reported from outcrop and subsurface data studies (Normark, 1970; Mutti and Ricci Lucchi, 1972; Walker and Mutti, 1973; Mutti, 1977; Posamentier and Kolla, 2003; Hadler-Jacobsen et al., 2005; Deptuck et al., 2008; Prélat et al., 2009; Hodgson, 2009; Mulder et al., 2010; Straub and Pyles, 2012) and the progradation of channelized lobes accompanied by compensational stacking is generally accepted as the main builder of submarine fans (Piper and Normark, 1983; Mutti and Normark, 1987; Twichell et al., 1992; Gardner et al., 2003; Straub et al., 2009). The submarine fans developed in accommodation and sediment-supply dominated basins, however, growth style of fans remains to be improved. Progradational deltas at the shelf-

edge are known to be a main supplier of sediment to deep-water turbidite lobes (Porębski and Steel, 2003). We propose here that aggradation and progradation style of deltas at the shelf-edge is linked with the evolution and stacking pattern of deep-water lobe complexes. To test this hypothesis, the evolution of 27 deep-water lobe complexes at the toe of two basin scale clinothems are documented using 630 closely (500 m to 3 km) spaced wells from the high sediment-supply Maastrichtian Washakie Basin where shelf margins prograded at rates of up to 40 km/My (Carvajal and Steel, 2006; Carvajal et al., 2009). We demonstrate a close relationship between the stacking pattern of the deep-water lobe complexes and the stacking pattern of the coeval shelf-margin depocenters (deltas).

GEOLOGY

Washakie Basin, one of the Laramide syn-tectonic basins, was formed between the Granite Mountains, Rawlins uplift, and Wind River Range during the early Maastrichtian (Steidtmann and Middleton, 1991) (Fig. 1.1). Washakie Basin infill contains some 16 clinothems (C1 to C16), each of ca. 100 Ky duration, formed by the early Maastrichtian fluvial Lance Formation, shoreline/shelf Fox Hills Sandstone, and deep-water Lewis Shale (Carvajal and Steel, 2006; Carvajal et al., 2009; Olariu et al., 2012). The undecompacted height of clinothems is between 230 m in the west and 430 m in the east due to the asymmetrical tilting of the basin. During a 1.8 My period, the shelf-margin prograded generally from north to south (west-east shelf-edge orientation) at a very high rate of >48 km/My and accumulated at rate of 267 m/My. The stratigraphy of the basin is divided into aggradational (C1 to C9) and progradational (C10 to C16) stages, based on the angle of the long-term shelf-edge trajectories (Carvajal et al., 2009).

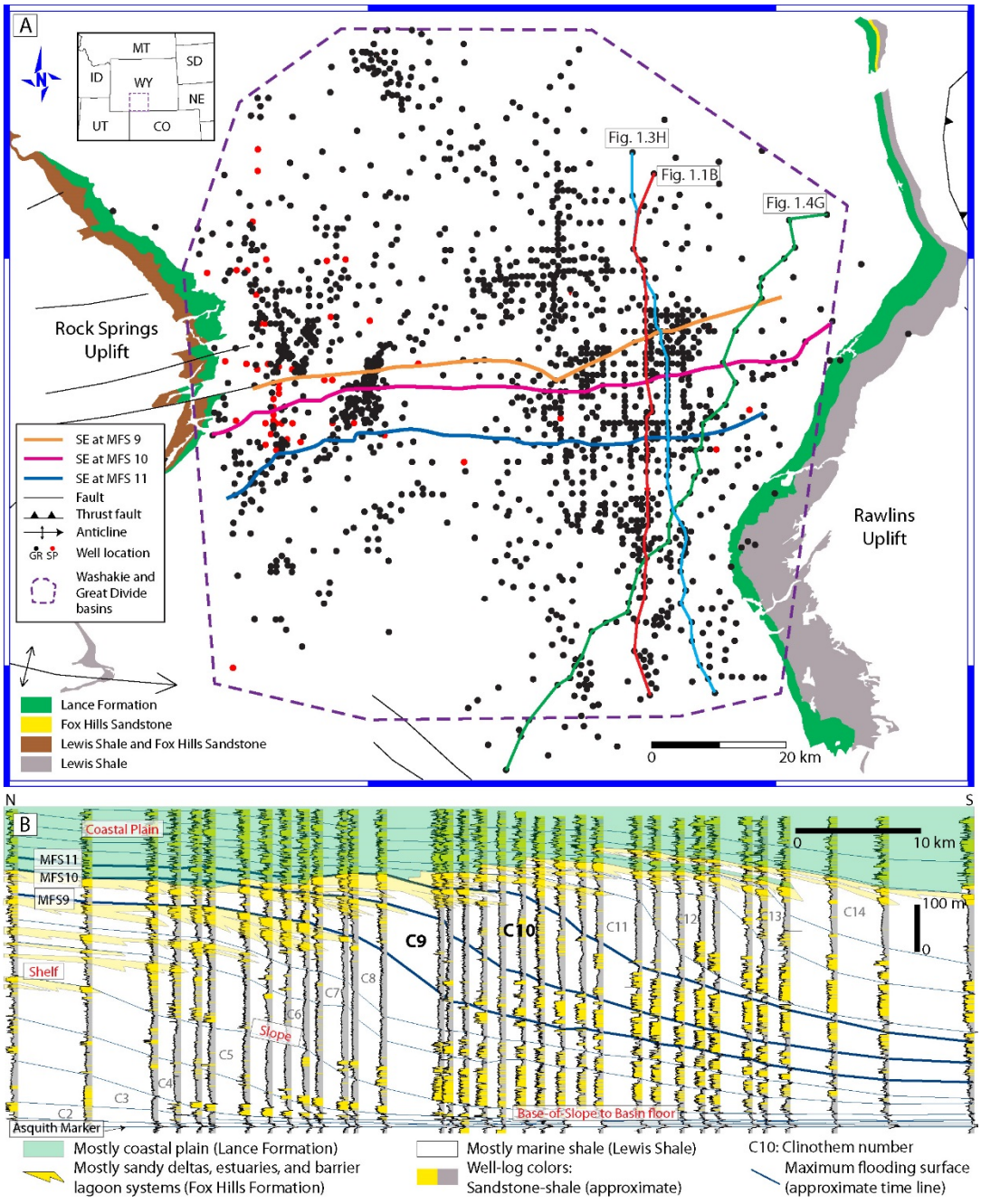

Figure 1.1: Location of Washakie Basin in Wyoming showing A) well locations and outcrop exposures and B) a dip-oriented cross-section through the linked fluvial (Lance Fm.) to shelf (Fox Hills Fm.) to deep-marine (Lewis Shale) depositional system, which is crossed by 16 clinothems (modified from Carvajal and Steel, 2009 and Olariu et al., 2012). GR: gamma ray; MFS: maximum flooding surface; SE: shelf edge; SP: spontaneous potential; ID: Idaho; MT: Montana; WY: Wyoming; SD: South Dakota; NE: Nebraska; CO: Colorado; UT: Utah.

DATA AND METHOD

A series of clinoform-bottomset intervals of submarine fan deposits, bounded by regionally traceable surfaces with high gamma-ray peaks, were defined within Clinothems 9 and 10, using 630 wells in the southern part of the Washakie Basin over an area around 6,200 km^2 (Fig. 1.1). The deposits within each study interval represent a relatively short time period (ca. 20 Ky for 5 to 6 intervals within a 100 Ky clinothem; Olariu et al., 2012). Within each mapped bottomset interval, the sandy deposits represent fan-lobe complexes whereas mudstone or heterolithic strata represent fringe or abandonment stages. The plan-view distribution of lobe complexes is shown by sandstone thickness maps for each interval, with a 10 to 90 API gamma cut-off. To begin the correlation, the early lobe complexes at the foot of Clinothem 9 were picked in topographic low areas. Channels associated with lobe complexes are identified from capping blocky units of low gamma-ray signal with a slight upward-fining pattern. Levees are recognized from repetition of thin beds interpreted from high gamma-ray serrated patterns. Unconfined lobe sheets were interpreted from repetition of units showing an upward-coarsening gamma-ray motif, and muddy beds from high gamma-ray signals within lobe complexes (Fig. 1.2, Appendix A).

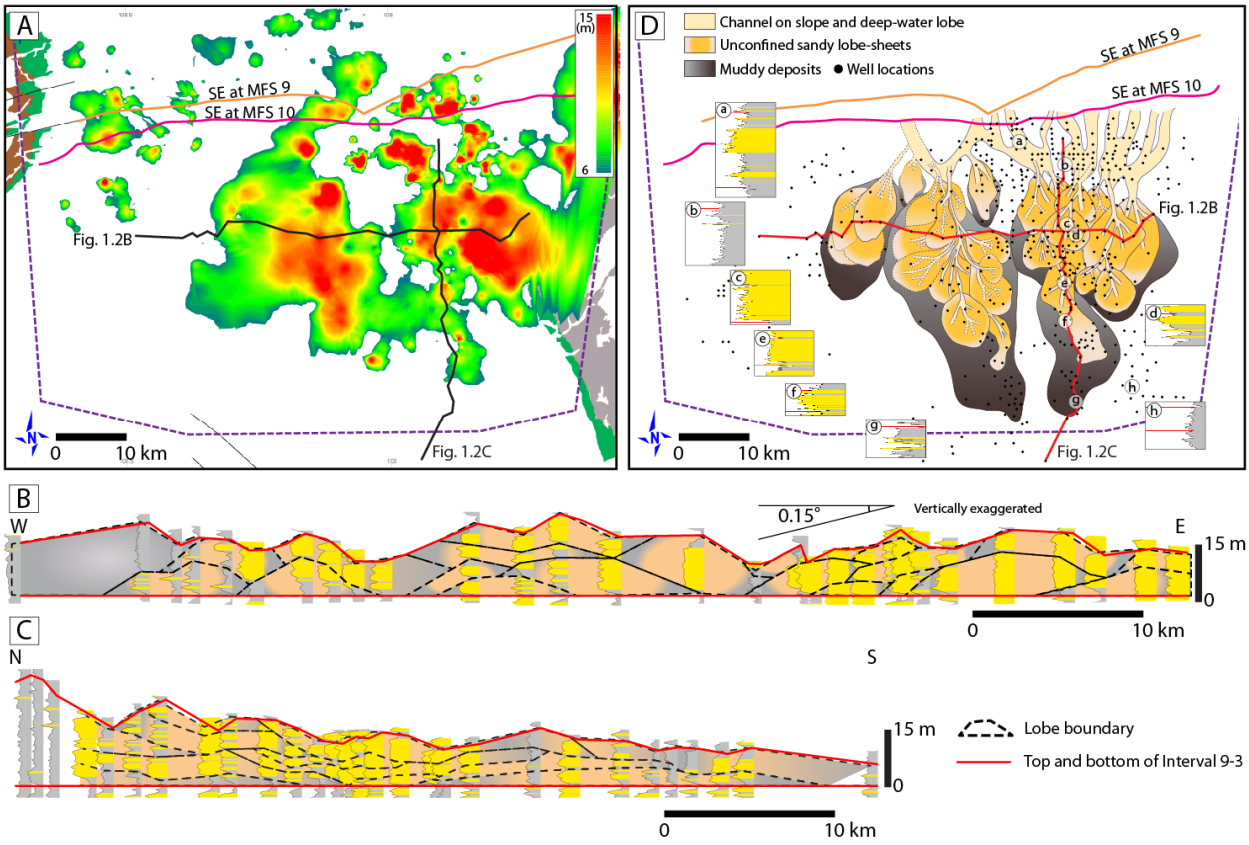

Figure 1.2: Lobe complexes in one (i.e., Interval 9-3) of five intervals mapped in Clinothem 9 fan. A) Sandstone thickness map showing two main lobe complexes. Cross-sections in depositional B) strike (W-E) and C) dip (N-S) directions. Cross-sections are flattened on the bottom horizon of Interval 9-3. Lobe complexes are thicker in the center and thin laterally displaying a compensational stacking pattern in the strike-section. In the dip direction, lobe complexes are asymmetrical with a convex-up geometry; the lobe complexes are thicker in proximal and thinner in distal parts. D) Lobe complexes interpreted by wireline gamma (GR) log motives showing amalgamated channels (blocky units of low GR), unconfined lobe sheets (upward coarsening GR), and muddy deposits (high GR) in the axis, fringe, and distal fringe of lobes respectively. The southwestern part of the basin was excluded from interpretation due to sparse well data.

RESULTS

Dimensions and Facies of Deep-Water Lobe Complexes

Lobate-elongate geometries can be recognized on sandstone isopach maps (Fig. 1.2A). The average size of a mapped lobe complex is about 28 km long, 15 km wide, and 21 m thick (Table 1.1). The average ratio of length to width is 1.9, showing that lobe complexes are elongated in depositional dip-direction (N-S trend). The strike-oriented cross section shows a convex-up lobe complex that is thicker in the center and thins laterally to the west and east (Fig. 1.2B), whereas an asymmetric convex-up shape, with thicker proximal and thinner distal parts, is observed in the depositional dip-direction of lobe complexes (Fig. 1.2C). Amalgamated channels, channel-levees, unconfined lobe sheets and muddy deposits are recognized in the axis, fringe, and distal fringe of lobes respectively (Fig. 1.2D). The channelized lobe axes contain blocky gamma log pattern (amalgamated structureless or weakly flat-laminated sandstone beds with possible mud clasts and erosional surfaces), whereas the levees with more "erratic" log pattern are created by thin, ripple cross-laminated sandstone beds, interlayered with siltstone and mudstone. The lobate distribution of coarsening-upward bedsets below channel-levees is interpreted in terms of a progradational unconfined lobe sheets. Mudstone with siltstone laminae and some hybrid beds with soft sediment deformation are probably deposited in the distal fringes of lobes and generate an irregular log pattern with thin sandstone beds.

Table 1.1: Dimension of lobe complexes in Clinothems 9 and 10 (Appendix B).

Inter-vals	Lobe complex	(A) Length (km)	(B) Width (km)	(C) = (A) / (B) Length / Width (ratio)	(D) Thickness at centroid (m)	(E) Area* (km^2)	(F) Volume (km^2 x m)
	9-2-1	29	15	1.9	20	198	2,486
9-2	9-2-2	34	13	2.6	17	272	3,506
	9-2-3	34	18	1.9	25	475	6,304
9-3	9-3-1	32	23	1.4	21	383	4,219
	9-3-2	30	19	1.6	15	350	3,849
	9-4-1	28	11	2.5	19	212	2,374
9-4	9-4-2	30	13	2.3	21	314	3,219
	9-4-3	36	23	1.6	14	618	6,388
9-5	9-5-1	23	13	1.8	17	211	1,937
	9-5-2	19	16	1.2	14	184	1,611
Maximum (C9)		36	23	2.6	25	618	6,388
Minimum (C9)		19	11	1.2	14	184	1,611
Average (C9)		**30**	**16**	**1.9**	**18**	**321**	**3,589**
10-1	10-1-1	31	19	1.6	15	397	3,938
	10-2-1	35	15	2.3	59	409	11,494
	10-2-2	29	11	2.6	35	298	7,938
10-2	10-2-3	27	15	1.8	25	340	5,477
	10-2-4	18	15	1.2	9	199	1,604
	10-2-5	19	9	2.1	21	125	1,415
	10-3-1	31	13	2.4	16	265	2,918
10-3	10-3-2	33	14	2.4	13	381	6,653
	10-3-3	26	14	1.9	16	273	4,321
	10-4-1	26	14	1.9	23	282	4,573
	10-4-2	34	16	2.1	24	391	6,464
10-4	10-4-3	35	17	2.1	27	367	5,576
	10-4-4	20	10	2.0	18	187	2,043
	10-4-5	19	11	1.7	23	149	1,487
	10-5-1	33	22	1.5	27	422	6,120
10-5	10-5-2	30	17	1.8	15	327	4,416
	10-5-3	25	17	1.5	12	280	3,355
Maximum (C10)		35	22	2.6	59	422	11,494
Minimum (C10)		18	9	1.2	9	125	1,415
Average (C10)		**28**	**15**	**2.0**	**22**	**300**	**4,694**
Total maximum		36	23	2.6	59	618	11,494
Total minimum		18	9	1.2	9	125	1,415
Total Average		**28**	**15**	**1.9**	**21**	**308**	**4,285**

Stacking Patterns of Deep-Water Lobe Complexes

Two distinct stacking patterns have been observed in the fans of Clinothems 9 and 10. In the earliest stage of Clinothem 9, no sandy lobe complexes were developed, only mudstones (Fig. 1.3A). The first deep-water lobe complexes developed in the south-central and south-east parts of the basin and were connected northwards with slope-channel systems (Fig. 1.3B). The lobe complexes of Clinothem 9 aggraded strongly through time, over an area of around 1,100 km^2 within about 35 km from the toe of slope, but they did not prograde or switch laterally much (Fig. 1.3B-D). The lobe complexes of Clinothem 9 eventually became smaller, and insignificant in volume (Fig. 1.3E, F). During the early development of Clinothem 10, the deep-water lobe complexes in the south-east part of the basin prograded sub-longitudinally towards the south-west (Fig. 1.4A). However, during the further growth of Clinothem 10, the deep-water lobe complexes continued to prograde to the south and south-west for another 20 km, and aggraded about 100 m during the evolution of Clinothem 10 fan (Fig. 1.4B-D). Smaller lobe complexes developed in the western part of the basin and migrated south-eastward with little aggradation (Fig. 1.4B, D, E).

Linkage between Submarine Fan Architecture and Shelf-Edge Trajectory

The Fox Hills shelf-edge had been previously analyzed in term of its trajectory and depositional environments (Olariu et al., 2012) and it had been particularly noted that through the series of 16 clinothems, rising shelf-edge trajectories tended to produce smaller fans than those that were more strongly progradational (Carvajal and Steel, 2006). This was because aggradation caused more of the total sediment budget to be stored on the shelf. We are now able to link the previous observations on the shelf-edge architecture with evolution of the lobe complexes within the basin-floor, deep-water fans. For Clinothem 9, the younger deltas developed on the inner shelf and were fluvial-dominated to tide-

influenced deltas (Olariu et al., 2012) that did not fed sediment to deep water (Fig. 1.3A). As the deltas approached the shelf edge after cross-shelf transit (mostly in the eastern part of the basin) more sediment was delivered to the shelf edge. The sediment became readily available to longshore currents that spread it along the shelf edge, eventually to be captured into the head of slope channels that funneled it to the deep water basin (Fig. 1.3B-D). During a late of clinothem growth the sea level was slowly rising as suggested by the smaller aggradation rates, and as a consequence thinner deltas developed at the shelf edge and smaller or no fans developed in the basin (Fig. 1.3E, F). The absence of significant deep water fans in the west can be explained by the fact that distributaries were few or small there, and most of the sandstone was concentrated in narrow elongate belts by eastwards longshore drift along the western shelf margin (Olariu et al., 2012) (Fig. 1.3G). The main sediment feeder for the deep-water lobes of Clinothem 9 were the shelf-edge deltas sited close to the slope channel heads on the upper slope, though wave-generated longshore drift of sand belts from the west also played an important supply role (Carvajal and Steel, 2009). The minimal lateral migration of the Clinoform 9 fan lobes is likely to have been caused by relatively fixed feeder channel systems at the shelf edge and on the slope. The dominantly aggradational pattern of the deep-water lobes of Clinothem 9 is interpreted as a response to the coeval shelf-edge aggradation rate of 50 m/100 Ky (Fig. 1.3H).

For Clinothem 10, the earliest deltas arrived at the shelf edge quickly, probably during highstand and were highly progradational suggesting significant sediment supply (Olariu et al., 2012). They almost reached the shelf edge in the eastern side of the basin providing sand to the deep water fans (Fig. 1.4A). The following cycles were mostly progradational and formed shelf edge deltas continually (Fig. 1.4B-D). High sediment flux and a relative sea-level fall are interpreted to have been responsible for the marked

progradation of the shelf-edge deltas with thin topsets (Fig. 1.4G) (Carvajal and Steel, 2009) and, in contrast to Clinothem 9, for the strongly prograding deep-water lobe complexes of Clinothem 10 in the southeast areas of the basin (Fig. 1.4B-D, F). The deep water lobe complexes migrated gradually to the west, probably as a result of the migration of the feeder channels and/or the compensational stacking processes related with topography. The lobe complexes in the south central and southwest of basin probably delivered from smaller river systems on the shelf or by the sporadic supply of longshore-drifted sediments along the southwestern shelf-edge (Fig. 1.4B, D, E).

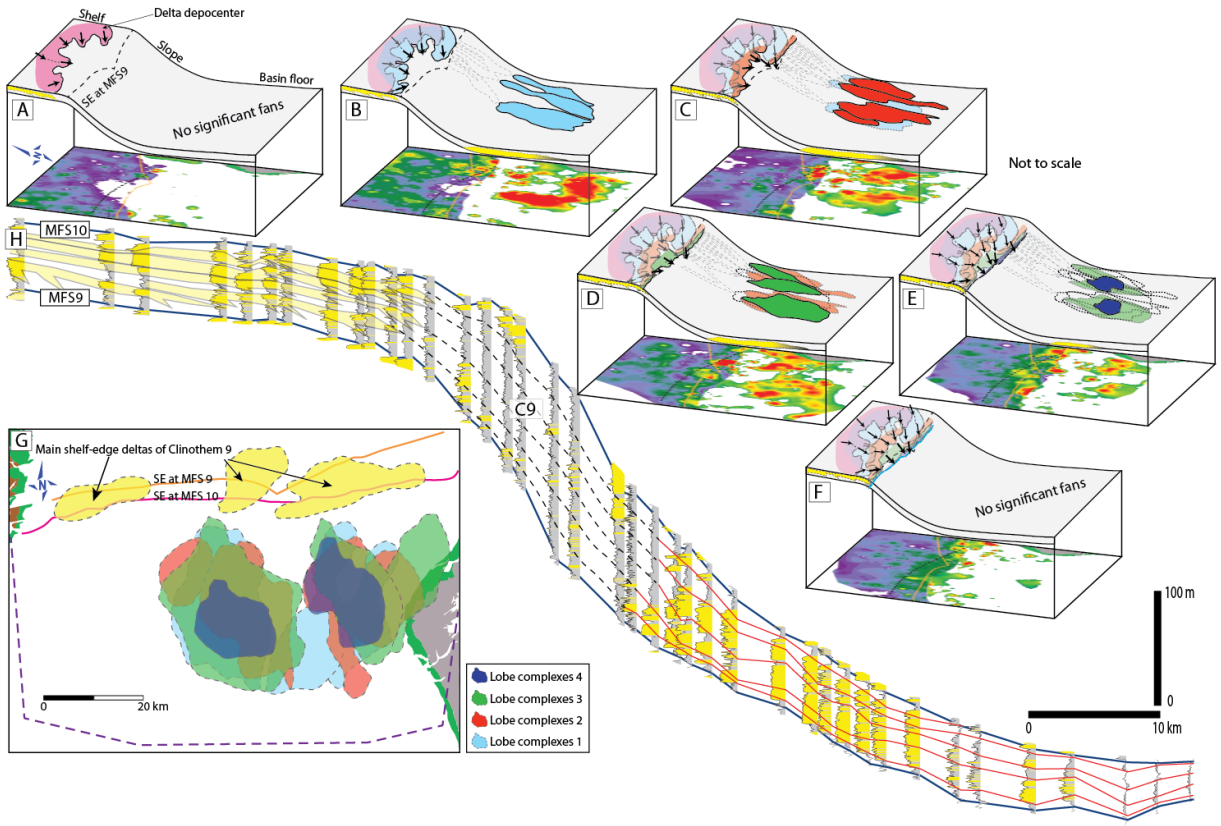

Figure 1.3: Three dimensional block diagrams of Clinothem 9, showing sandstone thickness map (on the bottom of block diagram) and the clinoform depositional environment (deltas and submarine fan-lobes) projected onto the top of block diagram at time steps from A) older to F) younger. The evolution of deep-water lobe complexes was linked with the distribution of delta depocenters on the shelf (modified from Olariu et al., 2012). G) Overlap of deep-water lobe complexes. The lobe complexes vertically stack on each other without significant progradation and lateral shifting. H) Dip cross-section of Clinothem 9. See also Figure 1.2 for the location of section.

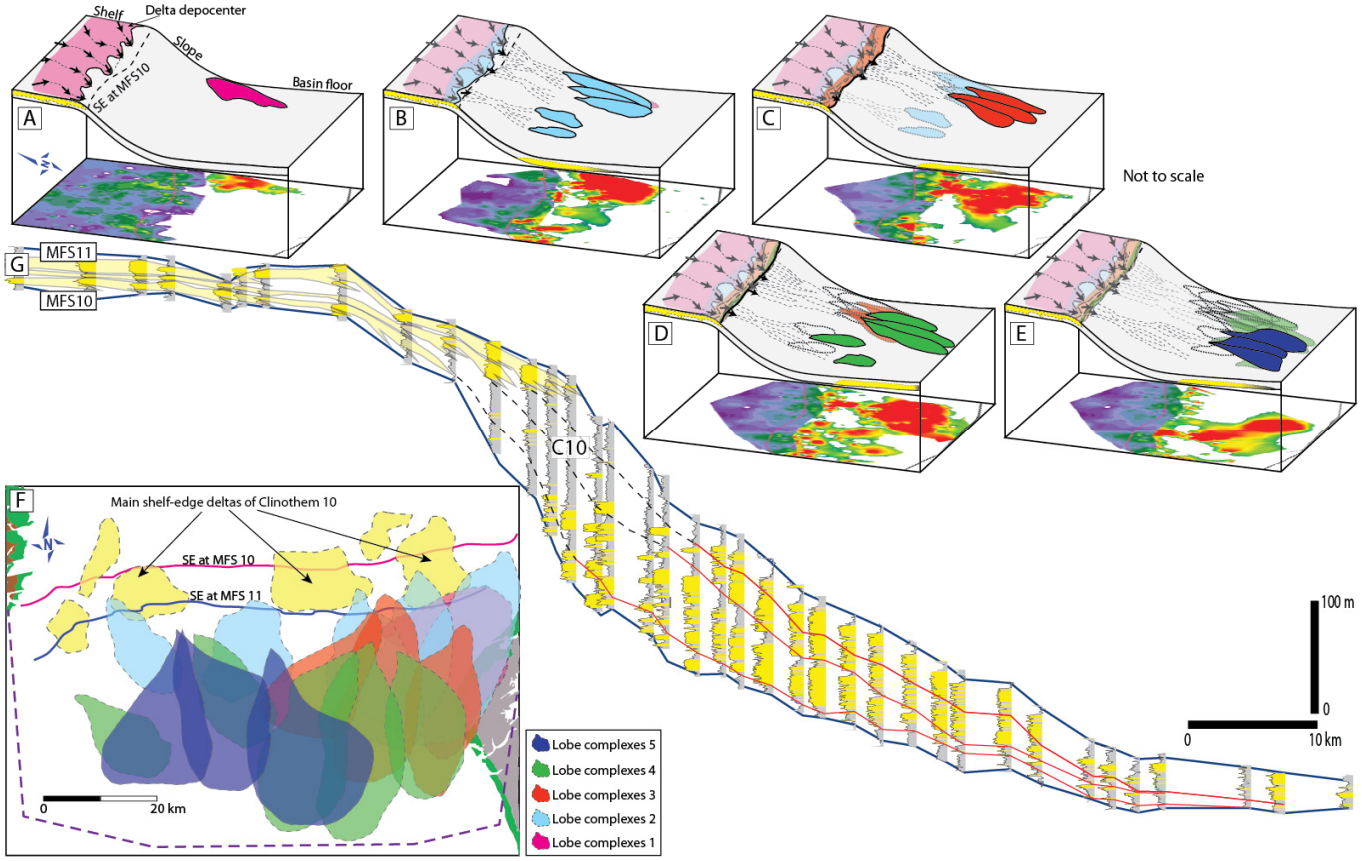

Figure 1.4: Three dimensional block diagrams of Clinothem 10, showing sandstone thickness map (on the bottom of block diagram) and the clinoform depositional environment projected onto the top of the block diagram at time steps from A) older to E) younger. The evolution of deep-water lobe complexes was linked with the distribution of delta depocenters on the shelf (modified from Olariu et al., 2012). F) Overlap of deep-water lobe complexes. The lobe complexes of Clinothem 10 prograde and shift significantly laterally compared to those of Clinothem 9. G) Dip cross-section of Clinothem 10. See also Figure 1.2 for the location of section.

DISCUSSION

Evolution of Submarine Fans in Accommodation-Dominated vs Sediment-Supply Dominated Margins

The general initiation-growth-retreat evolution of submarine fans (e.g., Hadler-Jacobsen et al., 2005) is probably widely applicable. The style of submarine fan growth, however, is likely distinctive, and driven by grain size, type of feeder system (Reading and Richards, 1994), relative sea-level behaviour (Van Wagoner et al., 1987; Posamentier and Vail, 1988), and sediment-supply rate (Carvajal and Steel, 2006, 2009). As noted above, there is growing agreement that the two end member models for margin growth are (1) the conventional accommodation-dominated model (Exxon Model) whereby delivery of sediment to the shelf edge and to the basin floor is driven by sea-level fall and reduced accommodation (Fig. 1.5A) (Van Wagoner et al., 1987; Posamentier and Vail, 1988; Kolla, 1993), and (2) a sediment-supply dominated model whereby sediment is delivered to the shelf edge and to the basin floor primarily by high sediment flux, irrespective of sea-level fall or rise (Fig. 1.5B) (Carvajal et al., 2009).

In the *accommodation-dominated model* above, sediment is supplied to submarine fans from the combination of normal fluvial erosion and delivery across the shelf and local erosion from valleys incised on the shelf, all of which is routed into deep-water during relative sea-level fall, even from modest-size rivers (Fig. 1.5Aa). During sea-level fall the shelf-edge progrades, but can be significantly eroded at times and sediments are likely delivered to deep water via slope channels and eventually, resulting in early-stage progradation of submarine fans. During sea-level rise, the shelf edge deltas and the basin

floor fan would be disconnected, but the deepwater slope would have continued to prograde, but with muddy fans and slumps and eventually a muddy prograding complex as sea level came back above the shelf edge (late lowstand wedge of Posamentier et al., 1991) prior to transgression back across the shelf. During shelf transgression fluvial channels and incised valleys on the shelf become widened and eventually filled (Heller et al., 2001; Strong and Paola, 2008). At this late stage, sediments are trapped mainly on the shelf and submarine fans receive little and/or no coarse grained (sand) sediment (Fig. 1.5Ab).

For the *supply-dominated margin model* (Fig. 1.5B), in contrast, high sediment flux allows deltas to transit the shelf, bypass onto the slope and form submarine fans at any sea-level stand (Covault et al., 2007). Unlike the conventional model, fan building here tends to continue during both fall (Fig. 1.5Ba) and rise (Fig. 1.5Bb) half cycles, but there can be additional influence of this rise and fall despite the high supply. During relative sea-level fall, sediment eroded from the shelf (restricted amount due to high sediment flux) and sediment bypassed through rivers build large submarine fans in deep-water. The progradation of submarine fans which are spatially extensive across shelf edge will be greater than that of localized fans connected with relatively fixed slope channels in accommodation-dominated settings, if sea-level fall rates are the same in both cases. However, what is different for high sediment-supply systems is that the shelf-edge will prograde despite relative sea-level rise (Carvajal and Steel, 2006) and slope channels consistently connect shelf edge deltas with basin floor (Fig. 1.5Bb).

The present data, both the calculation of sediment discharge and clinoform progradation rate (Carvajal and Steel, 2012), from Clinothems 9 and 10 in Washakie Basin show that the system can be classified as high sediment supply compared to other margin systems. It is therefore of some interest to look at the differences between Clinothems 9 and 10 within this high sediment flux setting. In Clinothem 10 we note that marked progradation of the shelf-edge caused a corresponding progradation of the genetically related submarine fan system, even during modest sea-level rise, as shown by the shelf-edge trajectory (Figs. 1.4, 1.5Ba). Further, in cases where the rate of relative sea-level rise became high, the shelf-edge aggraded (rising and prograding trajectory) and also resulted in dominantly aggradational submarine fans as seen in Clinothem 9 (Figs. 1.3, 1.5Bb). Toward the end of the aggradation stage the submarine fans retreated concurrently with the autogenic or allogenic retreat of the shelf-edge (Kim and Muto, 2007; Muto et al., 2007). Clinothems 9 and 10 of Washakie Basin thus demonstrate that the shelf-edge trajectory of a sediment-supply dominated margin can be significantly influenced by sea-level rise, and that this influence affected both shelf-edge trajectory and basin-floor fan behavior (staking pattern). This resulted in a supply-dominated but accommodation-influenced setting whereby an aggrading shelf-edge trajectory with coeval aggrading deep-water fan lobes changed to become a strongly prograding shelf-edge with coevally prograding fan-lobe complexes (Fig. 1.5B). To summarize the conditions for mirroring aggradation-progradation pattern between shelf-edge deltas and deep-water fans in high supply Washakie margin: (1) Clinothem 9 maintained the flux to the shelf-edge even during the relative sea-level rise and aggraded fans by sediments funneled through stable slope channels; (2) Clinothem 10 had high enough sediment supply for spatially extensive progradation across the shelf edge even during the relative sea-level fall concurrent with strong fan progradation.

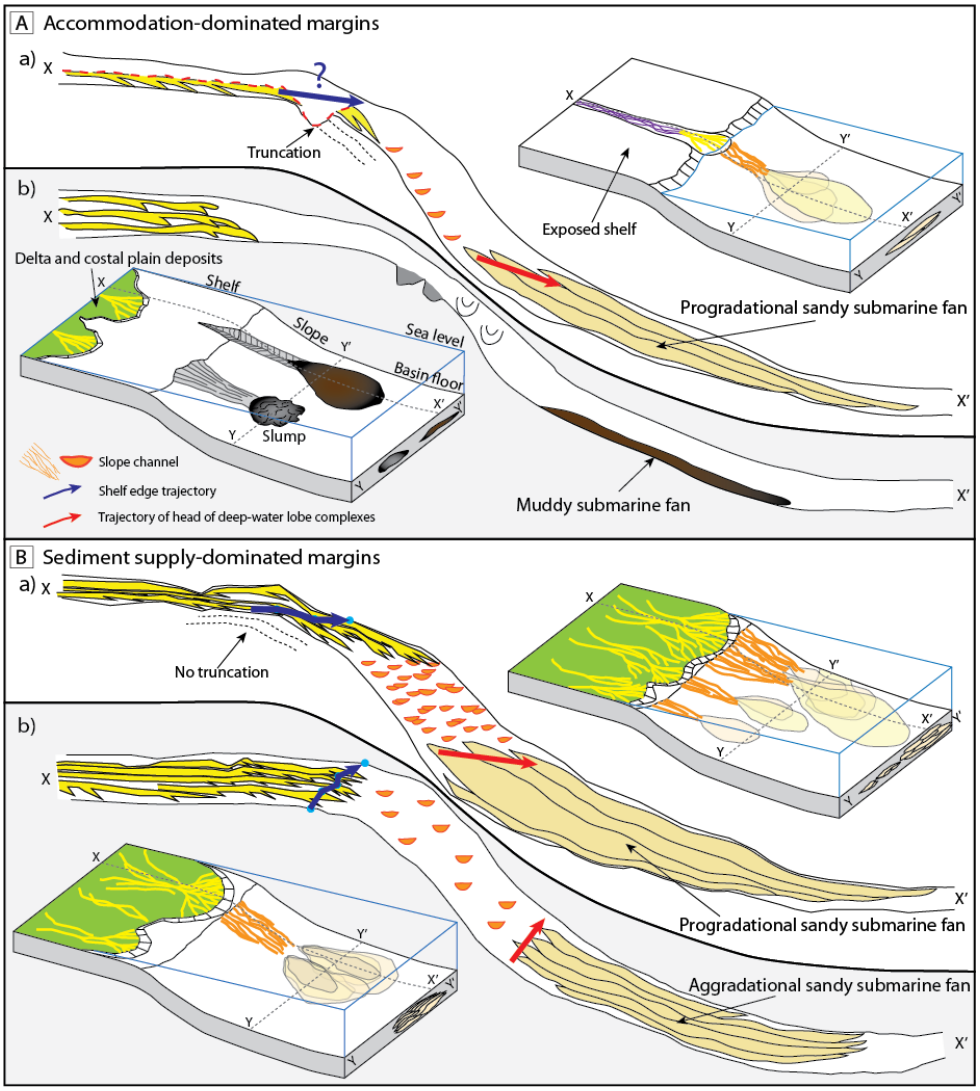

Figure 1.5: Schematic three dimensional block diagram with projected dip (X-X') and strike (Y-Y') cross-sections of clinoforms in A) accommodation-dominated margins. a) sea-level fall; with shelf and shelf-edge incisions with significant sand delivery to deep water. b) sea-level rise; with slumps and muddy failures on slope and basin floor. B) sediment supply-dominated margins. a) sea-level fall; with progradation dominant shelf-edge deltas and submarine fans. b) sea-level rise; with aggradation dominant shelf-edge deltas and submarine fans. Note that in sediment-supply dominated margins, shelf edge deltas are consistently connected with the basin floor by slope channels (more extensive channeling during sea-level fall) at any sea-level stand. In contrast, slope channels in accommodation-dominated margins connect the shelf edge deltas to the basin floor fans only during sea-level fall.

CONCLUSIONS

Deep-water fan-lobe complexes of the high-supply Washakie Basin evolved through stages of initiation, progradation, aggradation, and retreat. These stages of evolution are widely seen in staking of deep-water lobes within fans. However, it is observed that fan-lobe complex behavior (aggradation or progradation) can be linked to coeval shelf-edge trajectory behavior. This linkage was possible because (1) Washakie Basin was supply-dominated across the entire clinoform from top to bottom, despite times of stronger accommodation influence on some clinoforms, and (2) the sediment transport to deep water was quasi-continuous with consistent slope channel connection between shelf edge and basin floor during most of the sea-level cycle despite significant shelf-edge delta reworking by waves and tides. The latter condition contrasts with the discontinuous (lowstand) sediment delivery for low-supply, accommodation-dominated margins.

Chapter 2: Variability of Transitional Flows on Submarine Fan Fringes

ABSTRACT

The vertical and lateral lithofacies variation in the submarine fan-fringes of four clinothem-bottomsets in Washakie Basin, Wyoming, is examined at the scale from bed to submarine fan, using about 96 m of long cores from 4 wells as well as gamma-ray logs of closely spaced 1,585 wells. Submarine-fan lobes, and thereby lobe fringes are identified by (1) upward-coarsening gamma log motif at the scale (3 - 20 m) of prograding lobes, (2) intermediate thickness of structureless sandstones i.e., thinner than on axis and thicker than that of distal part of lobe, and (3) lobate patterns on sandstone thickness maps of clinothem bottomsets and thereafter the relative marginal locations on these fan lobes. Markov chains of vertical transitions of 1,236 lithofacies units from axis, fringe, and distal parts of submarine lobe-complexes and fans in four clinothems show a similar general-trend. The dominant transitions between deformed sandstones and structureless sandstones, up to laminated sandstones and laminated (or structureless) mudstones are observed from bottom to top of most bedsets in any location of a lobe as a consequence of deposition dominantly by high-concentration turbidity currents. In distal fringes, mud-clast muddy sandstones commonly overlie structureless sandstones. The common transition without intervening erosional surface, between structureless sandstones (representing turbidites) and mud-clast rich muddy sandstones (i.e., debrites) indicates that sedimentation on lobe fringes was typically associated with flow-transition from turbidity current to debris flow. In contrast, such transition of flow was not significant on the lateral fringe of fans Transition from other facies to mud-clast muddy sandstones in this position rarely develops. The relatively frequent transition from sandstones to mud-clast-rich sandstones on lateral fringes implies that high-concentration sandy turbidity currents were maintained as the dominant type of

flow along the lateral fringe. The fully transitional debris flows, derived from turbidity currents by entrainment of surrounding muds, during long run-out distances tend to develop mud-clast-rich muddy sandstones in the distal fringe of submarine lobes. Turbidity currents that did not undergo transition resulted in sandy turbidites with minor mud clasts after only short run-out distances. Where turbidity currents experience only partial transition, muddy matrix sandstones deposited with varying degrees of mud-clasts entrainment, depending on run-out distance. The basinward-elongated fans in Washakie Basin, defined by sandstone thickness maps, imply that the run-out distance of flow in north-south direction was longer than that in the west-east direction. Therefore, in spite of the heterogeneity in lobe fringes, the lateral fringes of fans are predicted to be characteristically sandier than distal fringes of submarine fans. Concerning submarine fan hydrocarbon reservoirs, although the main hydrocarbon flow-direction trends along the amalgamated channel-sandstones of the lobe axis, the second preferred flow-direction depends on the connectedness of sandy lateral-fringes and lobe-centers from different lobes, i.e., a direction generally (sub-) perpendicular to the axis of the submarine fan.

INTRODUCTION

The heterogeneity of pore-fluid flow, caused by inhomogeneous spatial distribution and stratigraphic stacking patterns of muddy deposits, has brought challenges on optimizing oil and gas production from deep-water sandstones (e.g., Gulf of Mexico, North Sea). The depositional process and resultant deposits of subaqueous sediment gravity flows have been actively studied from outcrop (e.g., Bouma, 1962; Walker and Mutti, 1973; Mutti, 1977; Piper and Normark, 1983; Mutti and Normark, 1987; Lowe, 1982; Hiscott, 1994; Kneller, 1995; Shanmugam, 1997), laboratory experiments (e.g., Kuenen, 1951;

Middleton, 1966a, 1966b, 1967; Middleton and Hampton, 1973; Kneller, 1995; Shanmugam, 2000), and perspective ideas (e.g., Postma, 1986; Shanmugam, 1996) for many decades. Notwithstanding numerous observation of debrites underlain by turbidites from outcropping ancient deposits (Hiscott and Middleton, 1979; Ricci-Lucchi and Valmori, 1980), subaqueous hybrid sediment gravity-flow deposits came into focus only in the last 15 years (Lowe and Guy, 2000; Haughton et al., 2003; Talling et al., 2004; Amy and Talling, 2006; Haughton et al., 2009; Hodgson, 2009; Baas et al., 2011; Kane and Pontén, 2012; Sumner et al., 2012; Talling et al., 2012; Talling, 2013). Haughton et al. (2003) were among the first studies to observe that a downslope-thickening, muddy clast-rich unit commonly covers a closely associated underlying downslope-thinning sandy bed, strongly suggesting that the sustained mobility of a debris flow with low basal friction on underlying watery sand, enabled such linked-debrites to develop mainly around the fringe of submarine fans. Kane and Pontén (2012) proposed that flows could transition from turbulent to laminar flow in order to explain the couplet of transient turbulent-laminar flows. The lateral variation of hybrid-flow deposits on the fringe around fans, however, still remains understudied. Our knowledge on three-dimensional (3-D) characteristics of hybrid flow deposits in deep-water is particularly immature and should be further investigated. Spatially dense (as close spaced as 500 m) wireline logs of the Washakie Basin make it possible to map and delineate the thickness and extent of submarine fans and their lobes. Detailed vertical stratigraphic patterns (< 1 cm - 2 m thick lithofacies) along the axis and on the fringe of lobe complexes are analyzed here by detailed observation of cores, and by using Markov chain analysis to confirm preferred vertical changes of lithofacies. The objectives here are 1) to show the systematic strike- and dip-directional variation of hybrid-flow deposits within fan lobe fringes and 2) to propose a conceptual

depositional model of subaqueous hybrid sediment gravity-flow on distal and lateral reaches of the fringe zone.

GEOLOGY

The Washakie Basin, one of the Laramide syn-tectonic basins (Fig. 2.1A), was formed adjacent to the Granite Mountains, Rawlins uplift, and Wind River Range during the early Maastrichtian (Steidtmann and Middleton, 1991). The Washakie Basin was filled by Lewis Shale, Fox Hills Sandstone, and Lance Formation in conditions of high subsidence (e.g., Flemings et al., 1986; Shuster and Steidtmann, 1988) and high sediment influx (Carvajal and Steel, 2006, 2009; Olariu et al., 2012) during the Bearpaw regression phase of the Western Interior seaway (Obradovich and Cobban, 1975; Merewether and Cobban, 1981). The Lewis Shale is represented by marine deep-water mudstone and sandstone turbidites up to 762 meters thick (Gill and Cobban, 1973). The nearshore Fox Hills Sandstone (up to 214 meters thick in southern Wyoming) and the paralic to alluvial Lance Formation (> 200 meters thick) overlie and inter-finger with the upper part of Lewis Shale (Gill et al., 1970; Winn et al., 1987) (Fig. 2.1B). The Washakie Basin fill, deposited during 1.8 My (ammonite zones calibrated to absolute ash dates), are sub-divided into 16 clinothems (C1 to C16), containing the early Maastrichtian fluvial-shelf-deep water deposits, by higher order maximum flooding surfaces (approximately every 100 Ky) (Fig. 2.2). The paleo-water depth of clinothem toes is conservatively estimated as approximately 430 meters from the undecompacted height of the1-2 degree dipping basin margin slope. Paleo-water depth would be deeper in the southeast of the basin based on the eastward syn-depositional tilt and therefore greater height of slopes toward the eastern part of the basin (Carvajal and Steel, 2009). During Maastrichtian, the entire sedimentary prism of shallow

to deepwater basin fill prograded generally from north to south at a very high rate of >48 km/My, while a west-east oriented shelf edge and shelf margin developed, and aggraded at a rate of 267 m/My (Carvajal and Steel, 2009). The prograding pattern of the basin fill is divided into dominantly aggradation and then dominantly progradational stages. The aggradation dominant period (from C1 to C9), inferred from the thick topsets of clinothems and slower rate of shelf-edge growth, resulted from a combination of high accommodation and high sediment flux. The high accommodation rate would have been caused by high subsidence rates of the basin floor related to active tectonic uplifts around the basin. In contrast, as the rate of accommodation later decreased due to slowed uplift, causing relatively thin but aerially extensive shelf topsets, as identified in the progradation dominant clinothems (C10 to C16) (Carvajal and Steel, 2009).

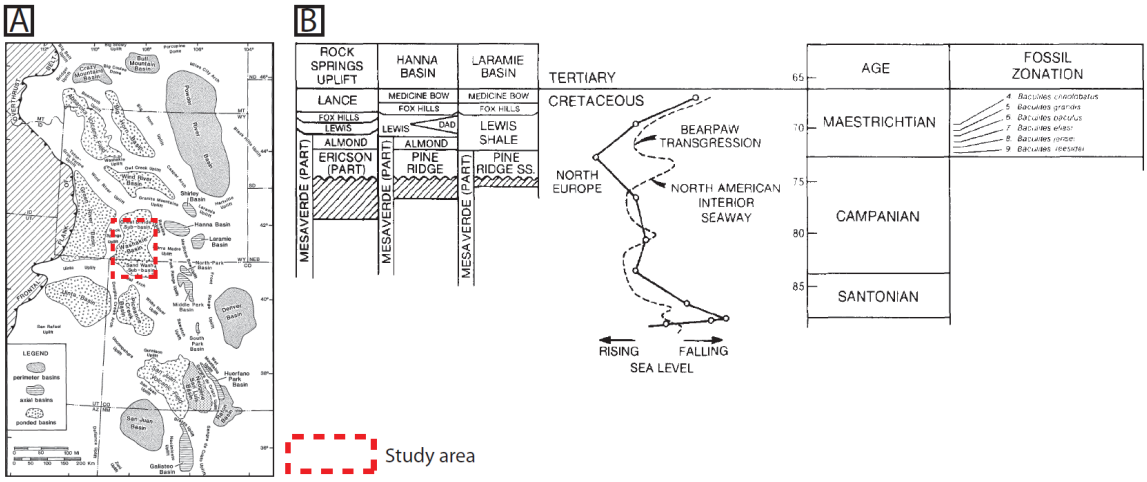

Figure 2.1: Simplified map showing A) location of Washakie Basin among Laramide basins (from Dickinson et al., 1988) and B) correlation of Upper Cretaceous formations of south-central Wyoming (Gill et al., 1970).

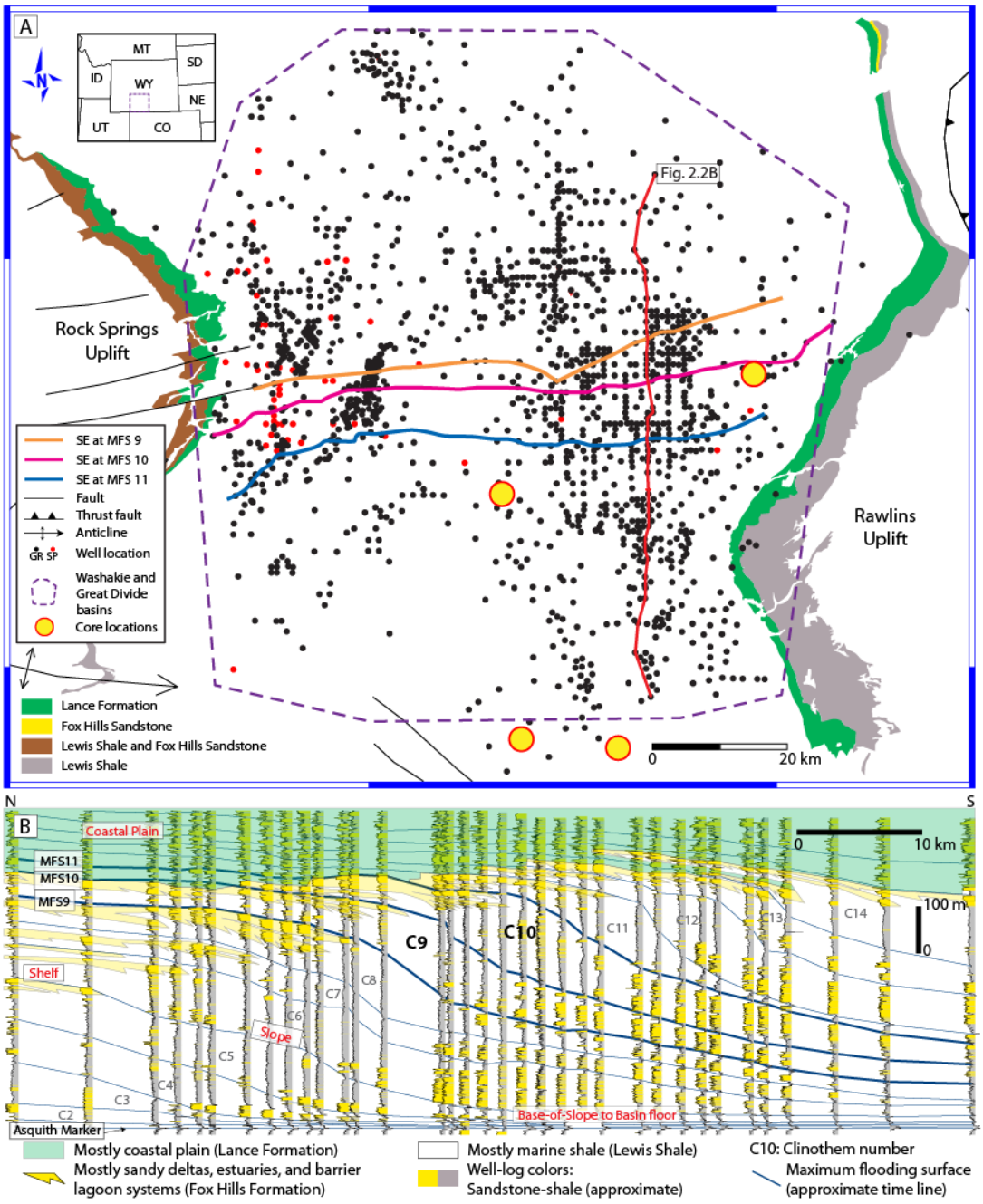

Figure 2.2: Location of Washakie Basin in Wyoming showing A) well locations and outcrop exposures and B) a dip-oriented cross-section through the linked fluvial (Lance Fm.) to shelf (Fox Hills Fm.) to deep-marine (Lewis Shale) depositional system, which is crossed by 16 clinothems (modified from Carvajal and Steel, 2009 and Olariu et al., 2012). GR: gamma ray; MFS: maximum flooding surface; SE: shelf edge; SP: spontaneous potential; ID: Idaho; MT: Montana; WY: Wyoming; SD: South Dakota; NE: Nebraska; CO: Colorado; UT: Utah.

DATA AND METHOD

Submarine fans, deposited over an area of 8,000 km^2 in the southern part of Washakie Basin, were mapped within the distal reaches of Clinothems 4, 5, 9, 11, and 12 using 1,585 wells. Each clinothem was delineated by correlation between maximum flooding surfaces in shallow-water (shelfal) deposits and abandonment muddy surfaces in the coeval deepwater deposits. These key clinothem-bounding surfaces are regionally traceable high gamma peaks on the well logs, calibrated by some unique conductivity kicks on the same logs (Carvajal and Steel, 2006, 2009). The deposits within each clinothem had an approximate duration of 100 Ky (Carvajal and Steel, 2009) within a succession of 1.8 My. Submarine fans of Clinothem 9 were sub-divided into lobe complexes based on gamma-log motif. Channels associated with lobe complexes were identified from capping blocky units of low gamma-ray signal with a slight upward-fining pattern. Levees are recognized from repetition of thin beds interpreted from high gamma-ray serrated patterns. Unconfined lobe sheets were interpreted from the repetition of units showing an upward-coarsening gamma-ray motif, and muddy beds from high gamma-ray signals within lobe complexes (Table 2.1). Submarine-fan distribution within Clinothems 4, 5, 9, 11, and 12 were defined by sandstone thickness maps of each clinothem with 90 API gamma cut-off (Fig. 2.3). About 96 m of cores from 4 wells (API No. 4903721476, 4903721741, 4903721922, and 4900722141) were observed and measured in detail (Table 2.2). Well 4900722141 was logged only by core photographs. The cores were collected from parts or complete intervals of Clinothems 4, 5, 9, 11, and 12. The depositional setting (e.g., axis, fringe, and distal part of submarine lobe complexes) of each interval was inferred from gamma-ray log patterns, core lithofacies, and locations of wells in submarine fans already defined by sandstone maps. Preferential trends of the vertical lithofacies transitions,

Markov chain analysis, were performed with transition proportion matrices, established from 1,236 lithofacies units (Tables 2.3-2.8).

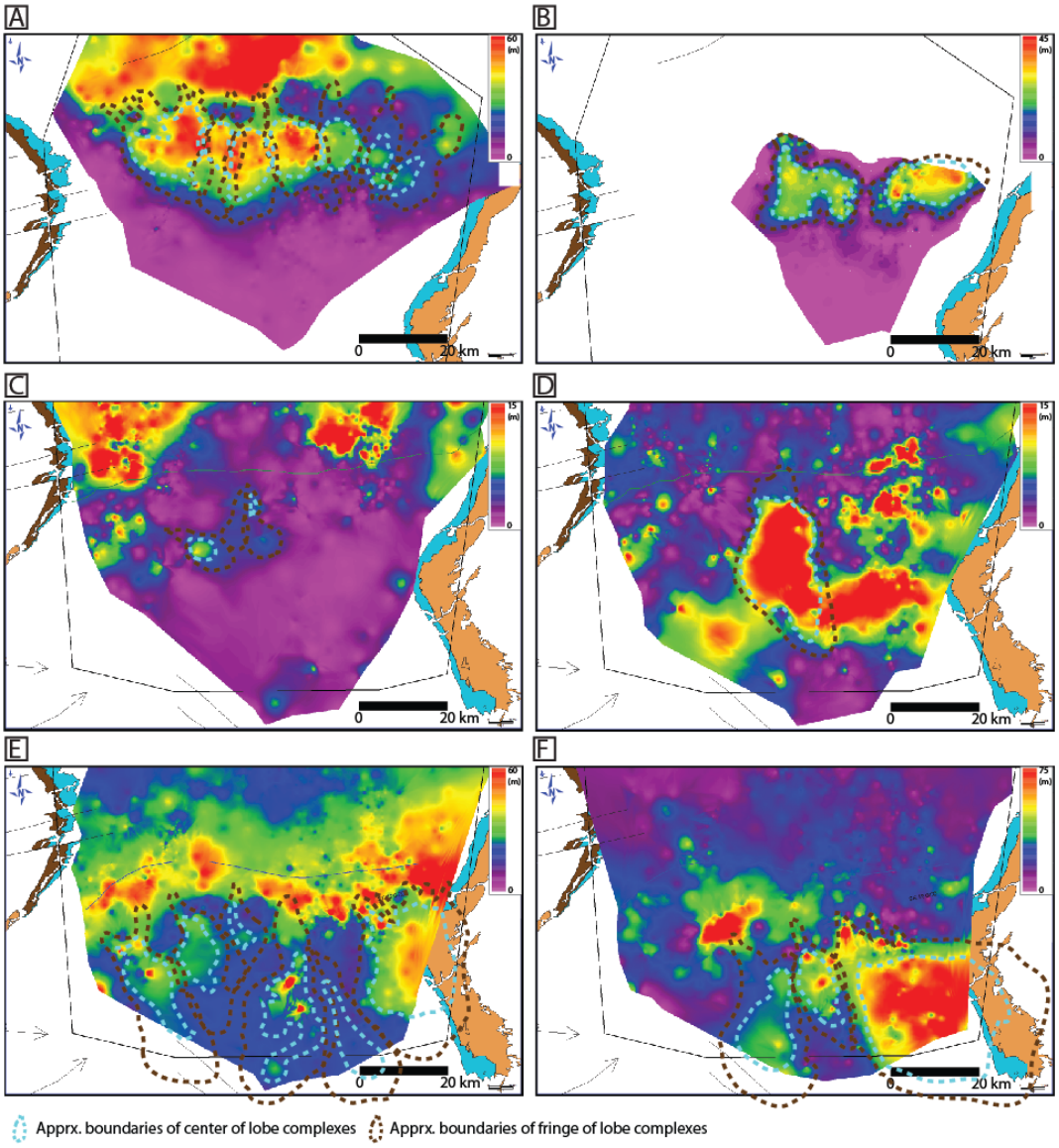

Figure 2.3: Sandstone thickness maps of A) Clinothem 4, B) Clinothem 5, C), D) Intervals 9-1 and 9-2 of Clinothem 9, E) Clinothem 11, and F) Clinothem 12 of Washakie Basin. The thickness of sandstones is estimated with 10-90 GR cutoff. Approximate boundaries of center and fringes of submarine lobe-complexes and fans are defined in lobate shaped sandstone bodies. The different scales are applied for thickness of each map in order to display clear lobate shapes of lobes in each clinothem and interval.

Table 2.1: Classification of gamma (GR) well log motifs (scale: 6-12 m between red lines; 90 GAPI cutoff for sandstones).

Image	Mark	Motif	Sediments	Dep. processes	Dep. setting	Core photo
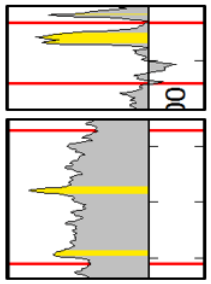		Relatively sharp based thin low GR within thick high GR interval	Erosional surface based sandstones overlain and underlain by mudstones	Deposition by turbidity currents erosive in base of current	Slope channel and overbank deposits (e.g. crevasse splay sandstones interbedding with mudstones)	
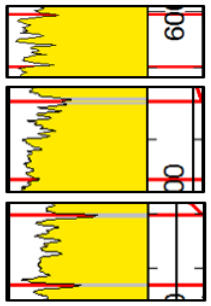		Blocky low GR in lower section and upward increasing GR at upper most tops	Amalgamated sandstones in lower section, and slight upward fining and thinning bed sets in the upper section	Deposition by high concentration turbidity currents, upper most normal grading by waning currents, and/or fining upward channel deposits	Amalgamated channels in proximal and center of fan axis beneath lobe-channels	
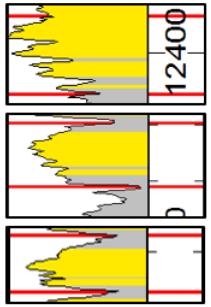		Upward decreasing and thickening GR, and upward increasing GR at upper most top	Upward coarsening and thickening bed sets, and upward fining and thinning bed sets at the most upper section	Sedimentation by waxing turbidity currents followed by waning current at upper most top	Prograding sheet-like lobe beneath lobe-channels in lobe fringes	

Table 2.1: (Continued)

Image	Mark	Motif	Sediments	Dep. processes	Dep. setting	Core photo
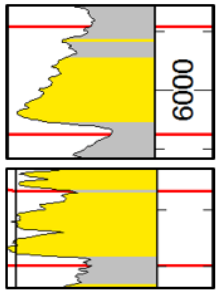	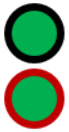	Upward increasing GR	Upward fining and thinning bed sets, potential transitional flow deposits (e.g. debrites with/without underlying sandstone)	Sedimentation by low-concentration turbidity currents and potentially transitional flow by entraining surrounding muds	Upward fining sheet-like lobe in distal lobe and transitional flow deposits in distal fringe of lobes	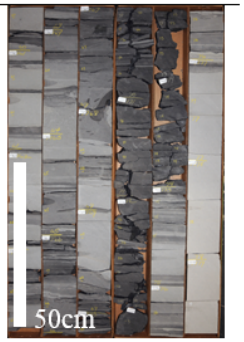
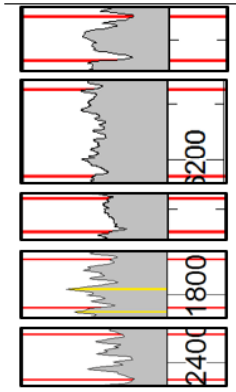		Blocky moderate to high GR with gentle upward decreasing or increasing GR	Structureless and laminated mudstones with thin siltstones and sandstones	Alternating deposition by hemipelagic fall out and dilute turbidity currents	Muddy slope, inter-lobe anywhere on top of fan-lobe if preserved, but dominant in distal lobes	
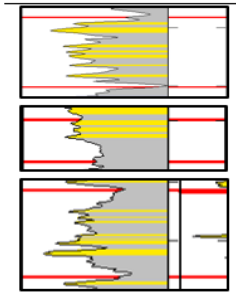		Serrated high and low GR peaks with gentle upward decreasing-increasing GR	Interbedded thin sandstones (planar-/ripple-laminated) and mudstones, but predominant mudstones	Sedimentation by dilute turbidity currents potentially followed by transitional flow	Channel-levee close lobe axis if preserved, dominant in lobe fringes	

Table 2.2: List of cores described in this study (Plates 2-5).

Well name	API No.	Depths (ft)		Clinothem
		Top	Bottom	
FILLMORE 2-19	4900722141	7,741	7,857	C4 and C5
1 USA-U	4903721476	10,730	10,822	C9
14-2 MCPHERSON SPRINGS	4903721741	10,425	10,505	C11 and C12
10 TRITON	4903721922	13,278	13,335	C12

Cores were provided by USGS Core Research Center. FILLMORE 2-19 was logged with core photos from USGS Core Research Center.

Table 2.3: Upward transition proportion matrix of lithofacies of Clinothem 9 from API No. 4903721476. Probability in brackets.

	SS1	SS2	LS1	LS2	LS3	MS1	MS2	HS	DS1	DS2	LM	DM1	DM2	SM
SS1		5 (14.3)		3 (8.6)	3 (8.6)	5 (14.3)	3 (8.6)	1 (2.9)	2 (5.7)	5 (14.3)	5 (14.3)			3 (8.6)
SS2	3 (42.9)			1 (14.3)					1 (14.3)		1 (14.3)			1 (14.3)
LS1				1 (25.0)				1 (25.0)						2 (50.0)
LS2	1 (14.3)		1 (14.3)					1 (14.3)			2 (28.6)			2 (28.6)
LS3	6 (85.7)					1 (14.3)								
MS1	1 (12.5)	1 (12.5)	1 (12.5)	1 (12.5)										4 (50.0)
MS2	1 (20.0)				1 (20.0)						1 (20.0)			2 (40.0)
HS					1 (12.5)					1 (12.5)	2 (25.0)			4 (50.0)
DS1	4 (80.0)				1 (20.0)									
DS2	5 (83.3)		1 (16.7)											
LM	6 (40.0)	1 (6.7)	1 (6.7)	1 (6.7)				3 (20.0)	1 (6.7)					2 (13.3)
DM1														
DM2														
SM	9 (42.9)				1 (4.8)	2 (9.5)	2 (9.5)	2 (9.5)	1 (4.8)		4 (19.0)			

Table 2.4: Upward transition proportion matrix of lithofacies of Clinothem 4 from API No. 4900722141. Probability in brackets.

	SS1	SS2	LS1	LS2	LS3	MS1	MS2	HS	DS1	DS2	LM	DM1	DM2	SM
SS1		7 (10.3)	14 (20.6)	4 (5.9)	2 (2.9)	14 (20.6)	8 (11.8)	1 (1.5)	1 (1.5)	2 (2.9)	6 (8.8)		1 (1.5)	8 (11.8)
SS2			6 (13.6)	1 (2.3)	1 (2.3)		12 (27.3)		2 (4.5)		5 (11.4)	1 (2.3)	1 (2.3)	15 (34.1)
LS1		4 (12.5)		4 (12.5)			3 (9.4)				3 (9.4)			18 (56.3)
LS2	3 (27.3)	2 (18.2)				1 (9.1)					1 (9.1)		1 (9.1)	3 (27.3)
LS3	1 (14.3)		1 (14.3)				2 (28.6)				1 (14.3)			2 (28.6)
MS1	1 (5.3)	4 (21.1)	2 (10.5)	1 (5.3)	1 (5.3)					2 (10.5)	5 (26.3)		1 (5.3)	1 (5.3)
MS2	2 (4.3)	9 (19.6)	1 (2.2)					2 (4.3)	3 (6.5)		6 (13.0)	3 (6.5)	9 (19.6)	11 (23.9)
HS	1 (16.7)								1 (16.7)		1 (16.7)			3 (50.0)
DS1	17 (54.8)	4 (12.9)	1 (3.2)		2 (6.5)	1 (3.2)	1 (3.2)			5 (16.1)				
DS2	7 (53.8)					3 (23.1)	1 (7.7)						1 (7.7)	1 (7.7)
LM	8 (22.9)	2 (5.7)	1 (2.9)	1 (2.9)			10 (28.6)	1 (2.9)	3 (8.6)					9 (25.7)
DM1			1 (20.0)				1 (20.0)				1 (20.0)			2 (40.0)
DM2	2 (14.3)		1 (7.1)				1 (7.1)		1 (7.1)		2 (14.3)			7 (50.0)
SM	26 (32.5)	12 (15.0)	4 (5.0)				7 (8.8)	2 (2.5)	20 (25.0)	4 (5.0)	4 (5.0)	1 (1.3)		

Table 2.5: Upward transition proportion matrix of lithofacies of Clinothem 5 from API No. 4900722141. Probability in brackets.

	SS1	SS2	LS1	LS2	LS3	MS1	MS2	HS	DS1	DS2	LM	DM1	DM2	SM
SS1		6 (11.8)	10 (19.6)	4 (7.8)	5 (9.8)	6 (11.8)	3 (5.9)	3 (5.9)	1 (2.0)	7 (13.7)	3 (5.9)			3 (5.9)
SS2	1 (5.6)		1 (5.6)				2 (11.1)		1 (5.6)		8 (44.4)		2 (11.1)	3 (16.7)
LS1							1 (8.3)				6 (50.0)			5 (41.7)
LS2		1 (20.0)				1 (20.0)		1 (20.0)			1 (20.0)			1 (20.0)
LS3	7 (70.0)	1 (10.0)											2 (20.0)	
MS1			1 (10.0)	1 (10.0)			1 (10.0)				7 (70.0)			
MS2	3 (15.8)	1 (5.3)			1 (5.3)			1 (5.3)	1 (5.3)		6 (31.6)		1 (5.3)	5 (26.3)
HS						1 (14.3)	1 (14.3)				1 (14.3)			4 (57.1)
DS1	18 (78.3)	1 (4.3)				1 (4.3)	2 (8.7)				1 (4.3)			
DS2	5 (71.4)						1 (14.3)		1 (14.3)					
LM	10 (27.8)	5 (13.9)			1 (2.8)	1 (2.8)	2 (5.6)	2 (5.6)	11 (30.6)					4 (11.1)
DM1							1 (100)							
DM2											1 (20.0)			4 (80.0)
SM	8 (26.7)	3 (10.0)			3 (10.0)		5 (16.7)		8 (26.7)		2 (6.7)	1 (3.3)		

Table 2.6: Upward transition proportion matrix of lithofacies of Clinothem 11 from API No. 4903721741. Probability in brackets.

	SS1	SS2	LS1	LS2	LS3	MS1	MS2	HS	DS1	DS2	LM	DM1	DM2	SM
SS1		7 (22.6)	2 (6.5)	1 (3.2)	1 (3.2)	6 (19.4)	4 (12.9)	1 (3.2)		1 (3.2)	1 (3.2)	1 (3.2)		6 (19.4)
SS2														7 (100)
LS1				1 (33.3)							1 (33.3)			1 (33.3)
LS2														2 (100)
LS3	1 (100)													
MS1	2 (25.0)		1 (12.5)							2 (25.0)				3 (37.5)
MS2	1 (20.0)													4 (80.0)
HS														1 (100)
DS1	3 (100)													
DS2	3 (100)													
LM	1 (25.0)					1 (25.0)			2 (50.0)					
DM1											1 (100)			
DM2														
SM	20 (83.3)					1 (4.2)	1 (4.2)		1 (4.2)		1 (4.2)			

Table 2.7: Upward transition proportion matrix of lithofacies of Clinothem 12 from API No. 4903721922. Probability in brackets.

	SS1	SS2	LS1	LS2	LS3	MS1	MS2	HS	DS1	DS2	LM	DM1	DM2	SM
SS1		2 (5.9)	2 (5.9)	8 (23.5)	3 (8.8)	3 (8.8)	3 (8.8)	1 (2.9)		1 (2.9)	3 (8.8)			5 (14.7)
SS2	1 (5.9)		1 (5.9)	1 (5.9)	2 (11.8)		3 (17.6)	1 (5.9)	1 (5.9)		2 (11.8)	1 (5.9)		4 (23.5)
LS1		2 (50.0)									2 (50.0)			
LS2	1 (8.3)	1 (8.3)					1 (8.3)	1 (8.3)			1 (8.3)			7 (58.3)
LS3	2 (20.0)	1 (10.0)				1 (10.0)	1 (10.0)				2 (20.0)			3 (30.0)
MS1				1 (25.0)				1 (25.0)			1 (25.0)			1 (25.0)
MS2	2 (12.5)							2 (12.5)	1 (6.3)		2 (12.5)		2 (12.5)	7 (43.8)
HS	3 (33.3)	1 (11.1)					1 (11.1)				1 (11.1)			3 (33.3)
DS1	8 (57.1)				3 (21.4)		1 (7.1)							2 (14.3)
DS2							1 (100)							
LM	4 (20.0)			1 (5.0)			2 (10.0)	2 (10.0)	4 (20.0)			1 (5.0)		6 (30.0)
DM1											1 (50.0)			1 (50.0)
DM2	1 (50.0)													1 (50.0)
SM	11 (27.5)	10 (25.0)		1 (2.5)	2 (5.0)		3 (7.5)	1 (2.5)	8 (20.0)		4 (10.0)			

Table 2.8: Upward transition proportion matrix of lithofacies of Clinothem 12 from API No. 4903721741. Probability in brackets.

	SS1	SS2	LS1	LS2	LS3	MS1	MS2	HS	DS1	DS2	LM	DM1	DM2	SM
SS1		3 (6.7)	1 (2.2)	5 (11.1)	2 (4.4)		1 (2.2)				13 (28.9)			20 (44.4)
SS2	3 (30.0)		1 (10.0)											6 (60.0)
LS1		2 (33.3)									1 (16.7)			3 (50.0)
LS2			1 (5.9)								7 (41.2)			9 (52.9)
LS3	1 (50.0)						1 (50.0)							0.0
MS1														
MS2	1 (12.5)	1 (12.5)	1 (12.5)					1 (12.5)			1 (12.5)			3 (37.5)
HS											3 (60.0)			2 (40.0)
DS1	2 (100)													
DS2														
LM	10 (32.3)	1 (3.2)		7 (22.6)			4 (12.9)	1 (3.2)	1 (3.2)					5 (16.1)
DM1														
DM2														
SM	28 (53.8)	3 (5.8)	2 (3.8)	5 (9.6)			2 (3.8)	3 (5.8)	1 (1.9)		4 (7.7)			

RESULTS

Lithofacies

Lithofacies in the study area were classified by grain sizes and sedimentary structures in core samples (Table 2.9, Fig. 2.4, Plate 1).

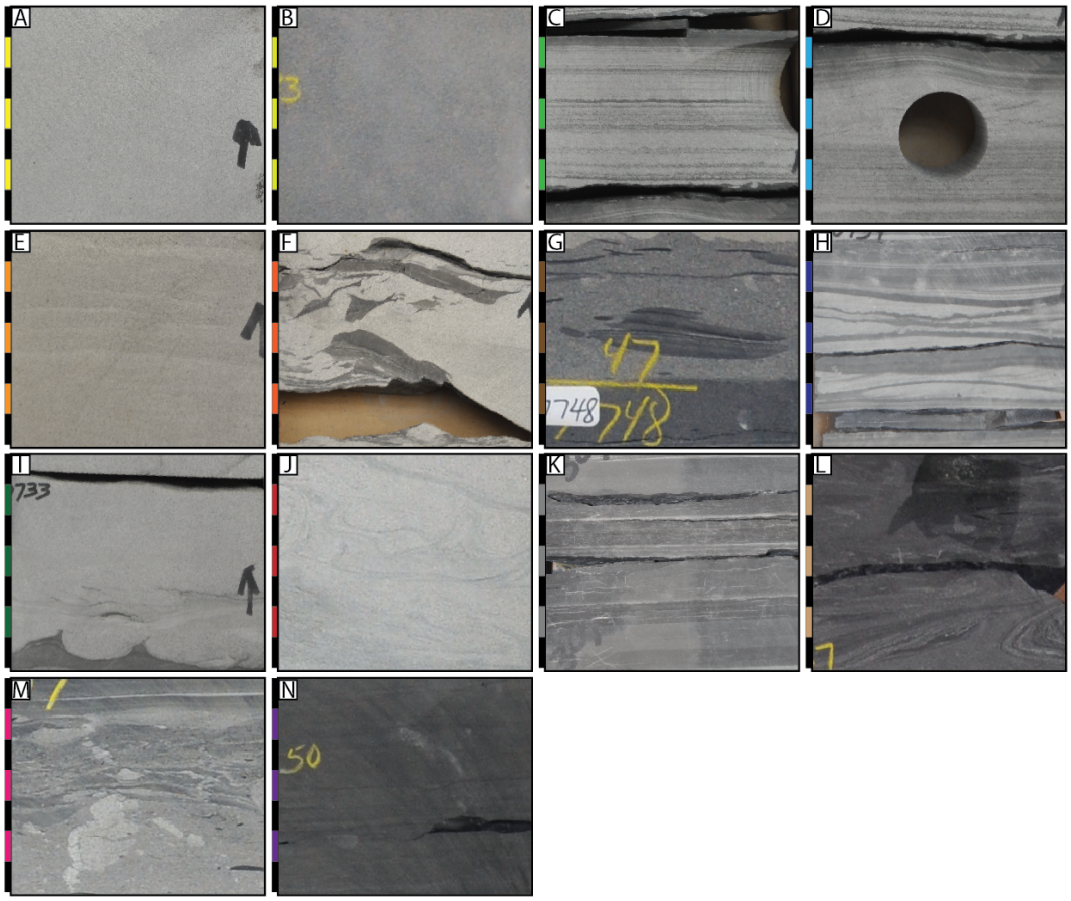

Figure 2.4: Representative core photographs of lithofacies in deep-water lobes of study areas, described and interpreted in Table 2.1 (Refer to Plates 2, 3, 4, and 5 for whole core photos). Structureless sandstone (SS) with A) sandy matrix (SS1) and B) muddy matrix (SS2). Laminated sandstone (LS) with C) planar laminae (LS1), D) ripple-laminae (LS2), and E) faint laminae (LS3). Mud-clast sandstone (MS) with F) sandy matrix (MS1) and G) muddy matrix (MS2). H) Heterolithic sandstone (HS). Deformed sandstone (DS) with I) loading structure (DS1) and J) contorted structure (DS2). K) Laminated mudstone (LM). Deformed mudstone (DM) with L) soft deformation (DM1) and M) injections (DM2). N) Structureless mudstone (SM). Scales in photos are in units of 1 cm. Colors of scale except black stand for each lithofacies.

Structureless sandstone (SS)

Description

Moderate to well-sorted siltstone and very fine to fine grained sandstones without sedimentary structures are identified in ranges of less than 1 cm to more than 2 m thick. These sandstones have sandy (SS1) or muddy (SS2) matrixes (Fig. 2.4A, B). This lithofacies is generally deposited above mudstones and/or deformed sandstone (DS) and overlain by laminated sandstones (LS) or mudstones, discussed below (Plate 2). Small mud-clasts or carbonaceous flakes (< 1mm diameter) are sometimes embedded in the sandstones sub-parallel to its bottom or dispersed without any preferential orientations throughout bed.

Interpretation

By the definition of turbidity current, sediments in turbidity currents should be supported by turbulence of flow (Sanders, 1965), and the resultant deposits of turbidity currents should be sediments settled from the suspended load. During sediment fall-out from suspension, segregation of sediment grains by sizes will result in a normally graded bed. Since many turbidite beds documented from previous studies are not normally graded, Shanmugam (1996) proposed another depositional mechanism of structureless sandstones as *en masse* freezing of sandy debris flow. Even though mechanism of sandy debris flow are not clearly understood yet, laboratory experiments show that as little as 0.7-5%wt clay (bentonite) in a sand-water mixture flow in a flume can form coherent debris flows (Marr et al., 2001). Structureless sandstones in the study area generally contain very small mud-clasts and/or carbonaceous flakes throughout bed with very low weight percentage in eye observation. This might be potential support for the notion that structureless sandstones with sandy or muddy matrixes were deposited from sandy and muddy debris flows respectively in the study area. In contrast, high-sediment concentration (density) turbidity

currents (e.g., Kuenen, 1950; Postma, 1986) is more widely accepted as a type of subaqueous sediment gravity-flow for the deposition of structureless sandstones in deep-water. A variety of this type of flow, hyperpycnal flow, making use of high sediment concentration already in a flooding river (with limited or no backwater zone) that debouches directly at the outer shelf and onto the deepwater slope, has been also used to interpret thick structureless beds (Plink-Björklund and Steel, 2004; Petter and Steel, 2006). In the present study area, structureless sandstone is mostly overlain by a normally graded thin portion of the bed and/or laminated sandstones, indicating that flows having both laminar and turbulent characteristics passed a location during short period. This could be explained by high-density turbidity currents which were laminar and turbulent in lower and upper part of flow respectively during high sediment fallout near the bed (Kuenen, 1950). Suppressed turbulence during high suspended-sediments settling in the lower part of high density turbidity currents would not form tractional structures, but would allow progressive aggradation of sand near the bed (Kneller and Branney, 1995), forming structureless sandstone beds even meters thick. If sediments fallout rates cannot be kept high, tractional sedimentary structures would be formed in the upper levels of structureless sandstones and it would be preserved unless eroded out by the following currents. Sandy matrix structureless sandstones could thus be deposited in a high energy setting such as the proximal part of fan lobes and/or lobe axis in which submarine lobe-channels become amalgamated. Muddy matrix structureless sandstones could be formed in any part of the lobe if the source of sediments was originally muddy. However, if the sediment source of turbidity currents was sandy, the lobe fringes would be the preferred sites for muddy matrix structureless sandstones to entrain mud as turbidity currents flow downstream.

Laminated sandstone (LS)

Description

Three types of laminated sandstone are observed in core. <1 - 35 cm thick, planar- and ripple-laminated (LS1 and LS2) siltstone and very fine to fine sandstone, that are usually capped by laminated or structureless mudstone and are underlain by structureless sandstone (Fig. 2.4C, D, Plate 2). Undulating light colored and light-grey colored very fine sandstone pairs form faintly laminated sandstone (LS3) in the thickness of 1-33 cm. Faint laminated sandstones usually underlie and/or are embedded within structureless sandstone (Fig. 2.4E, Plate 2).

Interpretation

Tractional sedimentary structures, planar to sub-planar laminae and rippled cross-laminae, are likely to have been formed by low-sediment concentrated turbidity currents (Talling et al., 2012) and/or by waning high density turbidity currents. Planar and ripple-cross laminated sandstones can be deposited in many settings, but they are more likely in lobe fringes and on the distal reaches of a lobe where channels rework deposits less than along the lobe axis. Faint laminated sandstones beneath structureless sandstones would be developed predominantly in proximal lobe areas or along lobe axes where turbulence could suppress high-density turbidity currents near the bed as traction carpets (Lowe, 1982; Hiscott, 1994). Weak grain dispersion stress among fine grains in currents hinders the forming of significant inverse grading in traction carpets (Sohn, 1997).

Mud-clast sandstone (MS)

Description

Mud-clasts, distributed subparallel to bedding and/or randomly in sandstone beds, are supported by sandy (MS1) and muddy (MS2) matrixes. In the study area, the shape of clasts are generally irregular or flat rather than sub-rounded. Mud clasts are generally grey

to dark grey color, and rarely with brownish color. The thickness of mud-clast rich sandstones ranges from <1 cm to about 120 cm. Structureless sandstones are sometimes overlain by mud-clast rich sandstones, but mud-clast rich sandstones also occur embedded in structureless sandstones (Fig. 2.4F, G, Plates 2, 3).

Interpretation

Mud-rich sandstones in a sandy matrix are likely to have been delivered by high-density turbidity currents. Irregular shaped mud clasts indicate weak abrasion of clasts with relatively short transportation from the original site (Smith, 1972). Mud clasts would have been entrained from an area closely upstream from the core locations rather than directly from the shelf. The random distribution of irregular clasts throughout this division is also showing that there was rapid deposition without significant segregation of grains and clasts in the flow (Plate 2). Sandy matrix, mud-clast rich sandstones may form dominantly in proximal lobe and lobe fringe areas. Mud clasts in sandstones with muddy matrix have a preferential orientation sub-parallel to the bottom of the bed, with an exception of deformed mud-clast and its surroundings (Plate 3). Mud clasts in sandstones with a muddy matrix are carried by high density turbidity currents but with less settling velocity. The preferential orientation of mud clasts occurs when the settling rate of sediments is low compared to those in sandstones with sandy matrix. As the mud content of a flow rises its capacity to carry clasts is increased, because of added cohesion. Therefore, the size and number of mud clasts in a flow with muddy matrix are expected to be larger and higher than those in a sandy matrix flow. If mud-clast-rich, muddy-matrix sandstone overlies a structureless sandstone containing water-escape structures such as dishes and pipes, discussed below, the muddy-matrix flow can be regarded as a linked-debrite which developed from transitional (hybrid) flow. Linked-debrites normally occur on lobe fringes (Haughton et al., 2003, 2009), and muddy high-density turbidity currents will deliver mud clasts down to

the distal lobe. If a mud-clast-rich muddy sandstone overlies mudstones or other facies, this muddy flow is likely to have transited from turbidity currents that entrainment fine mud and mud-clasts from the surroundings as it flowed downstream (Kane and Pontén, 2012).

Heterolithic sandstone (HS)

Description

Intervals of interbedded sandstones with dark grey mudstone are observed in <1 - 11 cm thick units. The interbeds often show small low angle discordances. Interbedded sandstones are frequently ripple or sub-planar laminated. The top and bottom of each interbedded sandstone with mudstone are clean and uneven (Fig. 2.4H, Plate 2).

Interpretation

The ripple and sub-parallel laminated interbedded sandstones result from low-concentration turbidity currents. Tractional currents caused the uneven top surface of underlying mudstones. Dilute turbidity currents that continuously form ripple-laminated sandstones which migrate down flow on partially consolidated muds tend to cause that surface to be loaded (load-casts) and incomplete rippled sandstone can become sunken into the underlying muddy substrate (Dzulynski and Kotlarczyk, 1962). Heterolithic sandstone facies can occur anywhere on the lobe if it is preserved, but it will be predominantly developed in a relatively low energy setting like the distal lobe area.

Deformed sandstone (DS)

Description

Two main sandstone deformation types are recognized in the study area. Loading and dewatering structures (DS1) such as flames and dishes occur and tend to be overlain by structureless sandstones. Sandstones with contorted laminae (DS2) also occur, and are

also overlain by and/or embedded in structureless sandstone intervals (Fig. 2.4I, J, Plates 2, 3). The thickness of this facies is generally less than 15 cm.

Interpretation

Flame and dish structures are formed as syn- or post-depositional soft deformation features caused by over-pressured pore-water (Sanders, 1965) during rapid differential deposition of high-density turbidity currents over weakly or un-consolidated substrates. Contorted laminae in sandstones can also be developed from fluidization of sediment due to rapid loading of sediments (Moslow and Davies, 1997) or by creeping and slumping high-density turbiditic flows on over-steepened surfaces, accompanying the soft-sediment deformation. Both types of deformation occur in high energy settings such as proximal lobe and lobe center.

Laminated mudstone (LM)

Description

Dark grey to black mudstones (occurring up to 219 cm thick) with sub-planar light-color laminae of silt and very fine to fine grained sandstones overlie and underlie all other lithofacies discussed above, but are mainly overlain by structureless mudstones, deformed or structureless sandstones (Fig. 2.4K, Plate 4). Tractional sedimentary structures are not present in the very thin sandstone beds (or laminae).

Interpretation

Iteration of suspended fine sediment fallout and low-density turbidity currents deposition forms laminated mudstone. Traction features in sandstone laminae or very thin beds are suppressed by the high mud content of the currents (Allen and Leeder, 1980). Meso- to micro-banded couplets of light colored, very fine sandstone and dark mudstones

could be also deposited by slurry flows (Lowe and Guy, 2000). Laminated mudstones can be deposited anywhere, but mainly in the low energy setting of a distal lobe.

Deformed mudstone (DM)

Description

2-71 cm thick units of soft deformed, dark grey mudstones with silt to very fine sandstone laminae (DM1) and up to 9 cm thick mudstones and muddy sandstones with vertically distorted silt to very fine sandstone streaks (DM2) are recognized in study area (Fig. 2.4L, M, Plate 3).

Interpretation

Post-depositional deformation of unconsolidated mud and silty sandstone substrates could have occurred during emplacement of debris flows (van der Merwe et al., 2009) or by collapsing of mud suspension into cohesive muddy flows (Kneller and McCaffrey, 2003) anywhere within lobes but especially in distal lobe areas. Partially consolidated or fluidized mud and muddy sandstones can be invaded by straight or sheared sand-injection from underlying sands bed syn-depositionally. Capping mudstones are generally not completely penetrated by sand injections. This supports the notion that the injection is a syn-depositional processes (Haughton et al., 2003). If it is preserved, it will be deposited at the top of the lobe, but it may become pervasive on the lobe fringe.

Structureless mudstone (SM)

Description

Strictly speaking, there is no perfectly structureless mudstone interval in the study area. However, dark grey to black mudstone with very rare faint silt laminae and/or faint soft deformations are observed in up to127 cm thick units in the study area (Fig. 2.4N, Plate 3).

Interpretation

Rarely structured or structureless mudstones deposited by hemipelagic suspension fallout or by *en masse* freezing of cohesive mud flow (McCave and Jones, 1988) is likely to occur dominantly in distal lobe areas.

Table 2.9: Lithofacies of submarine fan-lobes in Washakie Basin. Scales in photos are in units of 1 cm (Total 96 m cores from four wells).

Facies	Facies	Description	Sedimentary process	Environment
Structureless sandstone (SS)	SS1: Sandy matrix 	Structureless silt, very fine (vf) to fine (f) sandstone (SST) with dispersed small (< 1mm diameter) mud flakes, 0.4-200.6 cm thick, gradational and sharp boundaries at top and bottom (Fig. 2.4A, Plate 2)	Deposition by high-concentration (density) turbidity currents (e.g., Kuenen, 1950; Postma, 1986) and progressive aggradation of sands near bed (Kneller and Branney, 1995) by rapid falling of suspended sediments	High energy (proximal lobe and lobe center)
	SS2: Muddy matrix 	Structureless silt, vf to f muddy SST with dispersed small (< 1mm diameter) mud flakes and occasionally faint laminae, 0.3-49.2 cm thick, gradational and sharp boundaries at top and bottom (Fig. 2.4B, Plate 3)	Deposition by high-concentration (density) turbidity currents. Muddier than flow which is depositing SS1. Progressive aggradation of sands near bed (Kneller and Branney, 1995) by rapid falling of suspended sediments	High energy (anywhere in lobe if sediment source is muddy, but predominant in lobe fringe)
Laminated sandstone (LS)	LS1: Planar laminated 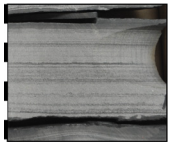	Planar and sub-planar laminated silt, vf to f SST, 0.4-34.4 cm thick, generally upward graded to mudstone (Fig. 2.4C, Plate 2)	Traction sedimentary structures by low-concentration turbidity currents or by waning high-density turbidity currents	High to low energy (anywhere in lobe, but more dominant in lobe fringe and distal lobe)
	LS2: Ripple-laminated 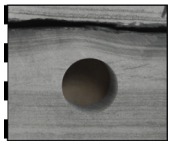	Ripple (frequently climbing ripple) cross-laminated silt, vf to f SST, 0.9-9.1 cm thick, generally gradational top and bottom boundaries (Fig. 2.4D, Plate 2)	Traction sedimentary structures by low-concentration turbidity currents or by waning high-density turbidity currents	High to low energy (anywhere in lobe, but more dominant in lobe fringe and distal lobe)
	LS3: Faint laminae 	Silt, vf to f SST with faint planar laminae and lenses, undulating light and greyish (slightly muddier) colored vf SST couplets, 1.1-33.0 cm thick, generally gradational top and bottom boundaries (Fig. 2.4E, Plate 2)	Faint lamination by high-density turbidity currents near bed (traction carpets) (Lowe, 1982; Hiscott, 1994) without significant reverse grading due to weak grain dispersion pressure of fine grains collision (Sohn, 1997)	High energy (proximal lobe and lobe center)

Table 2.9: (Continued)

Facies	Facies	Description	Sedimentary process	Environment
Mud-clast sandstone (MS)	MS1: Sandy matrix 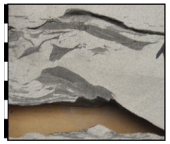	Silt, vf to f SST with irregular shaped and/or flat (subparallel to bedding) dark color (brownish, grey to dark grey) mud clasts, 0.6-16.4 cm thick, gradational top and bottom boundaries (Fig. 2.4F, Plate 2)	Mud clasts carried by high density turbidity currents. Relatively short transportation from its origin indicated by irregular shape of mud clasts (Smith, 1972)	High energy (anywhere in lobe, but dominant in proximal lobe, especially in lobe-channel)
	MS2: Muddy matrix 	Muddy matrix silt, vf to f SST with irregular shaped and/or flat (subparallel to bedding) brownish and dark color mud clasts with/without shearing, 0.3-122.3 cm thick, gradational top and sharp bottom boundaries (Fig. 2.4G, Plate 3)	Mud clasts carried by muddy high density turbidity currents, and/or transitional flows (e.g., linked-debrites (Haughton et al., 2003))	High energy (anywhere in lobe, but dominant in lobe fringe or distal lobe)
Heterolithic sandstone (HS)	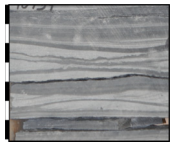	Heterolithic ripple or sub-planar laminated silt to vf SST interbedded with dark grey mudstone, 0.5-10.8 cm thick, uneven SST bottom and clean SST top (Fig. 2.4H, Plate 2)	Suspended mud fall deposits interlayered with deposits from low-concentration turbidity currents. Load-casted incomplete rippled vf SST (Dzulynski and Kotlarczyk, 1962) sunken into underlying muddy substrates	Low energy (anywhere in lobe if preserved, but dominant in distal lobe)
Deformed sandstone (DS)	DS1: Loading structure 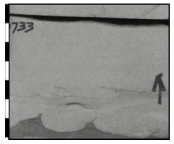	Soft deformed silt, vf to f SST underlain by mud or muddy SST. Loading (e.g., flame) and dewatering structures (e.g., dish), generally overlain by structureless SST, 0.3-7.7 cm thick (Fig. 2.4I, Plate 2)	Syn- and/or post-depositional soft deformation by overpressured pore-water (Sanders, 1965) during rapid deposition of high-density turbidity currents over weakly or un-consolidated substrate	High energy (anywhere in lobe, but dominant in proximal lobe and lobe center)
	DS2: Contorted structure 	Silt, vf to f SST with contorted laminae, 1.1-15.2 cm thick, gradational top and bottom boundary (Fig. 2.4J, Plate 3)	Sediment fluidization due to rapid loading of sediments (Moslow and Davies, 1997). Creeping and/or slumping sands accompanying with soft-sediment deformation, originally emplaced by high-density turbidity currents (?)	High energy (proximal lobe and lobe center)

Table 2.9: (Continued)

Facies	Facies	Description	Sedimentary process	Environment
Laminated mudstone (LM)	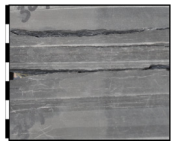	Dark grey to black mudstone with repeated sub-planar thin lighter color laminae silt, vf to f SST (structureless), 0.4-219.2 cm thick, rugged to sharp top and bottom boundaries, minor injection (Fig. 2.4K, Plate 4)	Suspended fine sediments fallout and low density turbidity currents deposition. Traction features (e.g., ripple, lamination) in SST laminae would be suppressed by high mud contents of currents (Allen and Leeder, 1980). Meso- to micro-band couplets of light-color vf SST and dark muddy from slurry-flow (Lowe and Guy, 2000)	Low energy (anywhere in lobe, but dominant in distal lobe)
Deformed mudstone (DM)	DM1: Soft deformed 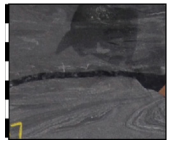	Soft deformed dark grey mudstone and silt to vf SST, 2.0-71.2 cm thick (Fig. 2.4L, Plate 3)	Post-depositional deformation of unconsolidated mud and silty substrates by emplacement of debris flows (van der Merwe et al., 2009) or by mud suspension collapse into cohesive muddy flow (Kneller and McCaffrey, 2003)	High to low energy (proximal lobe, if preserved, but dominant in distal lobe)
	DM2: Injections 	Mudstone and/or muddy SST with vertically distorted silt to vf SST streaks. Silt to vf SST lenses or laminae,0.3-9.3 cm thick (Fig. 2.4M, Plate 3)	Incomplete penetration of overriding mudstones by syn-depositional sand injection (Haughton et al., 2003) with or without deformation from underlying sand beds	High to low energy (at the top of lobe, if preserved, and in lobe fringe)
Structureless mudstone (SM)		Dark grey to black structureless mudstone with very rare faint siltstone laminae and/or faint soft deformation, 0.3-127.9 cm thick, sharp top and gradational bottom boundaries (Fig. 2.4N, Plate 3)	Hemipelagic sediment fallout and/or *en masse* freezing of cohesive mud flow (McCave and Jones, 1988)	Low energy (on top of the lobe, if preserved, and in distal lobe)

Facies distribution within different segments of fan lobes

Cores from the study area are located mainly in lobe axis (API No. 4903721476), lobe fringe (API No. 4903721922, 4900722141), and distal lobe (API No. 4903721741) settings (Figs. 2.5-2.8). This setting of each cored interval is inferred from initially constructed sandstone thickness maps of Clinothems 4, 5, 11, and 12, and two intervals (Intervals 9-1 and -2) of Clinothem 9 which are correlated in detail (See Chapter 1 for details). In order to analyze the vertical distribution of lithofacies and their preferred transitions in cored locations, Markov chain analysis on a total 1,236 lithofacies units was conducted (Tables 2.4-2.8, Figs. 2.5-2.8).

Lobe axis

Description

Upward coarsening gamma log-curve patterns are observed from Interval 9-1 of API No. 4903721476. In contrast, the gamma log motif of Interval 9-2 is characterized by a blocky, low gamma with mild serration pattern (Fig. 2.5). In core from API No. 4903721476, structureless sandstone is most dominant in Interval 9-2 (SS: 74% in thickness). The thickness percentage of laminated mudstones and structureless mudstones are 39 and 12% in Interval 9-1 but only 7 and 4% in Interval 9-2 (Fig. 2.5B-D). Each interval is located on the axis and slightly off-axis of lobe complexes in Interval 9-1 and 9-2 of Clinothem 9 as read from preliminary boundaries of lobe complexes by sandstone thickness maps (Fig. 2.5C, D).

Interpretation

The dominating structureless sandstone facies seen in the core is likely caused by amalgamation of lobe-channel sandstones close to the proximal lobe axis. In contrast, the relatively high percentage of laminated mudstone in Interval 9-1 (Fig. 2.5C) is because this

was only the initial emplacement of submarine fan lobes on the basin floor. (See discussion of Chapter 1 for details). The upward coarsening gamma ray and core patterns are also consistent with this being the initiation of the submarine lobe-complex deposition. The blocky low gamma ray motif and thick structureless sandstones of core together with the location of core in sandstone thickness maps support that API No. 4903721476 was close to the proximal lobe axis.

Lobe fringe

Description

Strong upward coarsening, gamma-ray log patterns are recognized in Clinothems 4, 5, 11, and 12 from API No. 4900722141, 4903721741, and 4903721922 (Figs. 2.6A, 2.7A, 2.8A). Thickness-percentages of structureless sandstones, as well as laminated and structureless mudstones is nearly constant (63-67%) in all four intervals. Thickness percentages of mud-clast sandstones with sandy and muddy matrices ranges also has a narrow range of 11-16% (Figs. 2.6C, D, 2.7C, 2.8C). The cores are located on the distal lobe fringes (Figs. 2.6C, D, 2.8C), and on the west-side lateral fringe (Fig. 2.7C) of lobe complexes in Clinothems 4 and 5 of 4900722141, Clinothem 12 of 4903721922, and Clinothem 11 of 4903721741 as shown by the sandstone thickness maps.

Interpretation

There are thinner structureless sandstones in the lobe fringe area than in the lobe axis area, but more than in distal lobe sites. The other unique characteristic of the lobe fringes in the study area is that they contain the highest thickness-percentages of mud-clasts sandstones. This suggests that most of the mud clasts in the sandstones are not transported from shelf-edge or upper slope, but sourced just upstream from the core locations. If mud clasts were sourced from shelf-edge or upper slope areas, the thickness-percentages of

mud-clast sandstones would have gradually decreased from proximal to distal lobe complexes with a pre-condition that there had been no flow transition during the of the mud clasts. The mud-clast sandstones with muddy matrix overlying structureless or deformed sandstones are interpreted as debrites on the lobe fringes, deposited by hybrid or transitional flows. The preferential location of hybrid or transitional beds are already reported as lobe fringes by Haughton et al. (2003, 2009), Hodgson (2009), and Kane and Pontén (2012). The lateral facies changes on lobe fringes, however, have not previously been documented, and will be discussed below.

Distal lobe

Description

Upward coarsening, gamma-ray log motifs, but gentler than those from lobe fringes, is observed in the interval of Clinothem 12 from API No. 4903721741 (Fig. 2.7A). The cored interval in Clinothem 12 of API No. 4903721741 is dominated by laminated (36%) and structureless (41%) mudstones. Minor structureless sandstones with sandy (7%) and muddy (3%) matrixes and mud-clast rich muddy sandstones (7%) are also recognized (Fig. 2.7B, D). Relatively thin sandstones with sub-planar and rippled laminae interbed with thicker mudstones. The location of this interval is inferred to be distal lobe for Clinothem 12 based on preliminary lobe complex boundaries on the sandstone thickness map (Fig. 2.7D).

Interpretation

Gentle coarsening upward gamma-ray log patterns indicate that the core is still located on a lobe complex. However, the core from Clinothem 12 of API No. 4903721741 is characterized as a lower energy setting than the lobe fringe, i.e., it is likely to be distal lobe based on the very high thickness percentage (77%) of laminated and structureless

mudstones. Thin ripple or planar laminated sandstones, deposited by dilute turbidity currents and interbedded with fallout mudstones, would have caused the gentle coarsening upwards seen on the gamma-ray log and cores.

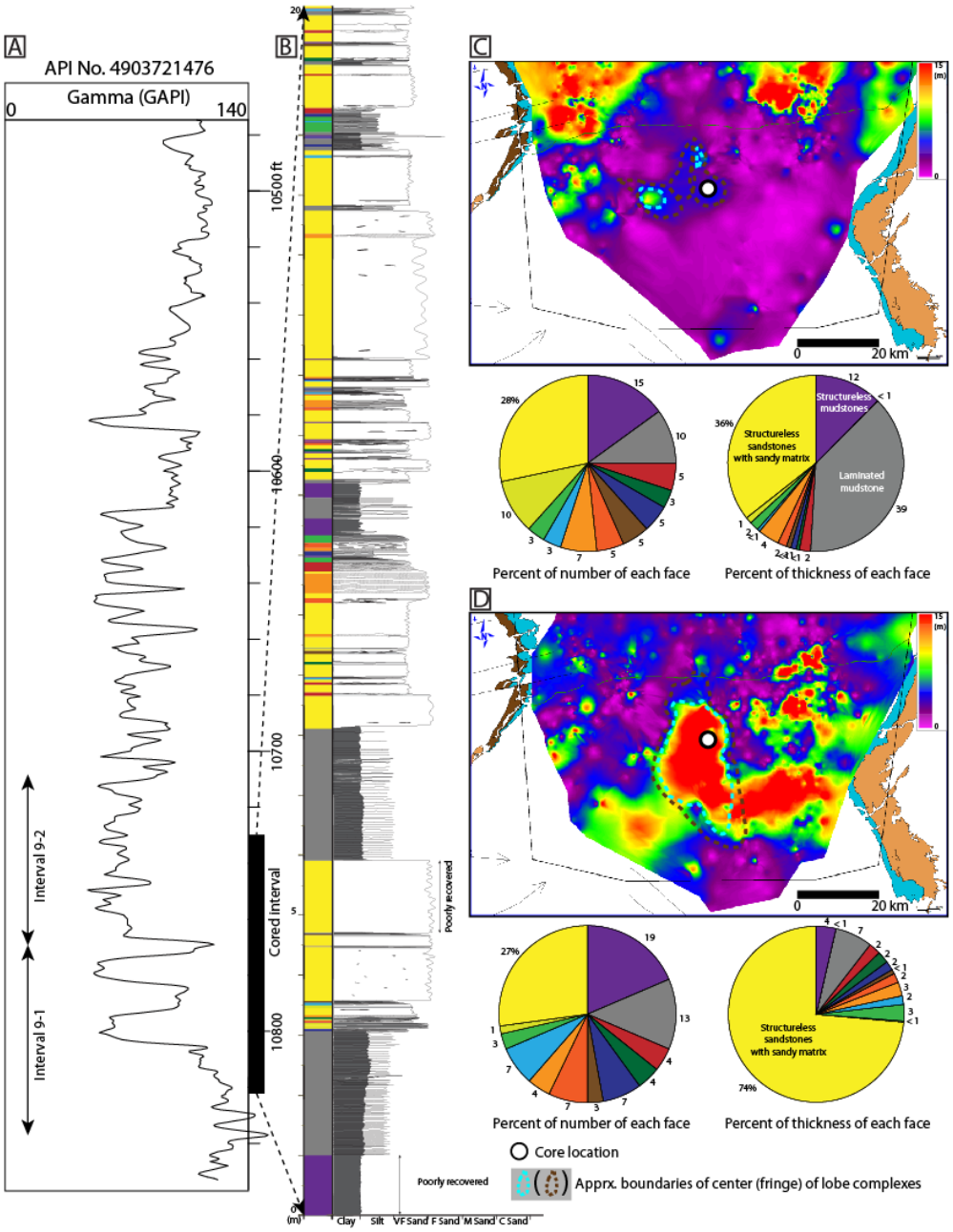

Figure 2.5: Correlation between A) gamma and B) core logs of a well (API 4903721476). Sandstone thickness map of C) Interval 9-1 and D) Interval 9-2 of Clinothem 9 with lithofacies number and thickness proportions. The core is located in axis and/or slightly off-axis of lobe complexes in Interval 9-1 and 9-2 with respect. Structureless sandstone is dominant lithofaices (SS: 27-28% of facies in number, and 36-74% in thickness). Amalgamation of sands is dominant sedimentary processes at or close to lobe axis by amalgamation of channels. Refer to Plate 1 for the detail log and Figures 2.1 and 2.8 for lithofacies legend.

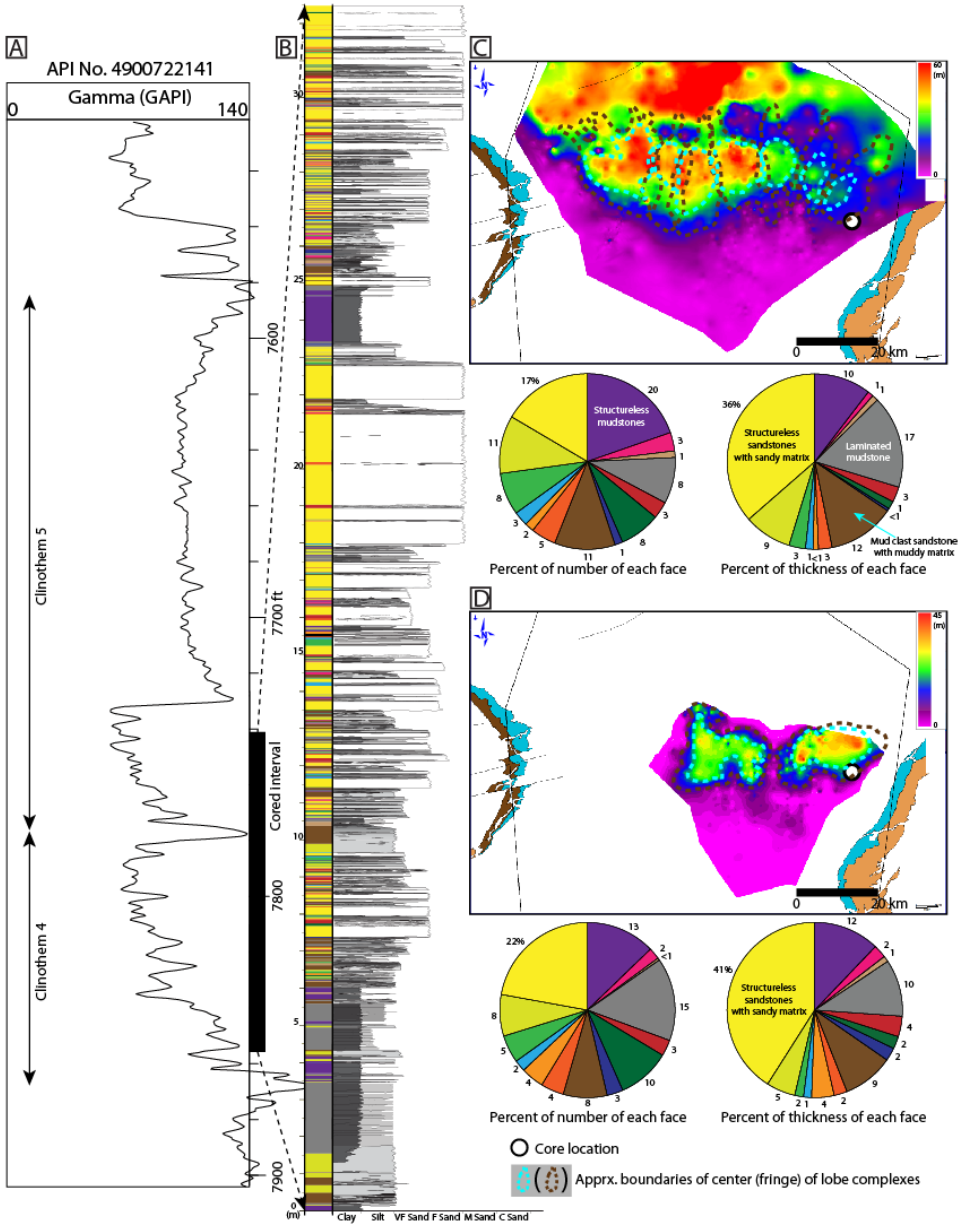

Figure 2.6: Correlation between A) gamma and B) core logs of a well (API 4900722141). Sandstone thickness map of Clinothems C) 4 and D) 5 with lithofacies number and thickness proportions. The core is located in fringe of lobe complexes in Clinothems 4 and 5. Note mud clasts rich sandstones frequently overlying structureless sandstones. Transitional flow deposits, linked-debrites, are observed more (MS2: 8-11% of facies in number, and 9-12% in thickness) than in succession of lobe axis (Fig. 2.5) and distal lobe (Fig. 2.7). Strong upward coarsening and thickening trend of GR and core logs indicate deposition of progradational submarine lobes by waxing flows. Refer to Plate 3 for the detail log and Figures 2.1 and 2.8 for lithofacies legend.

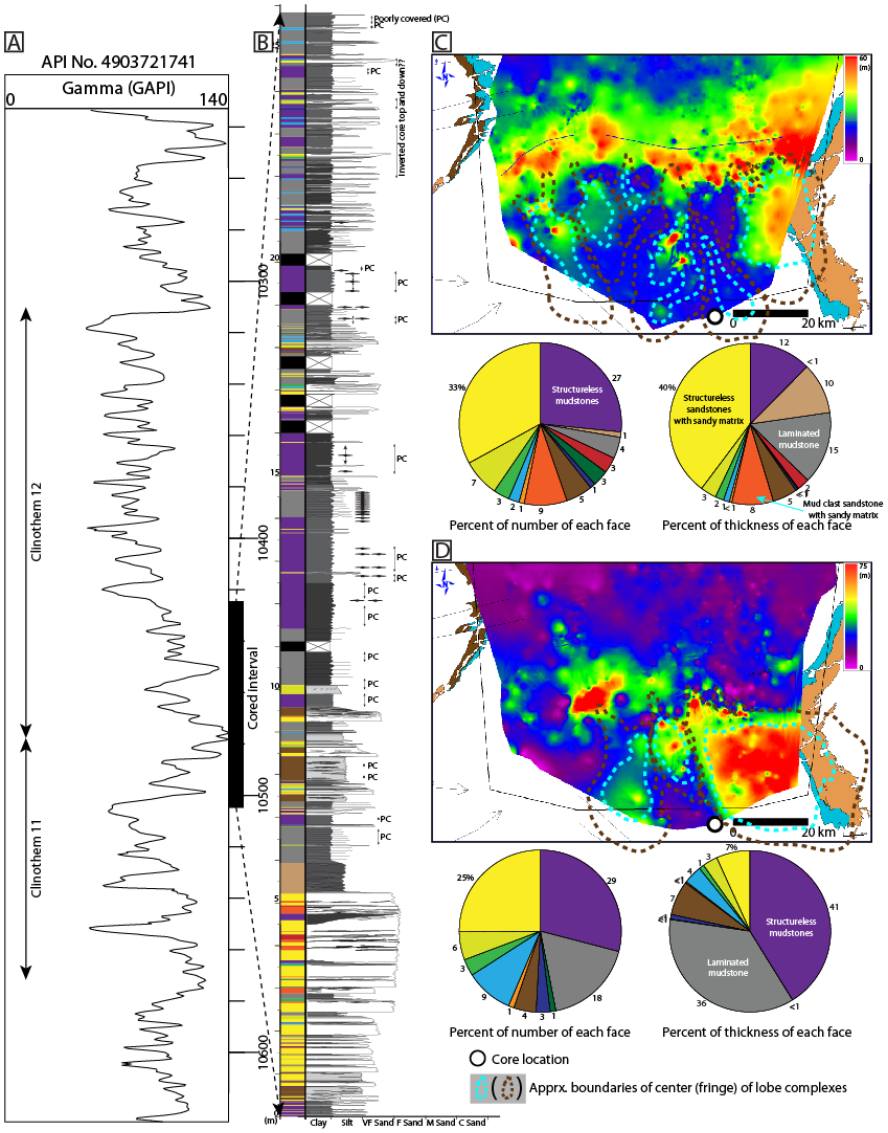

Figure 2.7: Correlation between A) gamma and B) core logs of a well (API 4903721741). Sandstone thickness map of Clinothems C) 11 and D) 12 with lithofacies number and thickness proportions. The core is located in fringe of and distal lobe complexes in Clinothems 11 and 12 respectively. Transitional flow deposits are observed (MS2: 5% of facies in number, and 5% in thickness) in the upper section of Clinothem 11. Upward fining and thinning GR and core logs would result from deposition of waning flows. Lower succession of Clinothem 12 is prevailed by mudstone with gentle upward coarsening (LM: 18% of facies in number, 36% in thickness; SM: 29% of facies in number, 41% in thickness), in contrast structureless sandstones are thin (SS: 25% of facies in number and 7% in thickness). Note the slight upward coarsening pattern of GR and core logs above Clinothem 11 showing turning from waning to waxing flows. Refer to Plate 4 for the detail log and Figures 2.1 and 2.8 for lithofacies legend.

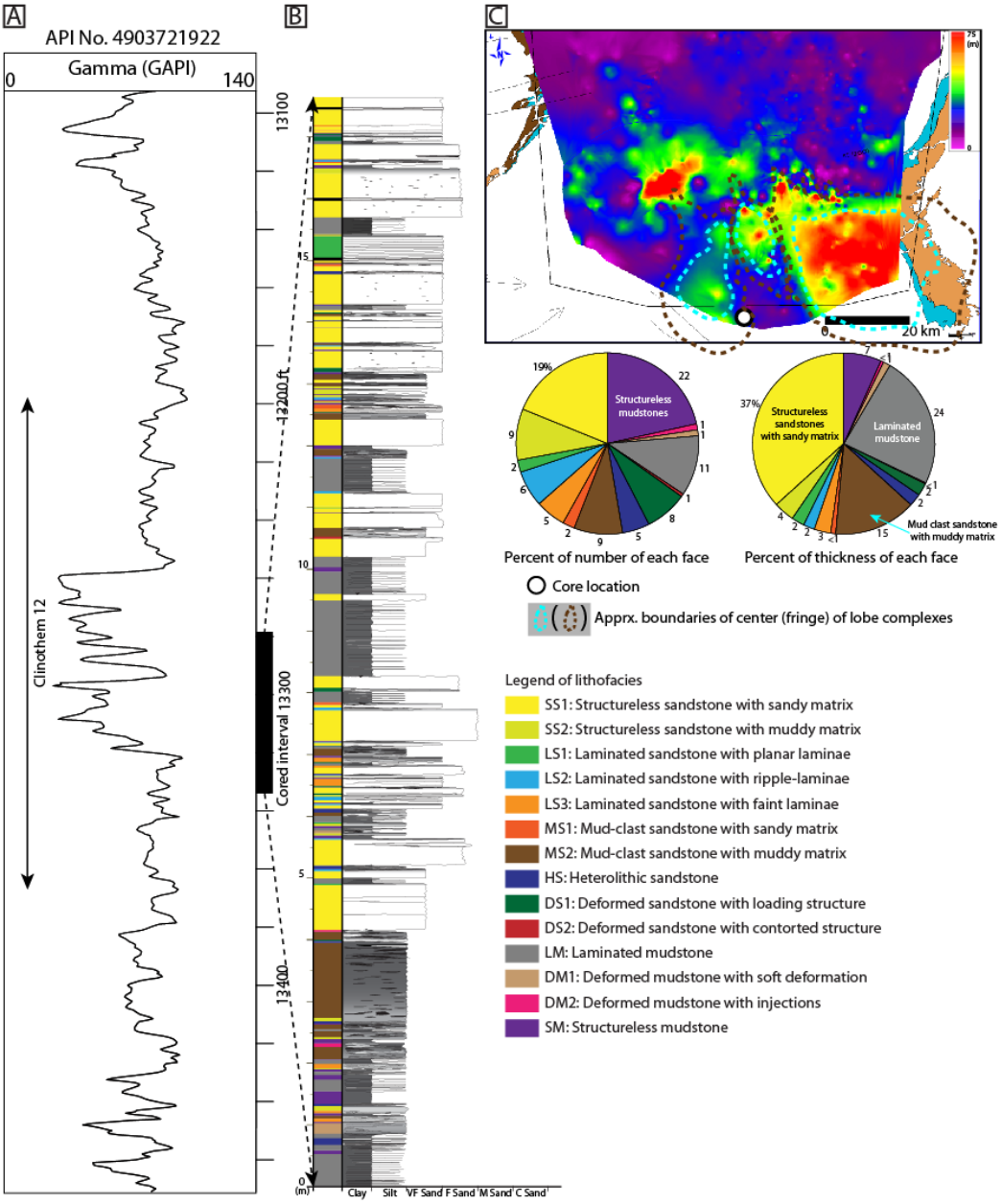

Figure 2.8: Correlation between A) gamma and B) core logs of a well (API 4903721922). C) Sandstone thickness map of Clinothem 12 with lithofacies number and thickness proportions. The core is located in fringe of lobe complexes in Clinothem 12. Note mud clasts rich sandstones frequently overlying structureless sandstones. Transitional flow deposits, linked-debrites, are observed more (MS2: 9% of facies in number, and 15% in thickness) than in succession of lobe axis (Fig. 2.5). Upward coarsening and thickening trend of GR and core logs might indicate deposition of progradational submarine lobes by waxing flows. Refer to Plate 2 for the detail log and Figure 2.1 for lithofacies legend.

Markov chain analysis

Transition proportion matrices (Tables 2.3-2.8) for lithofacies of the cored intervals in different clinothems were used to build Markov chains. The trend of vertical facies transition is extracted from Markov chains in lobe axis, fringe, and distal lobe settings (Figs. 2.9-2.11).

Lobe axis

The Markov chain of Well API No. 4903721476 which is located close to lobe axis shows three strong vertical facies transitions from deformed sandstones (DS1, DS2) to structureless sandstones (SS1) in over 80% of cases; from laminated sandstones (LS1, LS2) to laminated mudstones (LM) or structureless mudstones (SM) in about 30-50% of the transitions occasionally with mud-clast sandstones (MS1, MS2); and from structureless mudstones or laminated mudstones to structureless sandstones 43% and 40% respectively (Fig. 2.9A). These vertical transitions indicate that deformed sandstones and structureless sandstones are mostly capped by laminated mudstones or structureless mudstones. In contrast, structureless sandstones (SS1) are overlain by various facies of distorted sandstones (DS2) (14.3%), laminated mudstones (14.3%), mud clast sandstones (12.5%), and laminated sandstones (8.6%) without obvious vertical transition-pattern (Fig. 2.9B). There is no unique vertical facies transition for the lobe axis, but the most general vertical trend is observed to be deformed/structureless sandstones passing upward to laminated sandstones followed by laminated/structureless mudstones. In the lobe-axis area, vertical transitions involving mud-clast muddy sandstones are only rarely observed.

Lobe fringe

Markov chains of Clinothems 4, 5, 11, and 12 from API No. 4900722141, 4903721741, and 4903721922 display dominant trends of vertical facies transition similar

to those of the lobe axis. Deformed sandstones (DS1) - structureless sandstones (SS1) (54-100%), laminated sandstones (LS1, LS2) - laminated mudstones (LM)/structureless mudstones (SM) (20-100%), and structureless mudstones (SM)/laminated mudstones (LM) - structureless sandstones (SS1) (26-83%) are the dominant vertical facies transitions in any fringe location (mainly pink arrows in inset chains of Figure 2.10). These trends support the idea that sediment-deposition is mainly by turbidity currents also on the fringes of submarine fans. Because the transitions related with mudstones (SM, DM1, DM2, LM) and deformed sandstones (DS1) are in similar patterns from all fringe-locations, only parts of the Markov chains are used in the analysis of fringe of submarine fans, and transitions including mudstones and deformed sandstones are excluded (Fig. 2.10). Inset fan-diagrams of Figure 2.10 show locations of intervals in the fringes of fans from different clinothems. The locations of Figure 2.10A-C and 2.10D are defined as distal and lateral fringe in this study (Fig. 2.10).

In distal fringes (Fig. 2.10A-C), SS1, SS2, MS1, and MS2 facies pass upwards to each other frequently. Mud-clast sandstones with muddy matrix (MS2) overlie structureless sandstones (SS1, SS2) (9-29%). Structureless sandstones (SS1, SS2) are also overlain by mud-clast sandstones with sandy matrix (MS1) (13-20%). Structureless sandstones with muddy matrix (SS2) underlain by structureless sandstones with sandy matrix (SS1) (10-12%). These transitions explain hybrid-flow deposition by transitional and/or hybrid flows in the distal fringe. Structureless sandstones with sandy matrix (SS1) in the distal fringe might be deposited by non- or partially transformed turbidity currents, if flow-transition occurred. In lateral fringes (Fig. 2.10D), transitions related with mud-clast sandstones with muddy matrix (MS2) are less common, but transitions related with mud-clast sandstones with sandy matrix (MS1) do occur. Structureless sandstones with sandy matrix (SS1) overlie and are overlain by mud-clast sandstones with sandy matrix

(MS1) 25% and 19% of the time with respect. Structureless sandstones with sandy matrix (SS1) are also followed by mud-clast sandstones with muddy matrix (MS1) (23%). Structureless sandstones (SS1) with sandy matrix follow mud-clast sandstones with muddy matrix (MS2) (20%), but opposite transition is not observed. These trends indicate relatively minor hybrid-flow deposition in the lateral fringes of submarine fan in Clinothem 11 of Washakie Basin. The trend of vertical facies transition in lateral fringes in Clinothem 11, deformed sandstones (DS) - structureless sandstones (SS1) - mud-clast sandstones with sandy matrix (MS1) - SS1 - planar/ripple laminated sandstones (LS) - laminated/structureless mudstones (LM/SM) (Fig. 2.10D), is more similar with ones from axis than trends of distal fringes.

Distal lobe

The vertical facies transition of cored interval from Clinothem 12 in Well API No. 4903721741 is similar with that from Well API No. 4903721476. Transition from deformed sandstones (DS1) to structureless sandstones (SS1), from laminated sandstones (LS1, LS2) to laminated mudstones (LM) or structureless mudstones (SM), and from structureless mudstones or laminated mudstones to structureless sandstones are also the main transition-trends in this well (Fig. 2.11). However, the transition probabilities (44-60%) from laminated sandstones (LS1, LS2) and structureless sandstones (SS1, SS2) to structureless mudstones is higher than that (0-50%) of Well API No. 4903721476 due to the higher thickness percentage and number of mudstones in the well (Fig. 2.7D). The multiple transitions from various sandstone-facies (laminated, structureless, and heterolithic sandstones) to structureless or laminated mudstones indicates that sandstones are frequently interbedded with mudstones, supporting the deposition at low-energy setting.

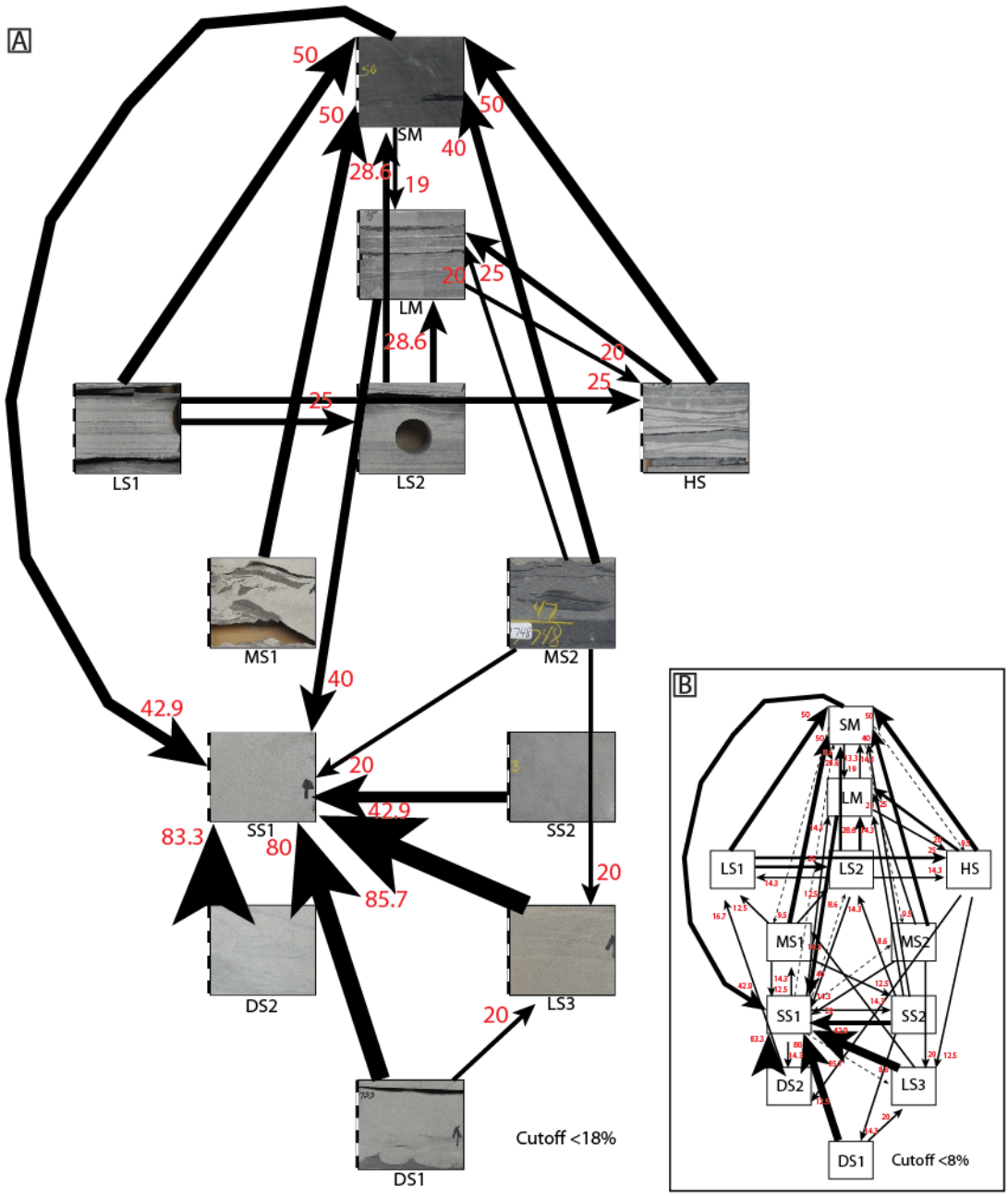

Figure 2.9: Markov chain of lithofacies with cutoff A) 15% and B) 8% from Clinothem 9 at the location of Well API No. 4903721476. Note that strong transition trend from deformed sandstones (DS1, DS2) to structureless sandstones (SS1), from laminated sandstones (LS1, LS2) to laminated mudstones (LM) or structureless mudstones (SM), and from structureless mudstones or laminated mudstones to structureless sandstones. In contrast, structureless sandstones (SS1) are followed by distorted sandstones (DS2), laminated mudstones, mud clast sandstones, and laminated sandstones without significant trend.

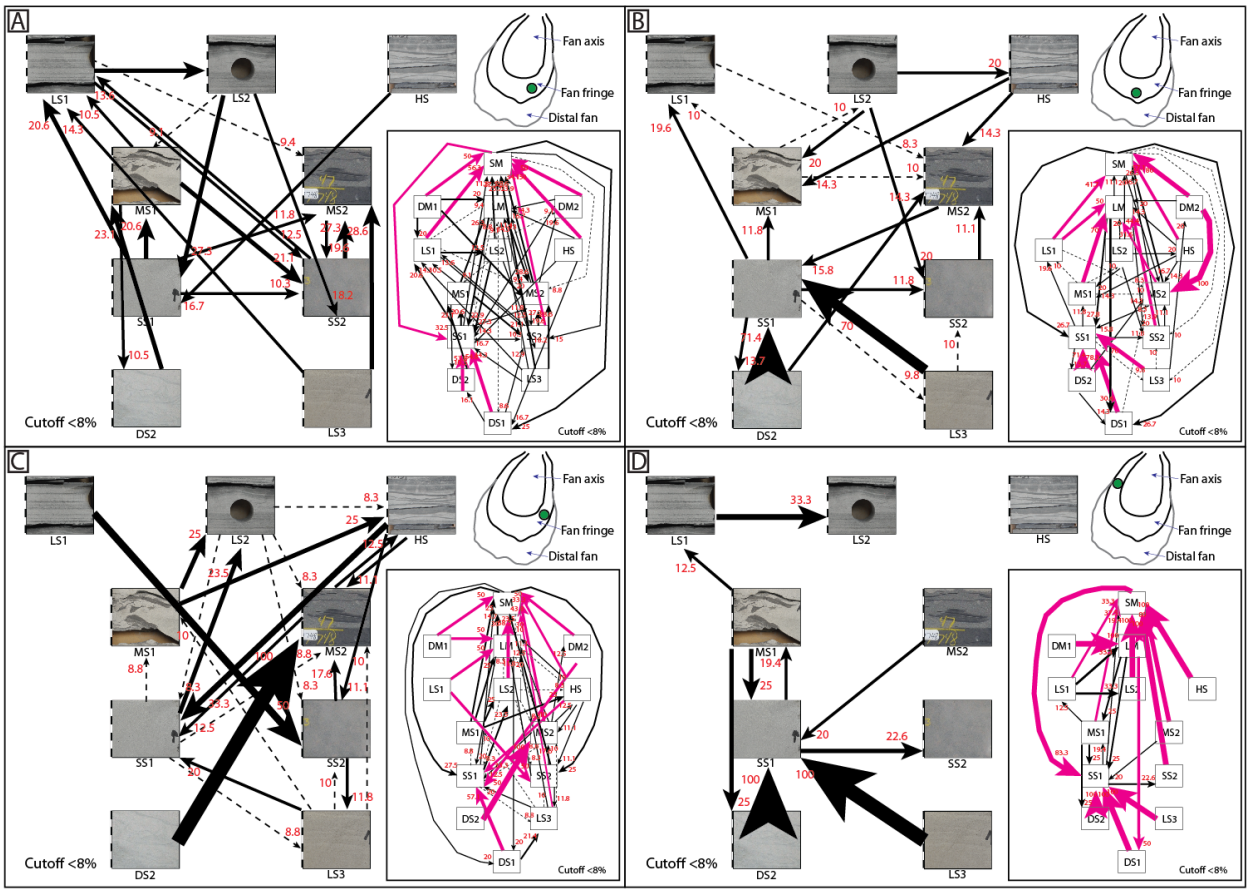

Figure 2.10: Parts of Markov chain of lithofacies with cutoff 8% from A) Clinothem 4 at the location of Well API No. 4900722141, B) Clinothem 5 at the location of Well API No. 4900722141, C) Clinothem 12 at the location of Well API No. 4903721922, and D) Clinothem 11 at the location of Well API No. 4903721741. Inset chain diagrams are full Markov chain with cutoff 8%. The transitions related with mudstones (SM, DM1, DM2, LM) and deformed sandstones (DS1) are excluded from chains in order to compare transitions mainly among structureless sandstones (SS1, SS2), mud-clast sandstones (MS1, MS2), and laminated sandstones (LS1, LS2). For convenience, transitions over 30% are marked in pink color. Inset fan diagrams show the relative locations (green circles) of core interval in the fringes of fans. Note that transitions of deformed sandstones (DS1) - structureless sandstones (SS1), laminated sandstones (LS1, LS2) - laminated mudstones (LM)/structureless mudstones (SM), and structureless mudstones / laminated mudstones - structureless sandstones are well observed in any locations fan-fringes. In distal fringes (A, B, C) transitions among SS1, SS2, MS1, and MS2 occur frequently. In lateral fringe (D) the interaction between MS2 and other facies is less common but active between MS1 and other facies.

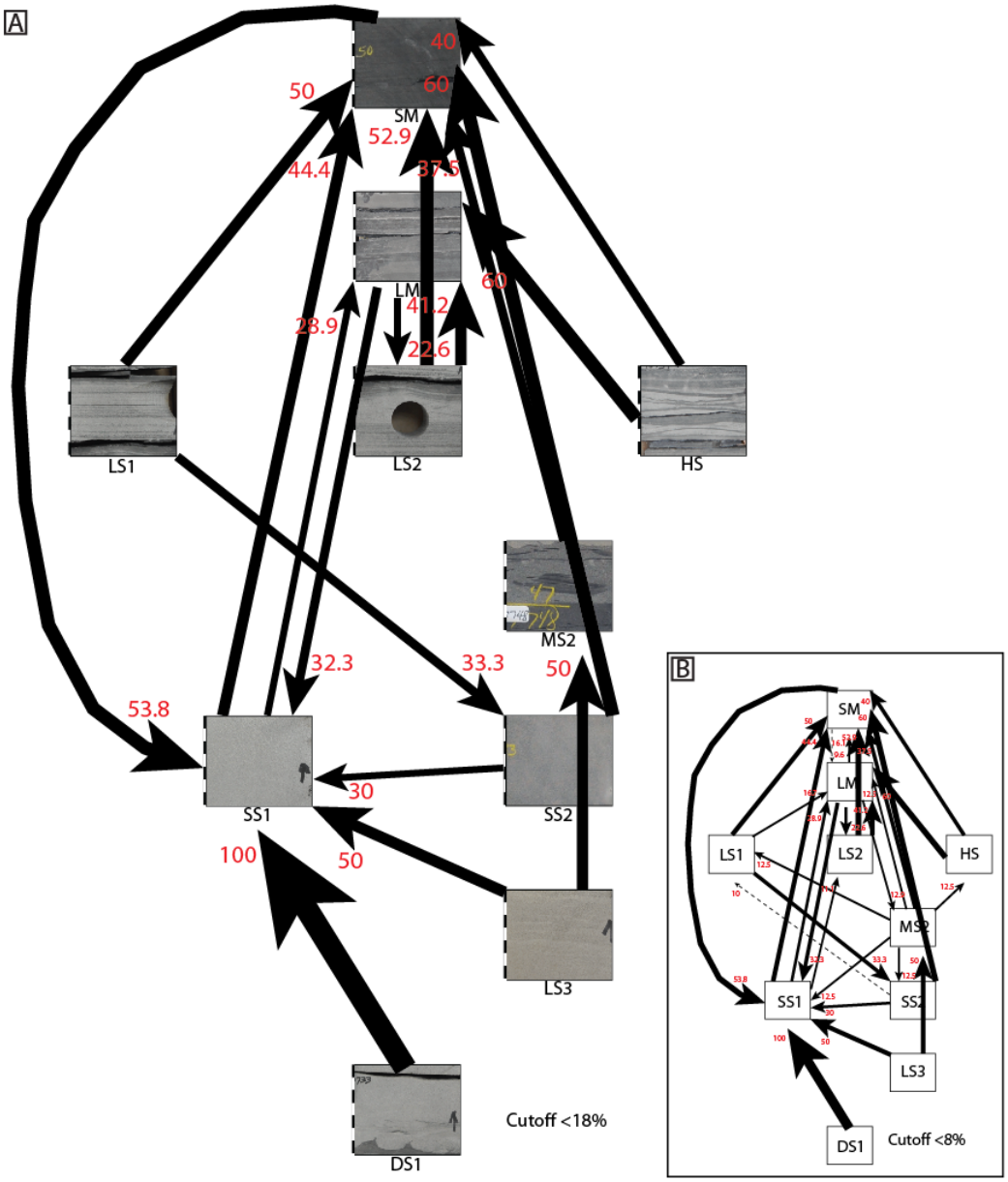

Figure 2.11: Markov chain of lithofacies with cutoff A) 18% and B) 8% from Clinothem 12 at the location of Well API No. 4903721741. Note that transition trends from deformed sandstones (DS1) to structureless sandstones (SS1), from laminated sandstones (LS1, LS2) to laminated mudstones (LM) or structureless mudstones (SM), and from structureless mudstones or laminated mudstones to structureless sandstones also observed in this well as Well API No. 4903721476. However, the transition to laminated/structureless mudstones from various is the most dominant trend of the well due to abundance of mudstones in the well, which supports low-energy depositional setting.

DISCUSSION

Depositional mechanisms of hybrid-flows on the fringe of lobes

There are different views on the depositional processes of hybrid flow. Haughton et al. (2003) proposed that linked-debrite is a result of debris flow riding on watery sands in genetically related subaqueous sediment-gravity flow, and suggested that linked-debrites always follow an underlying sand bed (Fig. 2.12A). Hybrid-flow deposits with multiple repetitions of turbidites and debrites (cm to meter thickness) are observed from cores collected from the fringes of submarine fans in Washakie Basin (Fig. 2.10). However, the debrites in the fan fringes do not always overlie precursor sand beds (Fig. 2.10). Kane and Pontén (2012) suggest that the longitudinal transition from turbulent to laminar flow by entraining clay content from nearby beds accounts for deposits of transient turbulent-laminar flow (Fig. 2.12B). To explain why there occurs frequent alternation of structureless sand beds and structureless sand with capping debrite beds, or just debrites, it is cumbersome and unrealistic to invoke alternation of linked debrites and transitional-flow deposits as these are very different mechanisms. This frequent changing of current-types unlikely occurs in a single lobe complex and/or even at submarine fan scale. Transitional flow, therefore, is more appropriate (sensu lato) to explain the trends of vertical facies transitions on the fringes of submarine fans in this study area, which show multiple debrites with or without underlying precursor sandstones. Mud-clast sandstones with muddy matrix would be originated from debris flows that experience transition from turbidity currents by entraining near bed muds. As turbidity currents erode the substrate, more clay would have been entrained within the gravity-flow. The increased clay content

and cohesiveness in the flow would have enhanced the capability of the flow to carry larger mud-clasts (Fig. 2.12C). The longer run-out turbidity currents in mud-rich systems would therefore be more likely to transform into debris flows (Kane and Pontén, 2012). This is also verified by the higher thickness percentages of mud-clast sandstones with muddy matrix (MS2) (9-15%) comparing to those with sandy matrix (MS1) (< 1-3%) (Figs. 2.2-2.5). Frequent vertical facies transitions from structureless sandstones (SS1, SS2) to mud-clast sandstones with muddy matrix, shown in Markov chains of this study (Fig. 2.8A-C) also support the idea that turbidity currents transformed to debris flows associated with long run-out distance. In contrast, because of the relatively short run-out distance to the lateral fringes from the lobe axis, turbidity currents would not be able to fully transform into debris-flows with abundant mud-clasts. The mud-clasts in partially or non-transformed flow would most likely originate from further upstream, and not from near depositional locations of these mud-clasts. Mud-clasts in lateral fringes would not be entrained from underlying muddy substrates, but would be delivered from further upstream by high concentration turbidity currents. The vertical facies transition from structureless sandstones with sandy matrix (SS1) to ones with muddy matrix (SS2) of a described core, located on a lateral fringe, implies an incomplete transition of turbidity currents into debris flow. The abundant embedded mud-clast sandstones with sandy matrix (MS1), noted by frequent transitions between MS1 and SS1, also supports the idea that high-concentration turbidity currents prevailed on the lateral fringes of lobes (Figs. 2.5B, 2.8D).

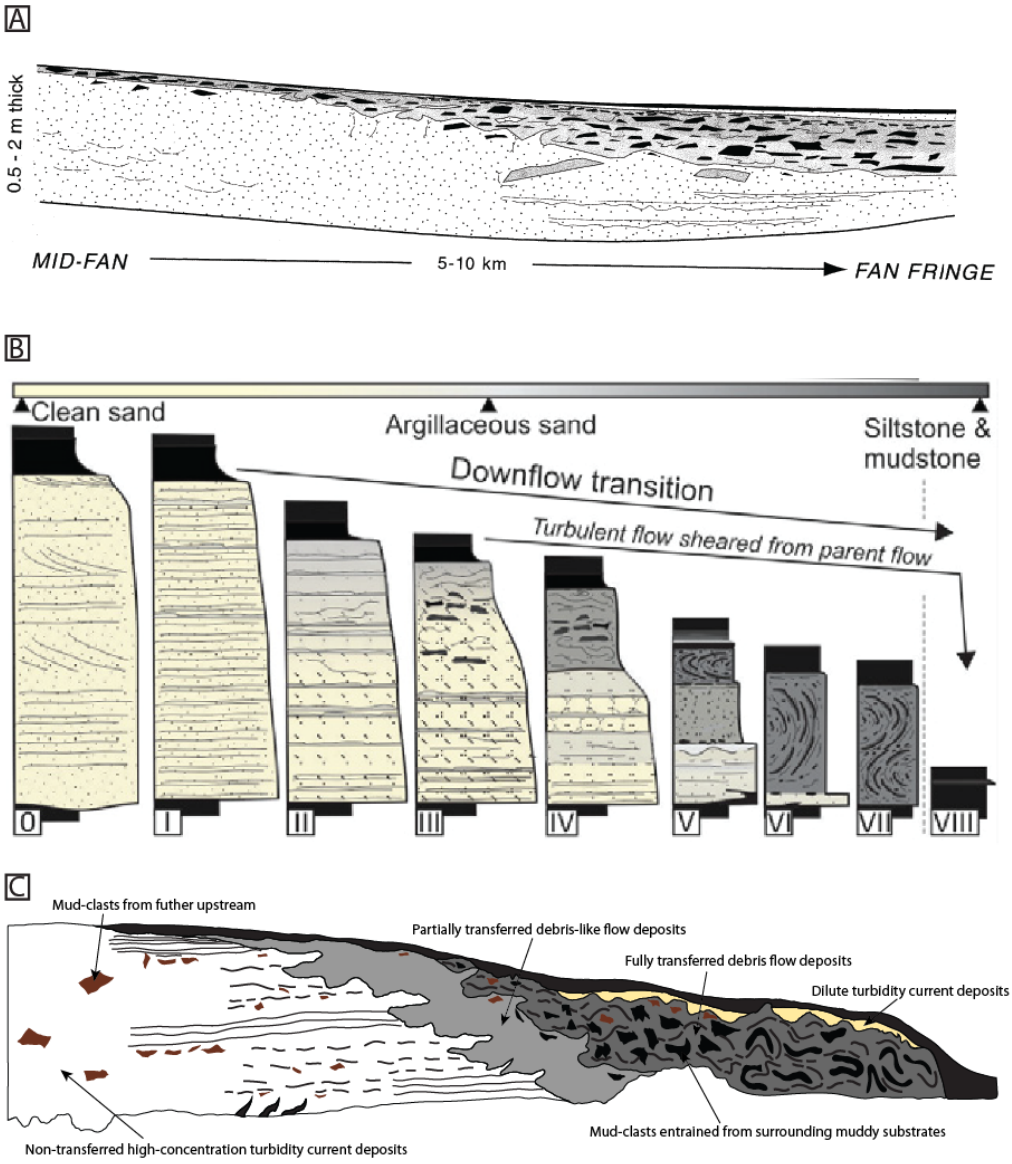

Figure 2.12: Lateral facies distribution of A) linked-debrites (Haughton et al., 2003), B) transitional flow-deposits (Kane and Pontén, 2012), and C) transitional hybrid flow-deposits (this study). Note that debrites of B and C do not always overlie precursor sand beds like A. As turbidity currents flow, entrained clay will be laden in the gravity-flow. The increased clay contents of flow enhances the capability of flow carrying larger mud-clasts by increasing cohesiveness of flow. The longer run-out turbidity currents in mud-rich systems will be preferably transferred into debris flows (Kane and Pontén, 2012). Mud clasts in this study might be origin both from further upstream (dark brown color) and/or near deposition locations (black color). Mud-clasts (dark brown) from further upstream are broken down as they flow downstream, but the sizes of ones from near beds (black color) increases as flow is transited into true debris flow. Flow direction is from left to right.

Conceptual model of lobe fringe and its application

The prominent distribution of hybrid-flow deposits on the fringes of fan lobes was suggested by recent studies (Haughton et al., 2003, 2009; Hodgson, 2009; Kane and Pontén, 2012). Hodgson (2009) agreed that hybrid flow-deposits are dominant on the fringe of lobes, but he also pointed out that hybrid beds are not always distributed symmetrically across a lobe (Fig. 2.13A). Here, I propose an updated model based on that of Hodgson (2009) for the fringes of lobe with lateral facies changes (Fig. 2.13B). As discussed above, the transformed mud-clast-rich, muddy-sandstones (i.e., debrites) develop preferentially in the distal fringes of fan lobes whereas partial- or non-transformed muddy or sandy turbidites deposit preferentially in the lateral fringes depending on run-out distance of flows. Therefore, even though there are heterogeneities of lithofacies on the fringes of lobes, the deposits on the lateral fringes are generally sandier than those on distal fringes (Figs. 2.13B, 2.14).

The elongated fan-shape, twice as long compared to width, in the bottomsets of clinothems in Washakie Basin (Refer to Table 1.1 and Figure 1.2 of Chapter 1) strongly suggest that there is a preferential distribution of mud-clast sandstones with muddy and sandy matrix in distal and lateral fringes respectively. In oil and gas reservoirs, hybrid-flow deposits in submarine fans critically impact permeability, flow direction, and reservoir compartmentalization. The preferential hydrocarbon flow-direction and permeability corresponds with the axial distribution of amalgamated channel-sandstones along the center of lobes. However, a second preferable flow-direction and permeability follows the connected paths of sandy lateral fringes of lobes, a direction generally perpendicular to the axis of submarine fans.

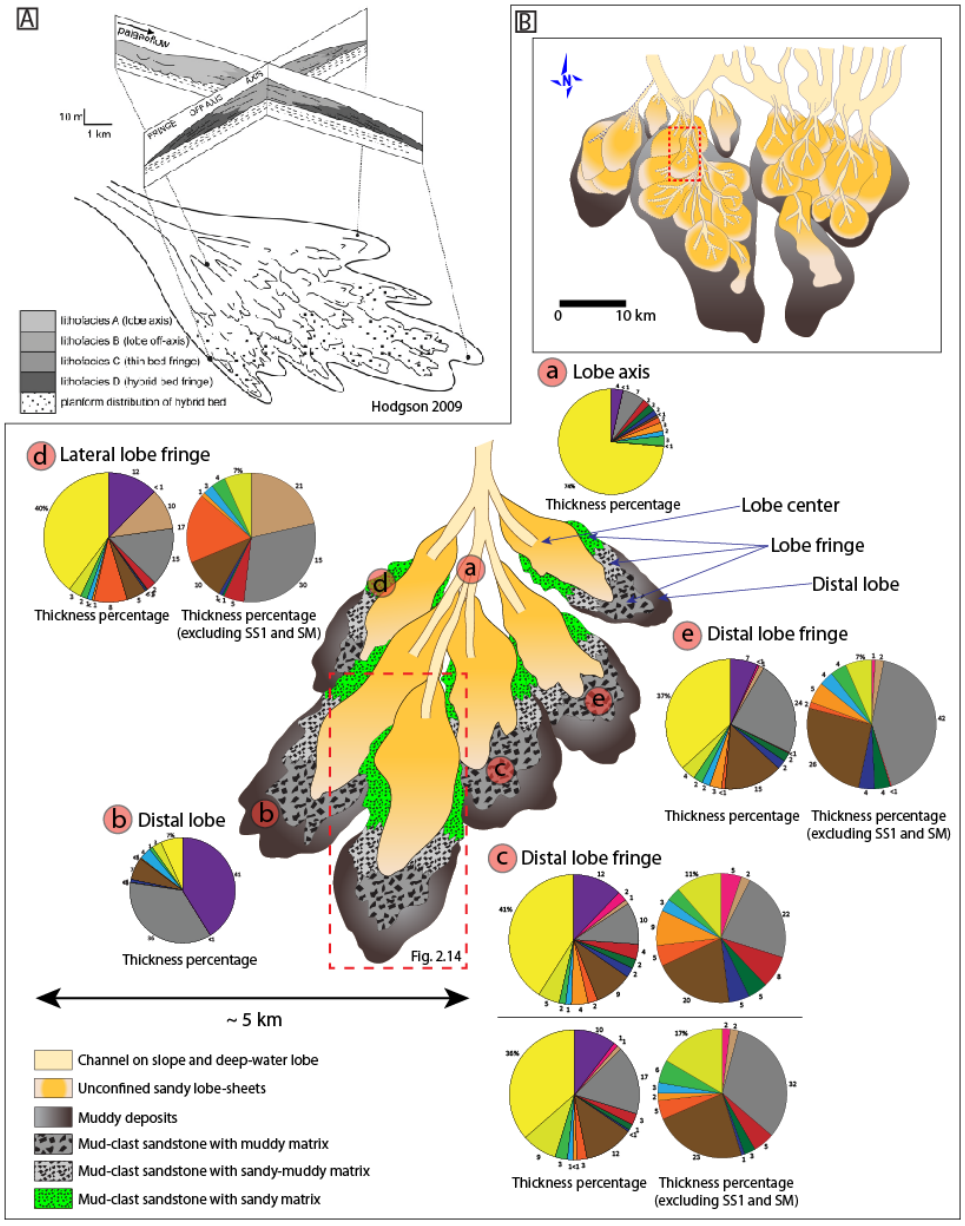

Figure 2.13: Conceptual models of submarine lobes of A) Hodgson (2009) and B) this study. In this study, the thickness of structureless sandstones in lobe fringes is thinner and thicker than ones of lobe axis and distal lobe with respect. The highest thickness-percentages of mud clasts sandstones is observed in lobe fringes. Note that the thickness percentages of mud-clast sandstones with muddy matrix in distal lobe fringe is higher than that of lateral lobe fringe. In contrast, mud-clast sandstones with sandy matrix is dominant in lateral fringe than in distal fringe. An inset diagram in B is lobe complexes which are defined by gamma well logs from Interval 9-2 in Clinothem 9 of Washakie Basin. See Chapter 1 for detail. Legend of pie charts is same with Figures 2.1, 2.8, and Plate 1.

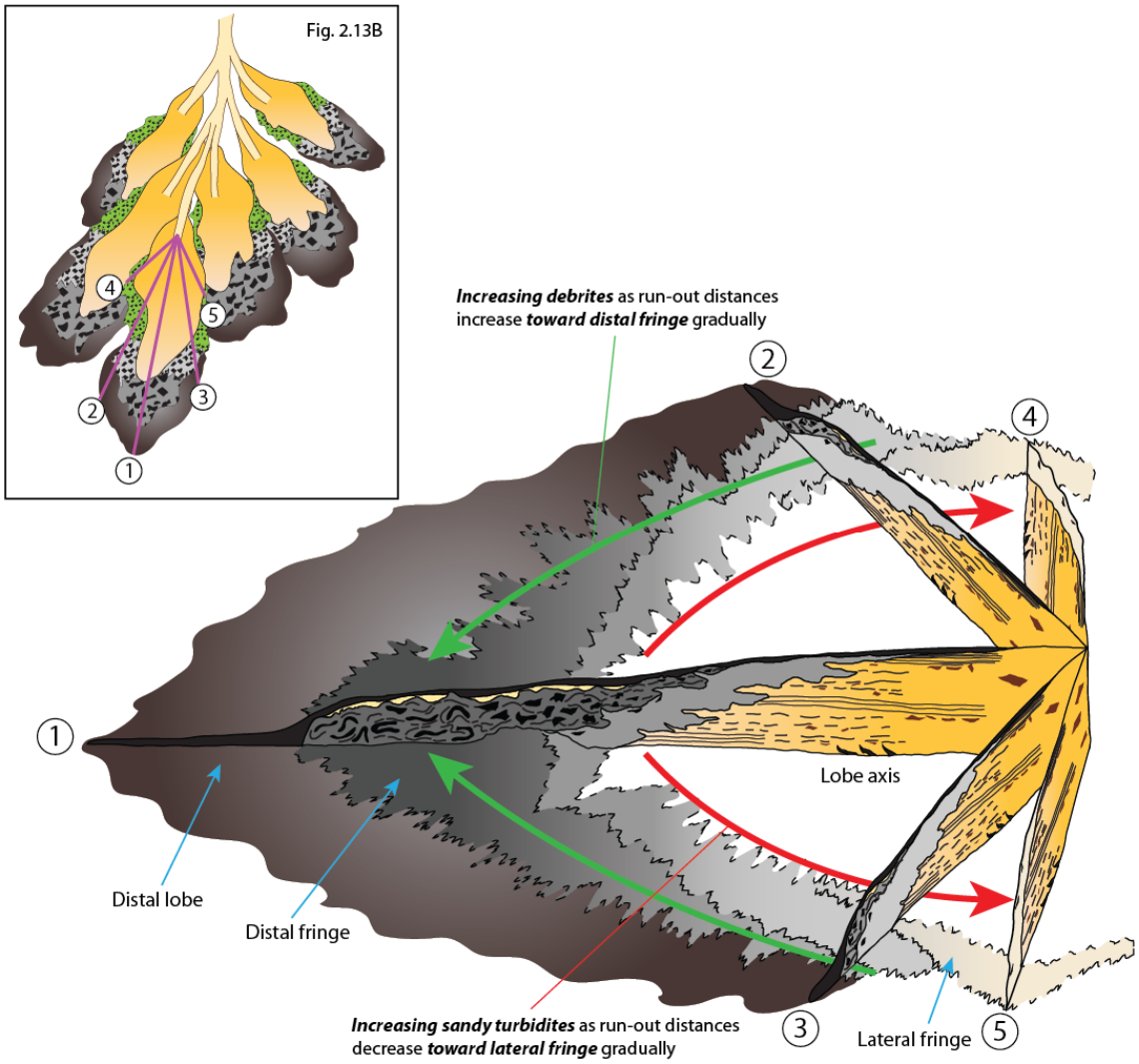

Figure 2.14: Fence diagram of submarine lobe in Washakie Basin. Mud-clast rich debrites are dominant in distal fringes in Cross-section 1. As the run-out distance of flow decreases like Cross-sections 2 and 3, partially transferred muddy turbidites and debrites are deposited in fringes. However, the portion of debrites in Cross-section 2 and 3 are much lower than that of Cross-section 1. In Cross-sections 4 and 5, sandy turbidites and/or slightly muddy turbidites are deposited in lateral fringes. This is because high concentration turbidity currents could not be transferred to debris flows due to too short run-out distance of flow comparing to Cross-sections 1, 2, and 3. Therefore, the lateral fringe of lobe would be sandier than distal fringe even though heterogeneities of lithofacies still exist in lobe fringes depending on the run-out distances of flows.

CONCLUSIONS

Two different depositional patterns are identified within the lateral and distal fringes of submarine fans in Washakie Basin, Wyoming. In the distal fringes with a long run-out distance in submarine fans on the basin floor, deposition can be strongly influenced by flow-transition from turbidity currents to debris flows and can involve multiple transitions without significant erosion between structureless sandstones (i.e., high-concentration turbidites) and mud-clast muddy sandstones (i.e., debrites). In contrast, there are far fewer such on the lateral fringes of fans due to the short run-out distance, which instead show a more sand-rich transit. The run-out distance of flow is an important factor on the transition of flow. Depending on run-out distance, flow can be fully, partially, or non-transformed, and results in deposition of mud-clast rich debrites, muddy turbidites, and sandy turbidites respectively. The longitudinally elongated fans in Washakie Basin were developed by long run-out distance of flow in north-south direction. The distal fringe of the submarine fans in Washakie Basin are muddier than the lateral fringe. An important secondary and more permeable flow-direction of such hydrocarbon reservoirs, generally sub-perpendicular to fan axis, is developed because of the sandy lateral-fringes on submarine fans.

Appendices

Appendix A is distribution maps of gamma-log motifs of Interval 9-3 in Clinothem 9 and Interval 10-3 in Clinothem 10. Sandstone thickness maps of six and five intervals in Clinothems 9 and 10 with respect are included in Appendix B.

Core logs with 1,236 lithofacies units (Plate 1) and photographs of four cores (Plates 2-5) are attached in a supplemental CD.

APPENDIX A: DISTRIBUTION MAPS OF LOG MOTIFS IN CLINOTHEMS 9 AND 10

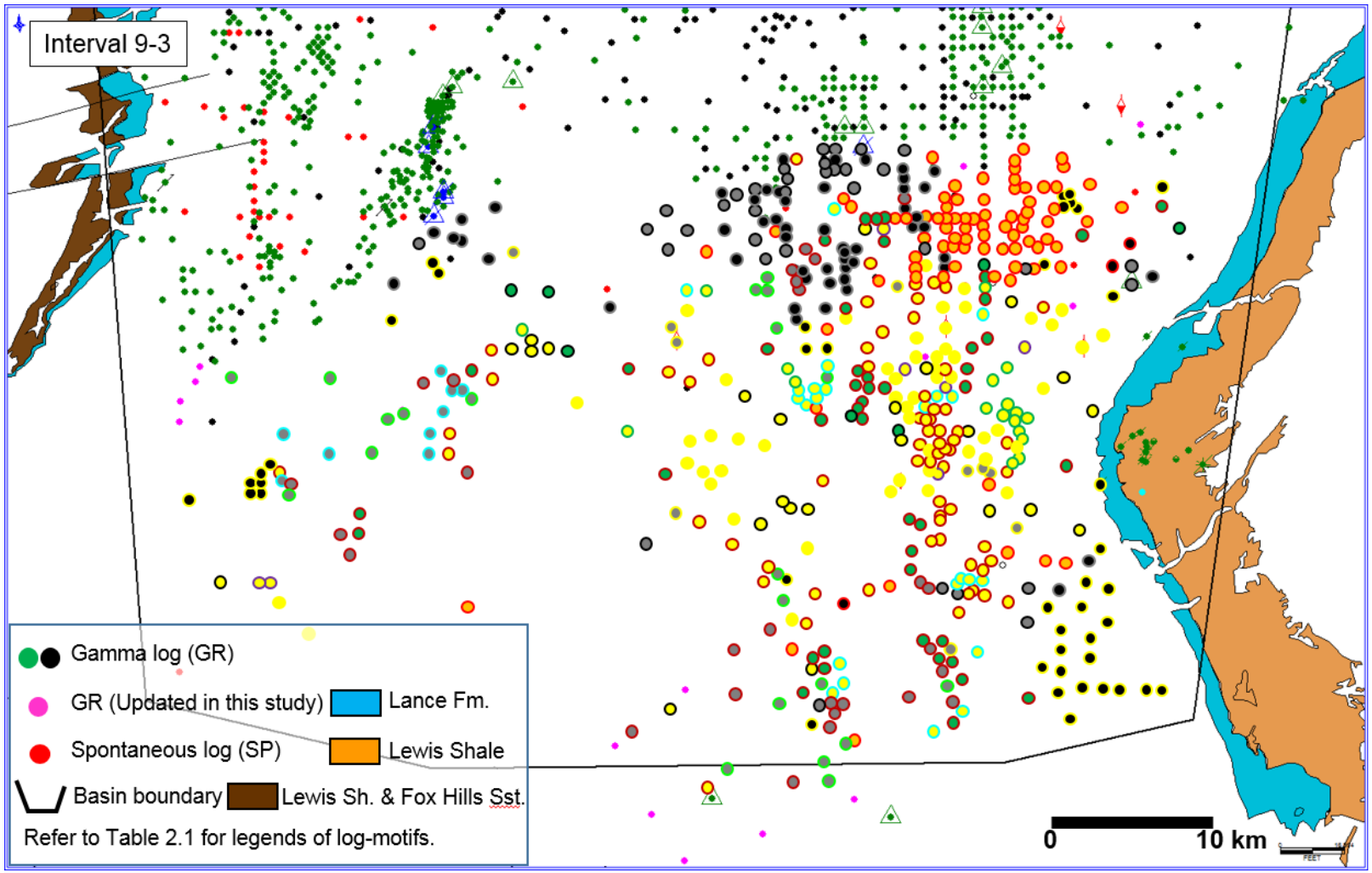

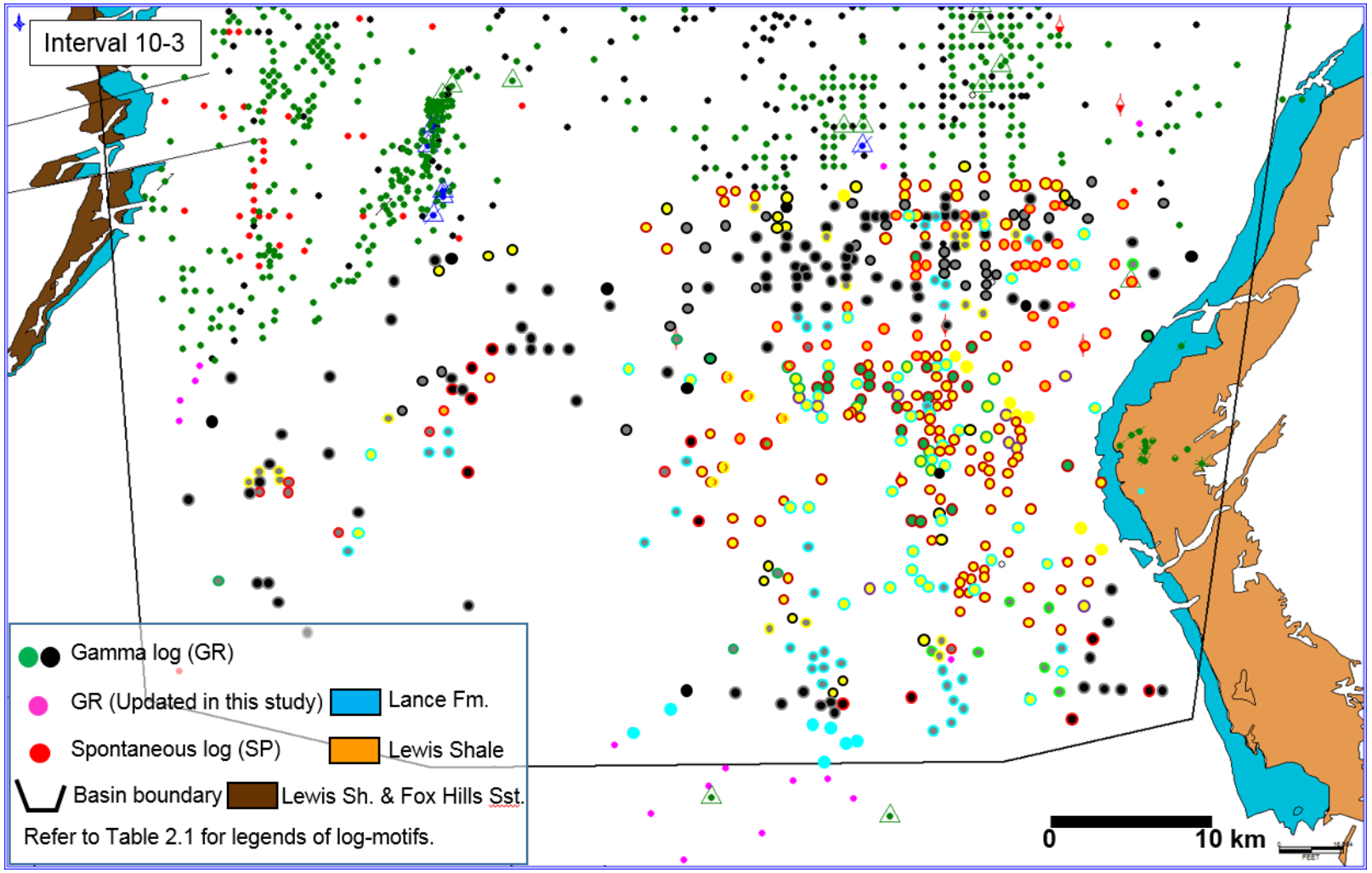
Interval 10-3
Gamma log (GR)
GR (Updated in this study)
Spontaneous log (SP)
Basin boundary
Lance Fm.
Lewis Shale
Lewis Sh. & Fox Hills Sst.
Refer to Table 2.1 for legends of log-motifs.
0
10 km

APPENDIX B: SANDSTONE THICKNESS MAPS IN CLINOTHEMS 9 AND 10

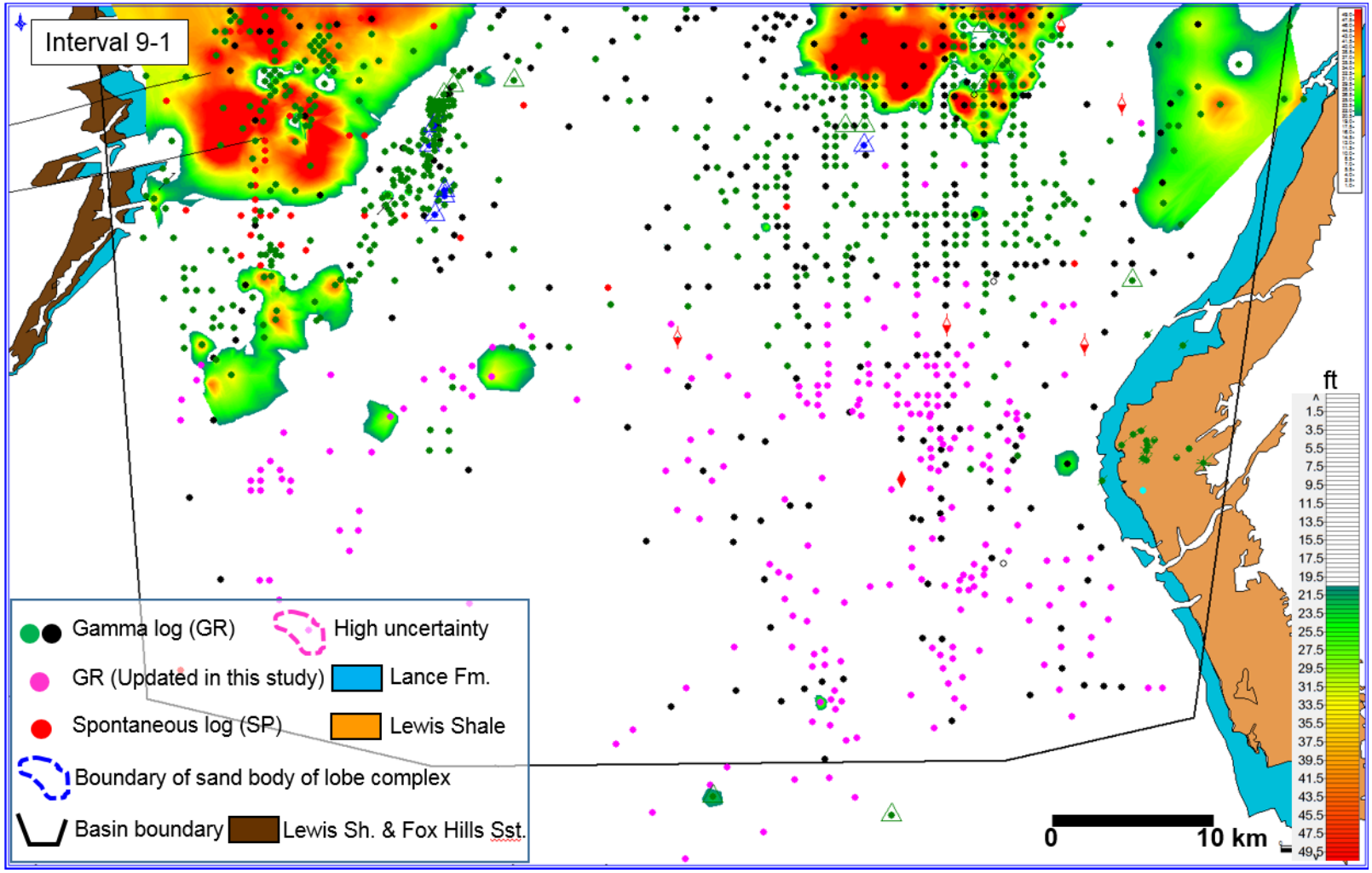

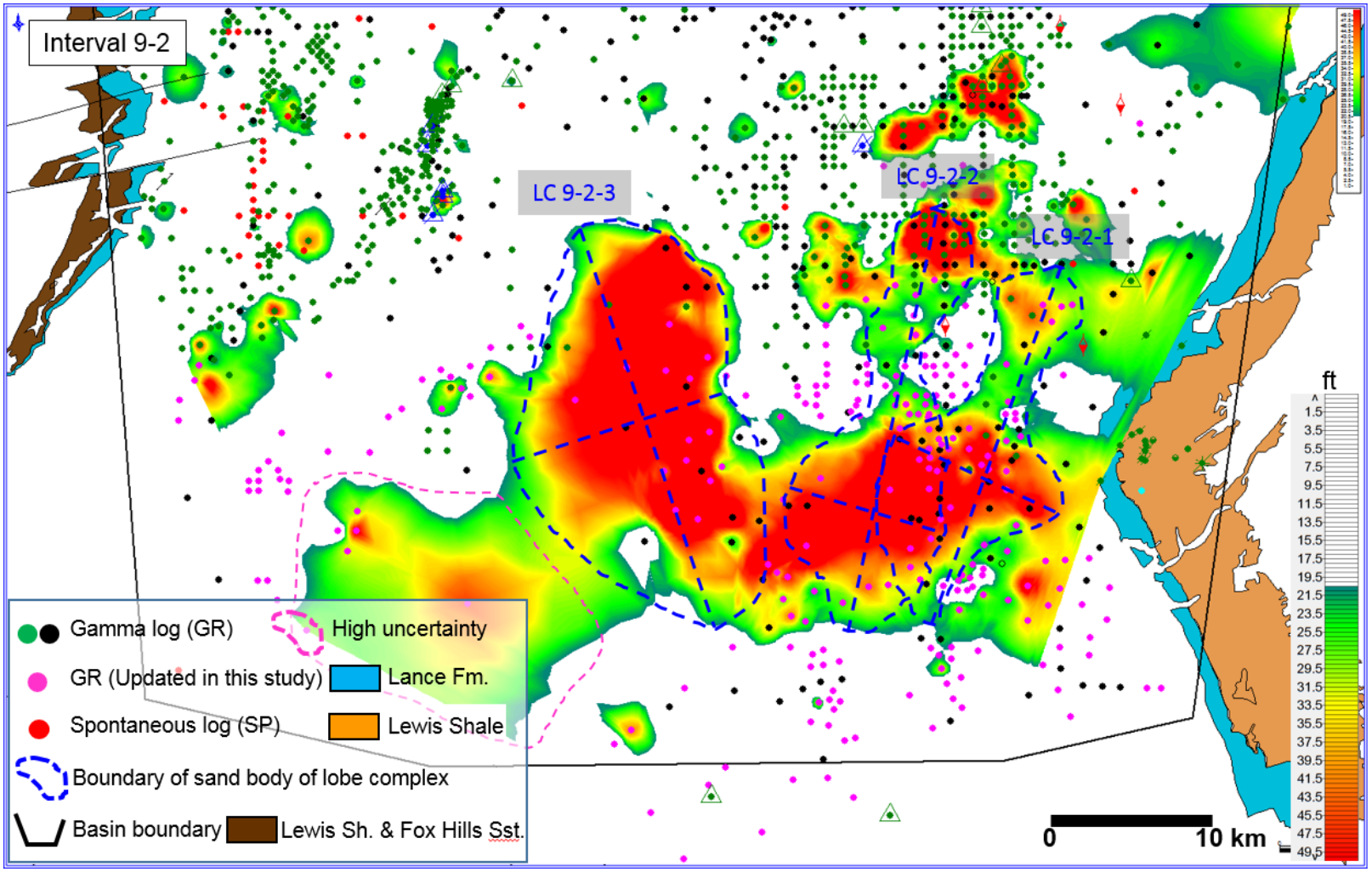
Interval 9-2
LC 9-2-3
LC 9-2-2
LC 9-2-1
ft
1.5
3.5
5.5
7.5
9.5
11.5
13.5
15.5
17.5
19.5
21.5
23.5
25.5
27.5
29.5
31.5
33.5
35.5
37.5
39.5
41.5
43.5
45.5
47.5
49.5
Gamma log (GR)
GR (Updated in this study)
Spontaneous log (SP)
Boundary of sand body of lobe complex
Basin boundary
High uncertainty
Lance Fm.
Lewis Shale
Lewis Sh. & Fox Hills Sst.
0
10 km

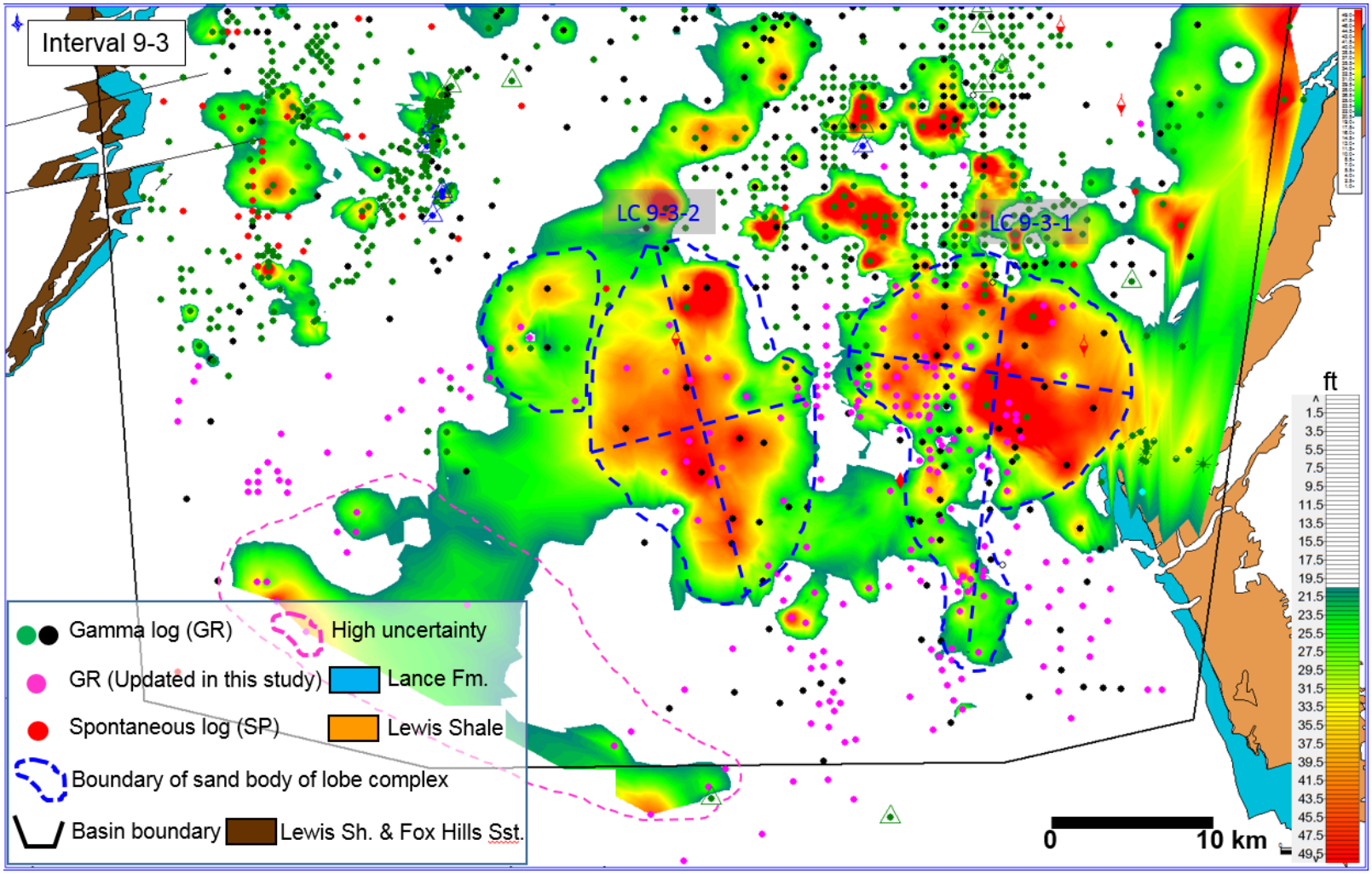
Interval 9-3
LC 9-3-2
LC 9-3-1
ft
1.5
3.5
5.5
7.5
9.5
11.5
13.5
15.5
17.5
19.5
21.5
23.5
25.5
27.5
29.5
31.5
33.5
35.5
37.5
39.5
41.5
43.5
45.5
47.5
49.5
Gamma log (GR)
GR (Updated in this study)
Spontaneous log (SP)
Boundary of sand body of lobe complex
Basin boundary
High uncertainty
Lance Fm.
Lewis Shale
Lewis Sh. & Fox Hills Sst.
0
10 km

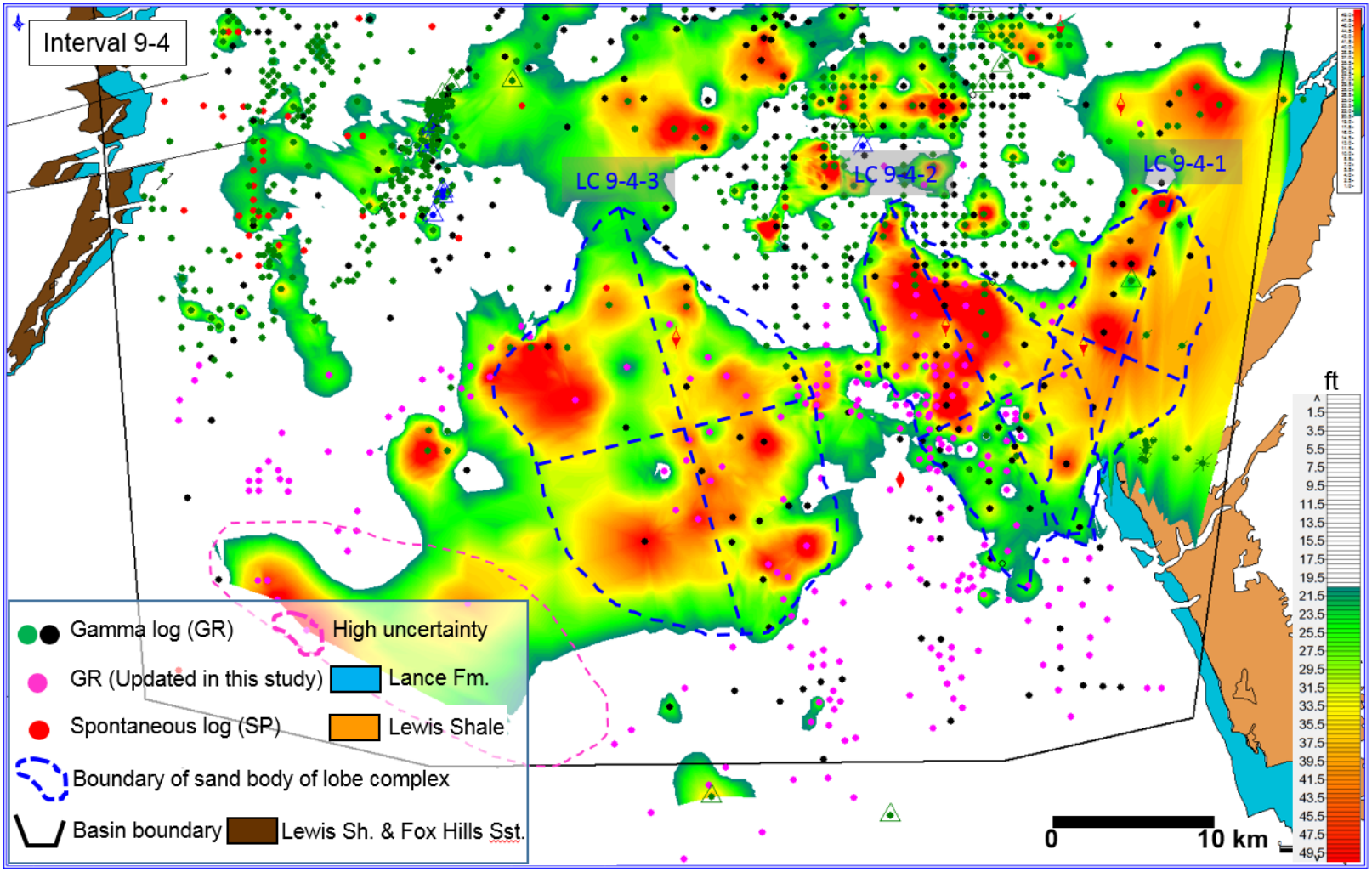
Interval 9-4
LC 9-4-3
LC 9-4-2
LC 9-4-1
ft
1.5
3.5
5.5
7.5
9.5
11.5
13.5
15.5
17.5
19.5
21.5
23.5
25.5
27.5
29.5
31.5
33.5
35.5
37.5
39.5
41.5
43.5
45.5
47.5
49.5
Gamma log (GR)
GR (Updated in this study)
Spontaneous log (SP)
Boundary of sand body of lobe complex
Basin boundary
High uncertainty
Lance Fm.
Lewis Shale
Lewis Sh. & Fox Hills Sst.
0
10 km

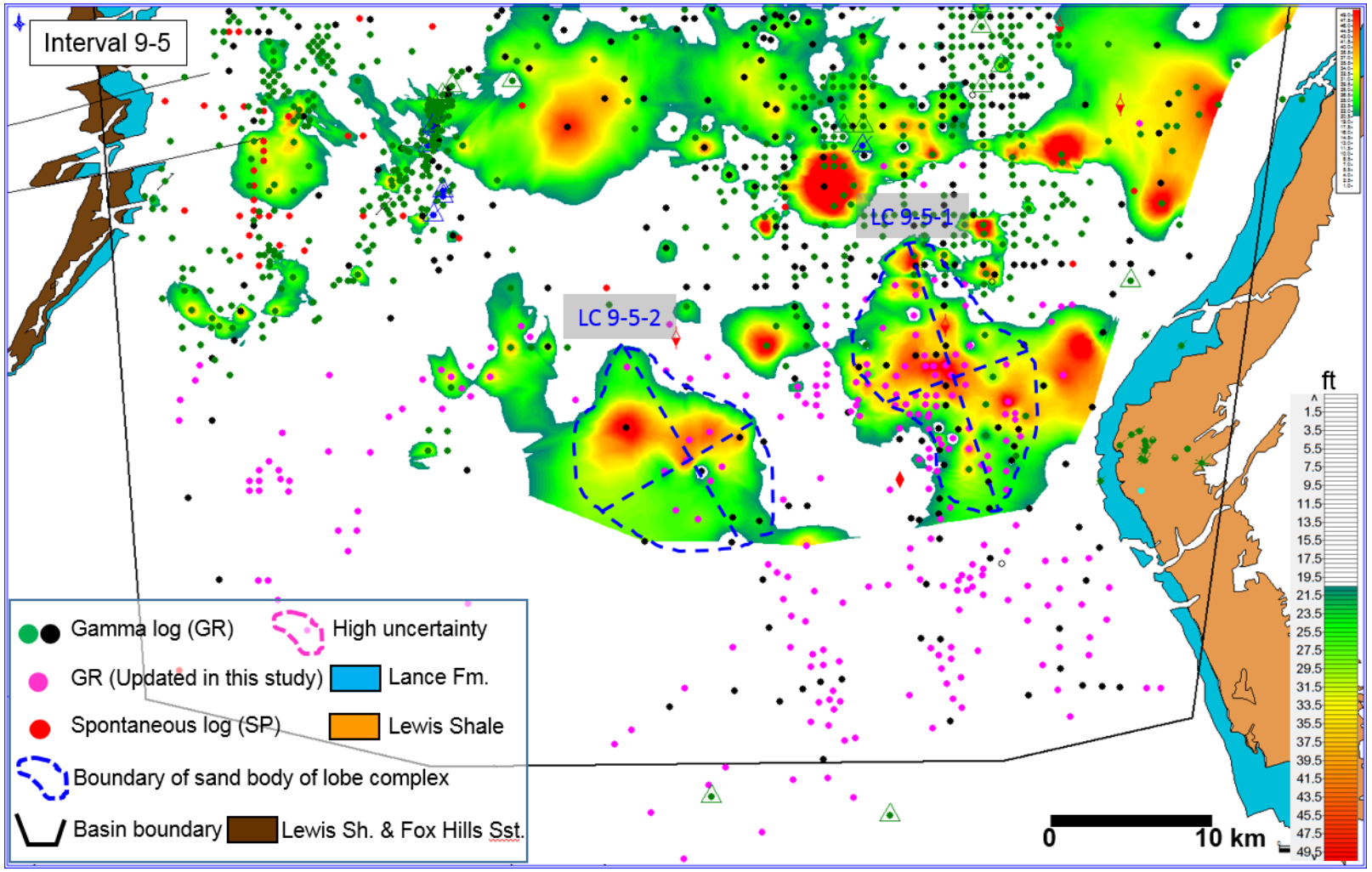
Interval 9-5
LC 9-5-1
LC 9-5-2
ft
1.5
3.5
5.5
7.5
9.5
11.5
13.5
15.5
17.5
19.5
21.5
23.5
25.5
27.5
29.5
31.5
33.5
35.5
37.5
39.5
41.5
43.5
45.5
47.5
49.5
Gamma log (GR)
High uncertainty
GR (Updated in this study)
Lance Fm.
Spontaneous log (SP)
Lewis Shale
Boundary of sand body of lobe complex
Basin boundary
Lewis Sh. & Fox Hills Sst.
0
10 km

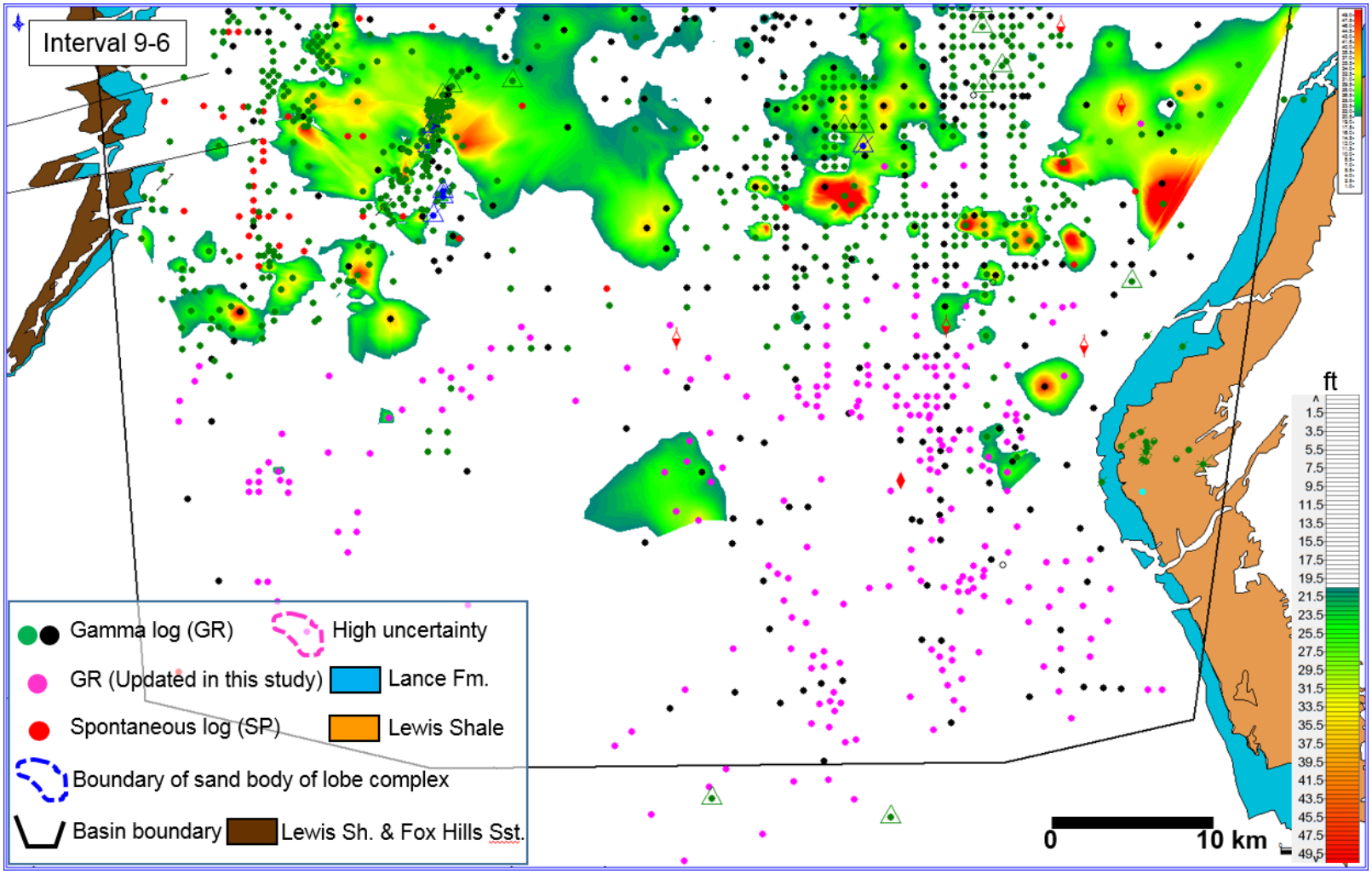
Interval 9-6
Gamma log (GR)
High uncertainty
GR (Updated in this study)
Lance Fm.
Spontaneous log (SP)
Lewis Shale
Boundary of sand body of lobe complex
Basin boundary
Lewis Sh. & Fox Hills Sst.
0
10 km
ft
1.5
3.5
5.5
7.5
9.5
11.5
13.5
15.5
17.5
19.5
21.5
23.5
25.5
27.5
29.5
31.5
33.5
35.5
37.5
39.5
41.5
43.5
45.5
47.5
49.5

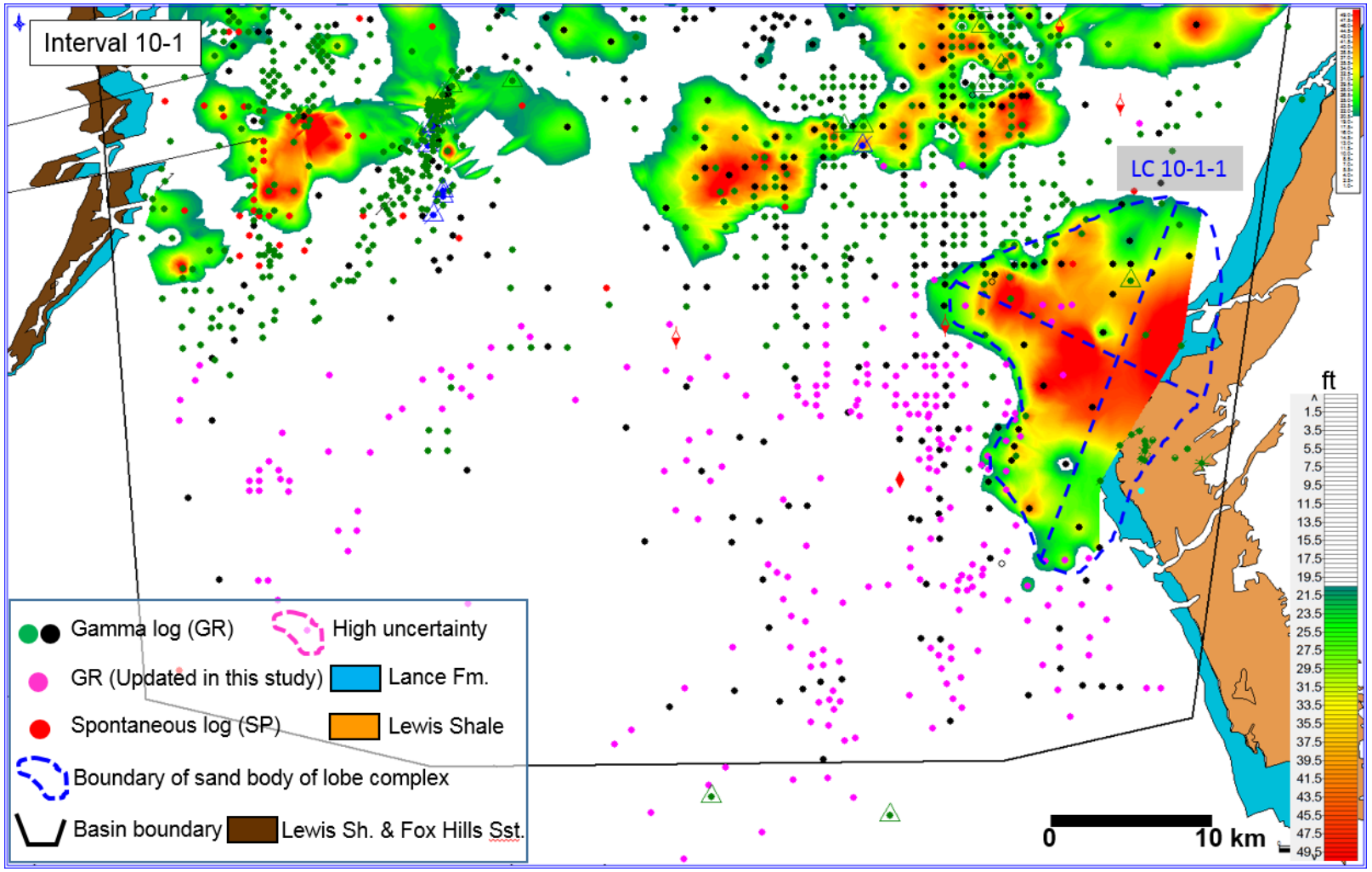
Interval 10-1
LC 10-1-1
ft
1.5
3.5
5.5
7.5
9.5
11.5
13.5
15.5
17.5
19.5
21.5
23.5
25.5
27.5
29.5
31.5
33.5
35.5
37.5
39.5
41.5
43.5
45.5
47.5
49.5
Gamma log (GR)
High uncertainty
GR (Updated in this study)
Lance Fm.
Spontaneous log (SP)
Lewis Shale
Boundary of sand body of lobe complex
Basin boundary
Lewis Sh. & Fox Hills Sst.
0
10 km

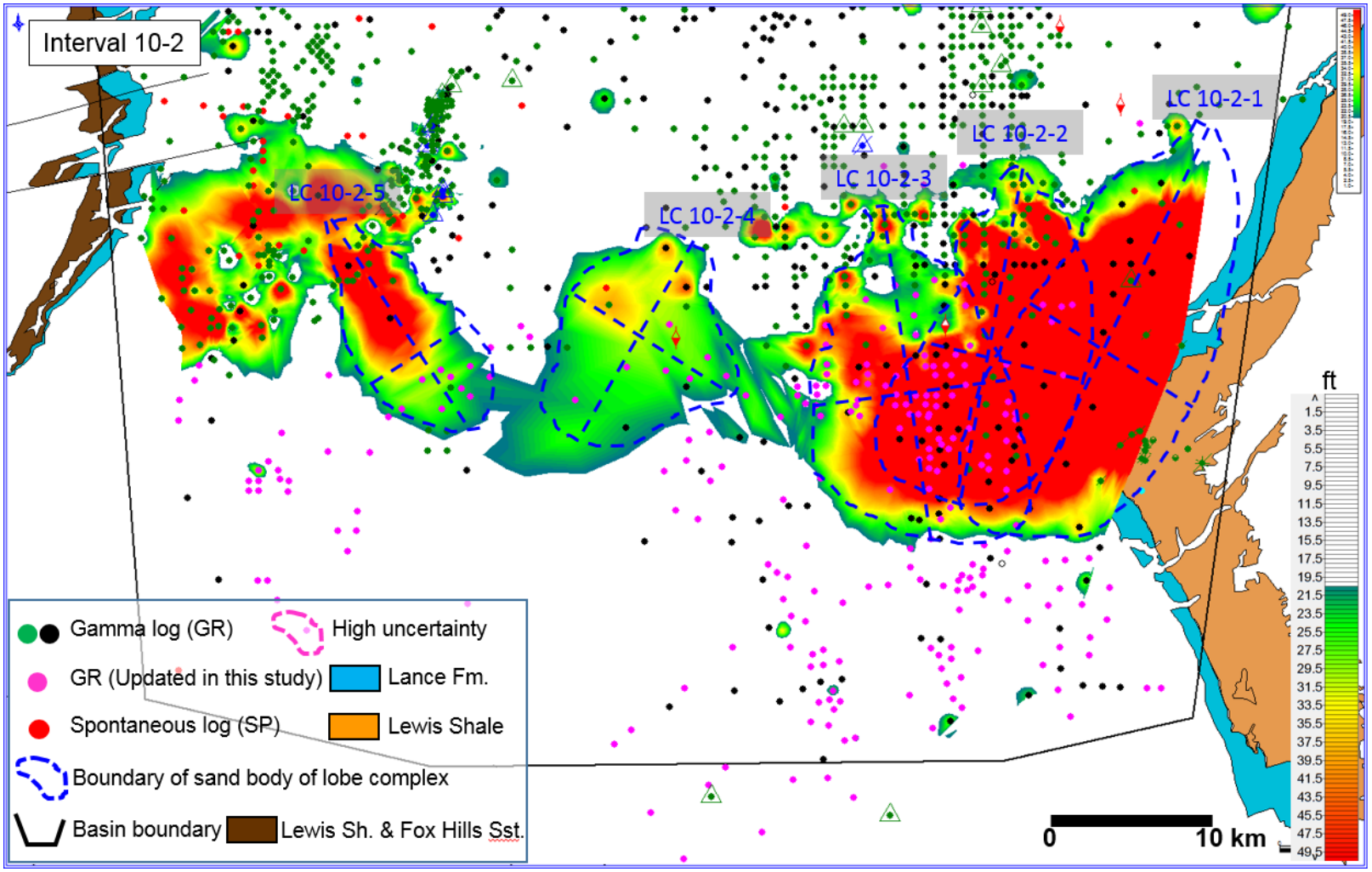
Interval 10-2
LC 10-2-1
LC 10-2-2
LC 10-2-3
LC 10-2-4
LC 10-2-5
ft
1.5
3.5
5.5
7.5
9.5
11.5
13.5
15.5
17.5
19.5
21.5
23.5
25.5
27.5
29.5
31.5
33.5
35.5
37.5
39.5
41.5
43.5
45.5
47.5
49.5
Gamma log (GR)
High uncertainty
GR (Updated in this study)
Lance Fm.
Spontaneous log (SP)
Lewis Shale
Boundary of sand body of lobe complex
Basin boundary
Lewis Sh. & Fox Hills Sst.
0
10 km

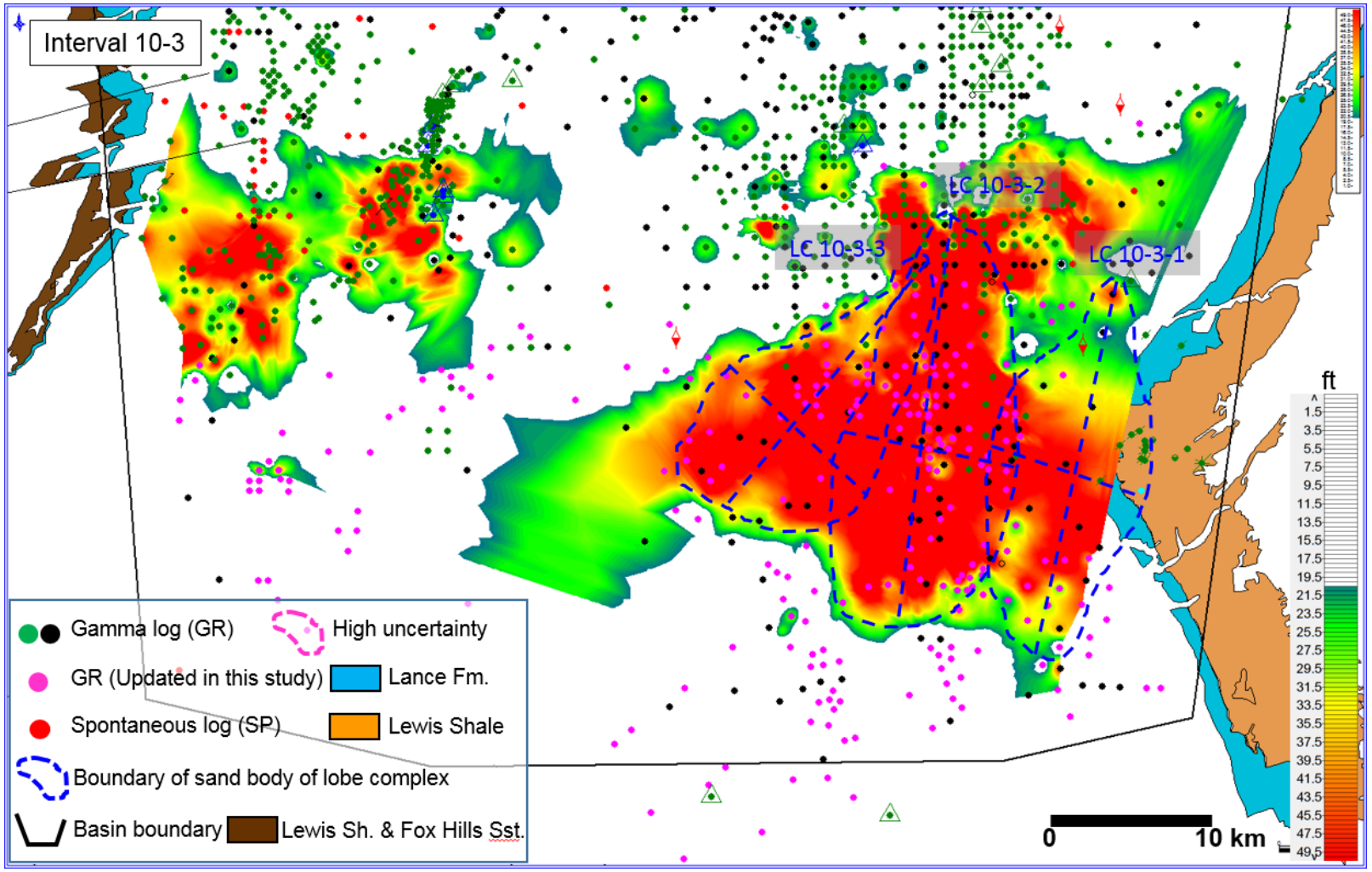
Interval 10-3
LC 10-3-2
LC 10-3-3
LC 10-3-1
ft
1.5
3.5
5.5
7.5
9.5
11.5
13.5
15.5
17.5
19.5
21.5
23.5
25.5
27.5
29.5
31.5
33.5
35.5
37.5
39.5
41.5
43.5
45.5
47.5
49.5
Gamma log (GR)
High uncertainty
GR (Updated in this study)
Lance Fm.
Spontaneous log (SP)
Lewis Shale
Boundary of sand body of lobe complex
Basin boundary
Lewis Sh. & Fox Hills Sst.
0
10 km

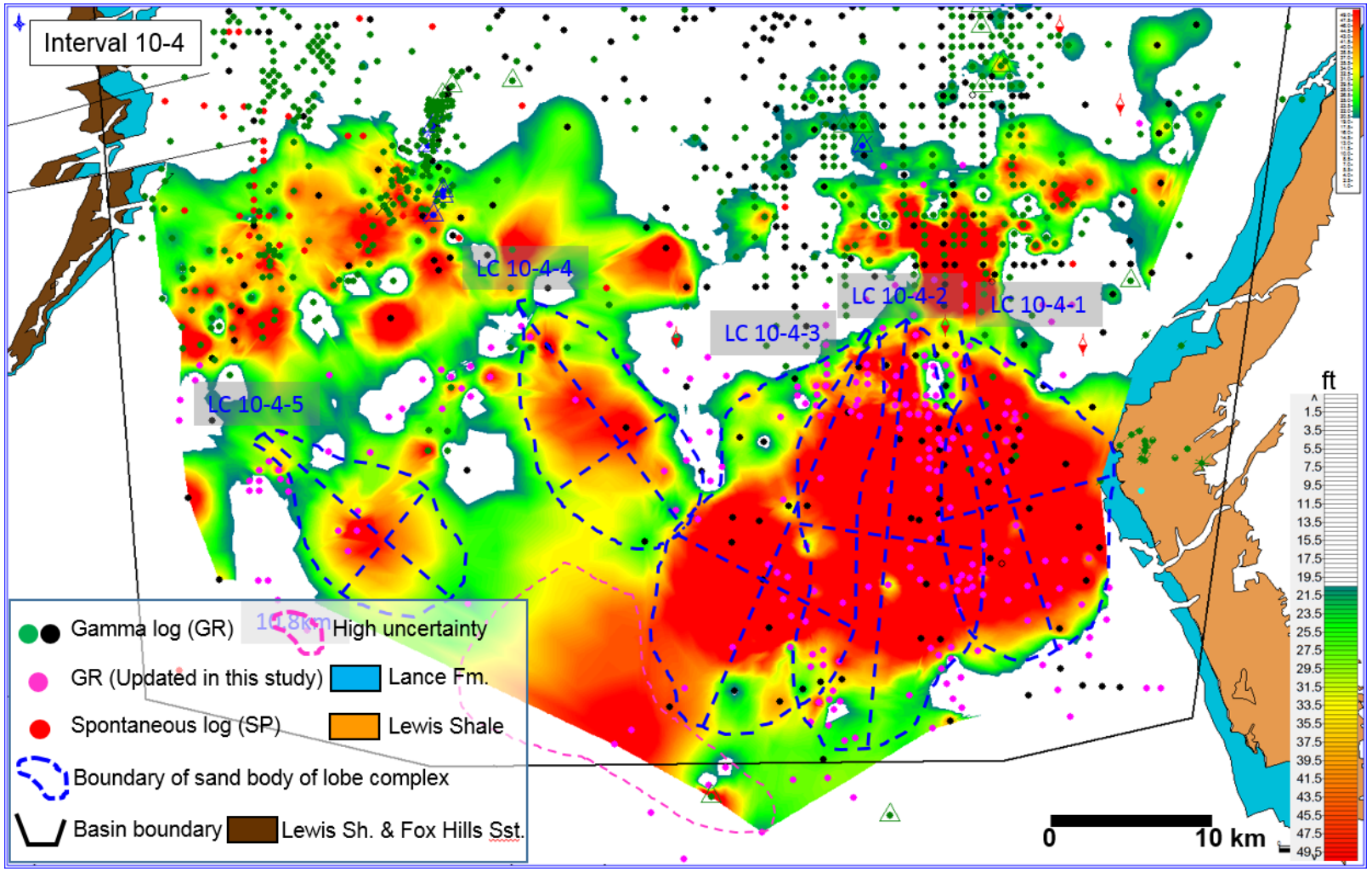
Interval 10-4
LC 10-4-4
LC 10-4-2
LC 10-4-1
LC 10-4-3
LC 10-4-5
ft
1.5
3.5
5.5
7.5
9.5
11.5
13.5
15.5
17.5
19.5
21.5
23.5
25.5
27.5
29.5
31.5
33.5
35.5
37.5
39.5
41.5
43.5
45.5
47.5
49.5
Gamma log (GR)
High uncertainty
GR (Updated in this study)
Lance Fm.
Spontaneous log (SP)
Lewis Shale
Boundary of sand body of lobe complex
Basin boundary
Lewis Sh. & Fox Hills Sst.
0
10 km

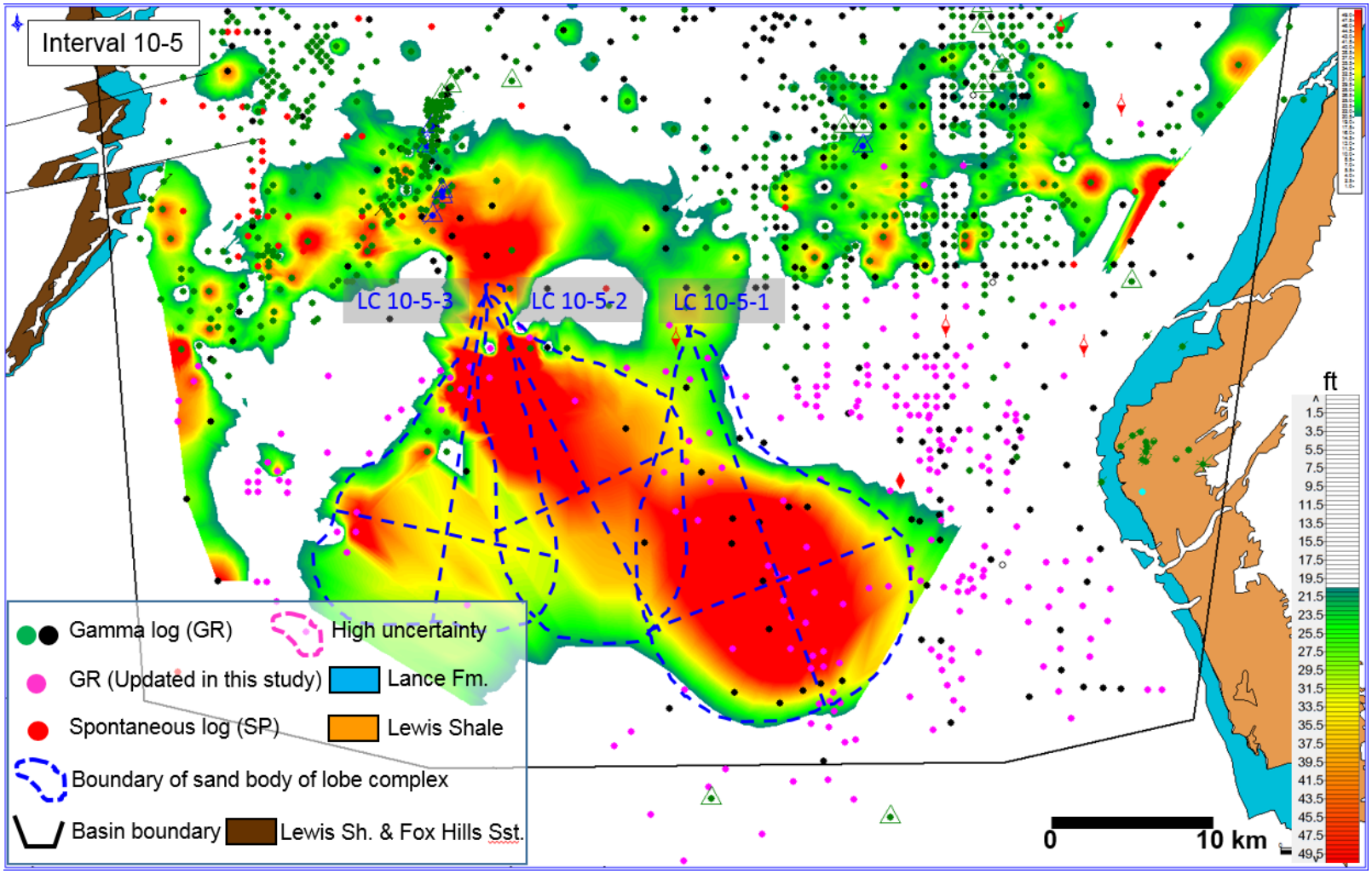
Interval 10-5
LC 10-5-3
LC 10-5-2
LC 10-5-1
Gamma log (GR)
High uncertainty
GR (Updated in this study)
Lance Fm.
Spontaneous log (SP)
Lewis Shale
Boundary of sand body of lobe complex
Basin boundary
Lewis Sh. & Fox Hills Sst.
0
10 km
ft
1.5
3.5
5.5
7.5
9.5
11.5
13.5
15.5
17.5
19.5
21.5
23.5
25.5
27.5
29.5
31.5
33.5
35.5
37.5
39.5
41.5
43.5
45.5
47.5
49.5

References

ALLEN, J.R.L., AND LEEDER, M.R., 1980, Criteria for the instability of upper-stage plane beds: Sedimentology, v. 27, p. 209-217.

AMY, L.A., AND TALLING, P.J., 2006, Anatomy of turbidites and linked debrites based on long distance (120 × 30 km) bed correlation, Marnoso Arenacea Formation, Northern Apennines, Italy: Sedimentology, v. 53, p. 161-212.

BAAS, J.H., BEST, J.L., AND PEAKALL, J., 2011, Depositional processes, bedform development and hybrid bed formation in rapidly decelerated (mud-sand) sediment flows: Sedimentology, v. 58, p. 1953-1987.

BOUMA, A.H., 1962, Sedimentology of some flysch deposits. A graphic approach to facies interpretation: Elsevier, Amsterdam, p. 168.

BURGESS, P.M., AND HOVIUS, N., 1998, Rates of delta progradation during highstands: consequences for timing of deposition in deep-marine systems: Geological Society of London, Journal, v. 155, p. 217-222.

CARVAJAL, C.R., AND STEEL, R.J., 2006, Thick turbidite successions from supply-dominated shelves during sea-level highstand: Geology, v. 34, p. 665-668.

CARVAJAL, C., AND STEEL, R., 2009, Shelf-edge architecture and bypass of sand to deep water: influence of shelf-edge processes, sea level and sediment supply: Journal of Sedimentary Research, v. 79, p. 652-672.

CARVAJAL, C., AND STEEL, R., 2012, Source-to-sink sediment volumes within a tectono-stratigraphic model for a Laramide shelf-to-deep-water basin: methods and

results: in Busby, C., and Azor, A., ed., Tectonics of Sedimentary Basins: Recent Advances, Part 2: New techniques and modeling, p. 131-151.

CARVAJAL, C., STEEL, R., AND PETTER, A., 2009, Sediment supply: the main driver of shelf-margin growth: Earth-Science Reviews, v. 96, p. 221-248.

COVAULT, J.A., NORMARK, W.R., ROMANS, B.W., AND GRAHAM, S.A., 2007, Highstand fans in the California borderland: The overlooked deep-water depositional systems: Geology, v. 35, p. 783-786.

DEPTUCK, M.E., PIPER, D.J.W., SAVOYE, B., AND GERVAIS, A., 2008, Dimensions and architecture of late Pleistocene submarine lobes off the northern margin of East Corsica: Sedimentology, v. 55, p. 869-898.

DICKINSON, W.R., KLUTE, M.A., HAYES, M.J., JANECKE, S.U., LUNDIN, E.R., MCKITTRICK, M.A., AND OLIVARES, M.D., 1988, Paleogeographic and paleotectonic setting of Laramide sedimentary basins in the central Rocky Mountain region: Geological Society of America Bulletin, v. 100, p. 1023-1039.

DIXON, J.F., STEEL, R.J., AND OLARIU, C., 2012, Shelf-edge delta regime as a predictor of deep-water deposition: Journal of Sedimentary Research, v. 82, p. 681-687.

DZULYNSKI, S., AND KOTLARCZYK, J., 1962, On load-casted ripples: Ann. Soc. Géol. Pologne, v. 32, p. 147-160.

FLEMINGS, P.B., JORDAN, T.E., AND REYNOLDS, S., 1986, Flexural analysis of two broken foreland basins: Late Cenozoic Bermejo Basin and early Cenozoic Green

River Basin (abstract): American Association of Petroleum Geologists, Bulletin, v. 70, p. 591.

GARDNER, M.H., BORER, J.M., MELICK, J.J., MAVILLA, N., DECHESNE, M., AND WAGERLE, R.N., 2003, Stratigraphic process-response model for submarine channels and related features from studies of Permian Brushy Canyon outcrops, West Texas: Marine and Petroleum Geology, v. 20, p. 757-787.

GILL, J.R., AND COBBAN, W.A., 1973, Stratigraphy and geologic history of the Montana Group and equivalent rocks, Montana, Wyoming, and North and South Dakota: U.S. Geological Survey professional paper 776, 37 p.

GILL, J.R., MEREWETHER, E.A., AND COBBAN, W.A., 1970, Stratigraphy and nomenclature of some Upper Cretaceous and lower Tertiary rocks in south-central Wyoming: U.S. Geological Survey professional paper 667, 53 p.

HADLER-JACOBSEN, F., JOHANNESSEN, E.P., ASHTON, N., HENRIKSEN, S., JOHNSON, S.D., AND KRISTENSEN, J.B., 2005, Submarine fan morphology and lithology distribution, in Dore, A.G., and Vining, B.A., eds., Petroleum Geology: North-West Europe and Global Perspectives-Proceedings of the 6th Petroleum Geology Conference: Geological Society, London, p. 1121–1145.

HAUGHTON, P.D.W., BARKER, S.P., AND MCCAFFREY, W.D., 2003, 'Linked' debrites in sand-rich turbidite systems-Origin and significance: Sedimentology, v. 50, p. 459-482.

HAUGHTON, P., DAVIS, C., MCCAFFREY, W., AND BARKER, S., 2009, Hybrid sediment gravity flow deposits - Classification, origin and significance: Marine and Petroleum Geology, v. 26, p. 1900-1918.

HELLER, P.L., PAOLA, C., HWANG, I., JOHN, B., AND STEEL, R., 2001, Geomorphology and sequence stratigraphy due to slow and rapid base-level changes in an experimental subsiding basin (XES 96-1): American Association of Petroleum Geologists, Bulletin, v. 85, p. 817-838.

HISCOTT, R.N., 1994, Traction-carpet stratification in turbidites - fact or fiction?: Journal of Sedimentary Research, v. 64, p. 204-208.

HISCOTT, R.N., AND MIDDLETON, G.V., 1979, Depositional mechanics of the thick-bedded sandstones at the base of a submarine slope, Tourelle Formation (Lower Ordovician), Quebec, Canada. In: Geology of Continental Slopes, in Doyle, L.J., and Pilkey, O.H., eds., SEPM Special Publication, v. 27, p. 307-326.

HODGSON, D.M., 2009, Distribution and origin of hybrid beds in sand-rich submarine fans of the Tanqua depocentre, Karoo Basin, South Africa: Marine and Petroleum Geology, v. 26, p. 1940-1956.

KANE, I.A., AND PONTÉN, A.S.M., 2012, Submarine transitional flow deposits in the Paleogene Gulf of Mexico: Geology, first published online 2 October 2012 doi: 10.1130/G33410.1.

KIM, W., AND MUTO, T., 2007, Autogenic response of alluvial-bedrock transition to base-level variation: Experiment and theory: Journal of Geophysical Research, v. 112, p. F03S14.

KIM, Y., KIM, W., CHEONG, D., MUTO, T., AND PYLES, D., 2013, Piping coarse-grained sediment to a deep-water fan through a shelf-edge delta bypass channel: Tank Experiments: Journal of Geophysical Research, v. 118, p. 2279-2291, DOI: 10.1002/2013JF002813.

KNELLER, B.C., 1995, Beyond the turbidite paradigm: physical models for deposition of turbidites and their implications for reservoir potential, in Hartley, A.J. and Prosser, D.J., eds., Characterization of Deep Marine Systems: Geological Society Special Publication, v. 94, p. 31-49.

KNELLER, B.C., AND BRANNEY, M.J., 1995, Sustained high-density turbidity currents and the deposition of thick massive sands: Sedimentology, v. 42, p. 607-616.

KNELLER, B.C., AND MCCAFFREY, W.D., 2003, The interpretation of vertical sequences in turbidite beds: the influence of longitudinal flow structure: Journal of Sedimentary Research, v. 73, p. 706-713.

KOLLA, V., 1993, Lowstand deep-water siliciclastic depositional systems: characteristics and terminologies in sequence stratigraphy and sedimentology: Bulletin of the Center for Research and Exploration-Production Elf Aquitaine, v. 17, p. 67-78.

KUENEN, P.H., 1951, Properties of turbidity currents of high density: SEPM Special Publication, v. 2, p. 14-33.

KUENEN, P.H., AND MIGLIORINI, C.I., 1950, Turbidity currents as a cause of graded bedding: Journal of Geology, v. 58, p. 91-127.

LOWE, D.R., 1982, Sediment gravity flows: II. Depositional models with special reference to the deposits of high-density turbidity currents: Journal of Sedimentary Petrology, v. 52, p. 279-297.

LOWE, D.R., AND GUY, M., 2000, Slurry-flow deposits in the Britannia Formation (Lower Cretaceous), North Sea: a new perspective on the turbidity current and debris flow problem: Sedimentology, v. 47, p. 31-70.

MARR, J.G., HARFF, P.A., SHANMUGAM, G., AND PARKER, G., 2001, Experiments on subaqueous sandy gravity flows: The role of clay and water content in flow dynamics and depositional structures: GSA Bulletin, v. 113, p. 1377-1386.

MCCAVE, I.N., AND JONES, K.P.N., 1988, Deposition of ungraded muds from high-density non-turbulent turbidity currents: Nature, v. 333, p. 250-252.

MEREWETHER, E.A., AND COBBAN, W.A., 1981, Mid-Cretaceous formations in eastern South Dakota and adjoining areas-stratigraphic, paleontologic, and structural interpretations, in Brenner, R.L., and others, eds., Cretaceous Stratigraphy and Sedimentation in Northwest Iowa, Northeast Nebraska, and Southeast South Dakota: Iowa Geological Survey Guidebook, Series 4, p. 43-56.

MIDDLETON, G.V., 1966a, Experiments on density and turbidity currents. I. Motion of the head: Canadian Journal of Earth Sciences, v. 3, p. 523-546.

MIDDLETON, G.V., 1966b, Experiments on density and turbidity currents. II. Uniform flow of density currents: Canadian Journal of Earth Sciences, v. 3, p. 627-637.

MIDDLETON, G.V., 1967, Experiments on density and turbidity currents. III. Deposition of sediments: Canadian Journal of Earth Sciences, v. 4, p. 475-505.

MIDDLETON, G.V., AND HAMPTON, M.A., 1973, Sediment gravity flows: mechanics of flow and deposition, in Middleton, G.V., and Bouma, A.H., eds., Turbidites and deep-water sedimentation: SEPM Pacific Section, Short Course Anaheim, p. 1-38.

MOSLOW, T.F., AND DAVIES, G.R, 1997, Turbidite reservoir facies in the Lower Triassic Montney Formation, west-central Alberta: Bulletin of Canadian Petroleum Geology, v. 45, p. 507-536.

MULDER, T., CALLEC, Y., PARIZE, O., JOSEPH, P., SCHNEIDER, J., ROBIN, C., DUJONCQUOY, E., SALLES, T., ALLARD, J., BONNEL, C., DUCASSOU, E., ETIENNE, S., FERGER, B., GAUDIN, M., HANQUIEZ, V., LINARES, F., MARCHÈS, E., TOUCANNE, S., AND ZARAGOSI, S., 2010, High-resolution analysis of submarine lobes deposits: seismic-scale outcrops of the Lauzanier area, SE Alps, France: Sedimentary Geology, v. 229, p. 160-191.

MUTO, T., STEEL, R.J., AND SWENSON, J.B., 2007, Autostratigraphy: a framework norm for genetic stratigraphy: Journal of Sedimentary Research, v. 77, p. 2-12.

MUTTI, E., 1977, Distinctive thin-bedded turbidite facies and related depositional environments in the Eocene Hecho Group, South-central Pyrenees, Spain: Sedimentology, v. 24, p. 107-131.

MUTTI, E., AND NORMARK, W.R., 1987, Comparing examples of modern and ancient turbidite systems: problems and concepts, in Leggert, J.K., and Zuffa, G.G., eds., Marine Clastic Sedimentology; Concepts and Case Studies: London, Graham and Trotman, p. 1-38.

MUTTI, E., AND RICCI LUCCHI, F., 1972, Le torbiditi dell'Appennino settentrionale: introduzione all'analisi di facies: Memorie della Societa Geologica Italiana, v. 11, p. 161-199.

NORMARK, W.R., 1970, Growth patterns of deep-sea fans: American Association of Petroleum Geologists, Bulletin, v. 54, p. 2170-2195.

OBRADOVICH, J.D., AND COBBAN, W.A., 1975, A time-scale for the Late Cretaceous of the western interior of North America, in Caldwell, W.G.E., eds., The Cretaceous System in the Western Interior of North America: Geological Association of Canada Special Paper, v. 13, p. 31-54.

OLARIU, M.I., CARVAJAL, C.R., OLARIU, C., AND STEEL, R.J., 2012, Deltaic process and architectural evolution during cross-shelf transits, Maastrichtian Fox Hills Formation, Washakie Basin, Wyoming: American Association of Petroleum Geologists, Bulletin, v. 96, p. 1931-1956.

PETTER, A.L., AND STEEL, R.J., 2006, Hyperpycnal flow variability and slope organization on an Eocene shelf margin, Central Basin, Spitsbergen: American Association of Petroleum Geologists, Bulletin, v. 90, p. 1451-1472.

PIPER, D.J.W., AND NORMARK, W.R., 1983, Turbidite depositional patterns and flow characteristics, Navy Submarine Fan, California Borderland: Sedimentology, v. 30, p. 681-694.

PLINK-BJÖRKLUND, P., AND STEEL, R.J., 2004, Initiation of turbidity currents: outcrop evidence for Eocene hyperpycnal flow turbidites: Sedimentary Geology, v. 165, p. 29-52.

PORĘBSKI, S.J., AND STEEL, R.J., 2003, Shelf-margin deltas: their stratigraphic significance and relation to deepwater sands: Earth-Science Reviews, v. 62, p. 283-326.

POSAMENTIER, H.W., ERSKINE, R.D., AND MITCHUM JR, R.M., 1991, Models for submarine-fan deposition within a sequence-stratigraphic framework, in Weimer, P., and Link, M.H., eds., In Seismic facies and sedimentary processes of submarine fans and turbidite systems: Frontiers in Sedimentary Geology, p. 127-136.

POSAMENTIER, H.W., AND KOLLA, V., 2003, Seismic geomorphology and stratigraphy of depositional elements in deep-water settings: Journal of Sedimentary Research, v. 73, p. 367-388.

POSAMENTIER, H.W., AND VAIL, P.R., 1988, Eustatic controls on clastic deposition: II, sequence and systems tract models, in Wilgus, C.K., Hastings, B.S., Ross, C.A., Posamentier, H.W., Van Wagoner, J., and Kendall, C.G.St.C., eds., Sea-Level Changes: An Integrated Approach: SEPM, Special Publication 42, p. 125-154.

POSTMA, G., 1986 Classification for sediment gravity-flow deposits based on flow conditions during sedimentation: Geology, v. 14, p. 291-294.

PRÉLAT, A., HODGSON, D.M., AND FLINT, S.S., 2009, Evolution, architecture and hierarchy of distributary deep-water deposits: a high-resolution outcrop investigation from the Permian Karoo Basin, South Africa: Sedimentology, v. 56, p. 2132-2154.

READING, H.G., AND RICHARDS, M., 1994, Turbidite systems in deep-water basin margins classified by grain size and feeder system: American Association of Petroleum Geologists, Bulletin, v. 78, p. 792-822.

RICCI LUCCHI, F., AND VALMORI, E., 1980, Basin-wide turbidites in a Miocene, over-supplied deep-sea plain: a geometrical analysis: Sedimentology, v. 27, p. 241-270.

SANDERS, J.E., 1965, Primary sedimentary structures formed by turbidity currents and related resedimentation mechanisms, in Middleton, G.V., eds., Primary sedimentary structures and their hydrodynamic interpretation: SEPM Special Publication, v. 12, p. 192-219.

SHANMUGAM, G., 1996, High-density turbidity currents: are they sandy debris flows?: Journal of Sedimentary Research, v. 66, p. 2-10.

SHANMUGAM, G., 1997, The Bouma Sequence and the turbidite mind set: Earth-Science Reviews, v. 42, p. 201-229.

SHANMUGAM, G., 2000, 50 years of the turbidite paradigm (1950s-1990s): deep-water processes and facies models-a critical perspective: Marine and Petroleum Geology, v. 17, p. 285-342.

SHUSTER, M.W., AND STEIDTMANN, J.R., 1988, Tectonic and sedimentary evolution of the northern Green River basin, western Wyoming: Geological Society of America, Memoir 171, p. 515-529.

SMITH, N.D., 1972, Flume experiments on the durability of mud clasts: Journal of Sedimentary Petrology, v. 42, p. 378-383.

SOHN, Y.K., 1997, On traction-carpet sedimentation: Journal of Sedimentary Research, v. 67, p. 502-509.

STEIDTMANN, J.R., AND MIDDLETON, L.T., 1991, Fault chronology and uplift history of the southern Wind River Range, Wyoming: Implications for Laramide and post-Laramide deformation in the Rocky Mountain foreland: Geological Society of America Bulletin, v. 103, p. 472-485.

STRAUB, K.M., PAOLA, C., MOHRIG, D., WOLINSKY, M.A., AND GEORGE, T., 2009, Compensational stacking of channelized sedimentary deposits: Journal of Sedimentary Research, v. 79, p. 673-688.

STRAUB, K.M., AND PYLES, D.R., 2012, Quantifying the hierarchical organization of compensation in submarine fans using surface statics: Journal of Sedimentary Research, v. 82, p. 889-898.

STRONG, N., AND PAOLA, C., 2008, Valleys that never were: time surfaces versus stratigraphic surfaces: Journal of Sedimentary Research, v. 78, p. 579-593.

SUMNER, E.J., TALLING, P.J., AMY, L.A., WYNN, R.B., STEVENSON, C.J., AND FRENZ, M., 2012, Facies architecture of individual basin-plain turbidites: comparison with existing models and implications for flow processes: Sedimentology, v. 59, p. 1850-1887.

TALLING, P.J., 2013, Hybrid submarine flows comprising turbidity current and cohesive debris flow: Deposits, theoretical and experimental analyses, and generalized models: Geosphere, v. 9, p. 460-488.

TALLING, P.J., AMY, L.A., WYNN, R.B., PEAKALL, J., AND ROBINSON, M., 2004, Beds comprising debrite sandwiched within co-genetic turbidite: origin and widespread occurrence in distal depositional environments: Sedimentology, v. 51, p. 163-194.

TALLING, P.J., MASSON, D.G., SUMNER, E.J., AND MALGESINI, G., 2012, Subaqueous sediment density flows: depositional processes and deposit types: Sedimentology, v. 59, p. 1937-2003.

TWICHELL, D.C., SCHWAB, W.C., NELSON, C.H., KENYON, N.H., AND LEE, H.J., 1992, Characteristics of a sandy depositional lobe on the outer Mississippi fan from SeaMARC IA sidescan sonar images: Geology, v. 20, p. 689-692.

VAN DER MERWE, W.C., HODGSON, D.M., AND FLINT, S.S., 2009, Widespread syn-sedimentary deformation on a muddy deep-water basin-floor: the Vischkuil Formation (Permian), Karoo Basin, South Africa: Basin Research, v. 21, p. 389-406.

VAN WAGONER, J.C., MITCHUM, R.M., POSAMENTIER, H.W., AND VAIL, P.R., 1987, Seismic stratigraphy interpretation using sequence stratigraphy, Part 2: Key definitions of sequence stratigraphy, in Bally, A.W., eds., Atlas of seismic stratigraphy: American Association of Petroleum Geologists Studies in Geology 27, v. 1, p. 11-14.

WALKER, R.G., AND MUTTI, E., 1973, Turbidite facies and facies associations: *in* Middleton, G.V., and Bouma, A.H., eds., Turbidites and deep-water sedimentation: SEPM Pacific Section, Short Course, p. 119-157.

WINN, R.D., BISHOP, M.G., AND GARDNER, P.S., 1987, Shallow-water and sub-storm-base deposition of Lewis Shale in Cretaceous Western Interior Seaway, south-central Wyoming: American Association of Petroleum Geologists, Bulletin, v. 71, p. 859-881.